INAUGURAL-DISSERTATION
zur
Erlangung der Doktorwürde

der
Naturwissenschaftlich-Mathematischen
Gesamtfakultät

der
Ruprecht-Karls-Universität
Heidelberg

vorgelegt von
Dipl.-Phys. Dagmar Sigrun Isert
aus Waiblingen

Tag der mündlichen Prüfung: 14. Februar 2001

Transporttheorie für skalare Quarks und Gluonen

Gutachter: Prof. Ph D Sandra P. Klevansky

Prof. Dr. Michael G. Schmidt

Dissertation
submitted to the
Combined Faculties for the Natural Sciences and for Mathematics
of the Rupertus Carola University of
Heidelberg, Germany
for the degree of
Doctor of Natural Sciences

Transport Theory for scalar Quarks and Gluons

presented by

Diplom-Physicist Dagmar Sigrun Isert
born in Waiblingen, Germany

Heidelberg, 14.02.2001

Referees: Prof. Ph D Sandra P. Klevansky
Prof. Dr. Michael G. Schmidt

Transporttheorie für skalare Quarks und Gluonen

Zusammenfassung

In dieser Arbeit werden die sogenannten Transport- und Constraintgleichungen für skalare Quarks und Gluonen aufgestellt. Es wird gezeigt, dass die Transportgleichung ohne Berücksichtigung der Constraintgleichung in der Quasiteilchennäherung zu einer Boltzmann-artigen Gleichung führt. Die Analyse aller auftretenden Selbstenergiegraphen macht deutlich, welche Rolle sie spielen: Einige Graphen führen zu den erwarteten Wirkungsquerschnitten, während andere Graphen Feynman-Diagramme von Streuprozessen niedrigerer Ordnung renormieren.

Bei der Berechnung der Transportgleichung treten in einzelnen Selbstenergiegraphen sogenannte Pinch-Singularitäten auf. Durch eine explizite Rechnung kann gezeigt werden, dass sie sich im Gleichgewicht wegheben. Für Systeme im Nicht-Gleichgewicht werden verschiedene Ansätze untersucht, die allerdings nicht zur Aufhebung aller Pinch-Singularitäten führen.

Bei Berücksichtigung der Constraintgleichung erhalten die Propagatoren eine endliche Breite, wodurch die Pinch-Singularitäten nicht mehr auftreten. Dafür wird die Berechnung der Transportgleichung komplizierter, und sie kann nicht mehr in eine Boltzmann-artige Form gebracht werden.

Transport theory for scalar quarks and gluons

Abstract

In this work, we have detailed the calculations of the transport and constraint equations for a theory of scalar quarks and gluons with self-interactions. Special care has been taken in particular in understanding how the transport equation, taken on its own, leads to a Boltzmann-like equation when considered in the quasiparticle approximation. Through the analysis of all self-energy graphs that occur it is evident which role they play: certain graphs give rise to the expected cross sections, while others serve to renormalize diagrams of lower order scattering processes.

In the calculation of the transport equation, so-called pinch singularities arise in individual self-energy diagrams. We demonstrate explicitly how they cancel in equilibrium. For the case of non-equilibrium, several ansätze are investigated, but none of them leads to the cancellation of all pinch singularities.

Finally, the constraint equation is considered. This leads to the introduction of a finite width into the propagators. The main advantage of this is that no pinch singularities can possibly occur. The disadvantage, however, is that the calculations become very cumbersome and it is no longer straightforward to cast the transport equation into a form which can be recognized as being Boltzmann-like.

Contents

Chapter 1

Introduction

In searching for the fundamental particles of matter, many new hadrons were found in accelerator experiments in the 1950/60's. In order to organize this 'hadron-zoo', quarks were postulated as fundamental particles. Due to the Pauli-principle for quarks in hadrons, it was necessary to postulate a new quantum number called color which is the charge of the strong interaction. The number of colors (three) is confirmed by several experiments. Under normal conditions only color neutral objects (hadrons) are observed, i.e. three quark states (baryons) or quark-antiquark pairs (mesons). Nevertheless, one believes that this confinement falls away for matter under extreme conditions.

In the hadronic phase, confinement plays a dominant role and the chiral symmetry is spontaneously broken. For sufficiently high temperatures and/or baryonic density a phase transition is believed to take place. The new phase is the so-called quark-gluon plasma (QGP); quarks and gluons are free particles that are deconfined and the chiral symmetry is restored. Note that it is often assumed that both phase transitions take place simultaneously, i.e. at the same temperature.

In a naive view, this phase transition is frequently given heuristically as shown in Fig. 1.1. There it is assumed that an equilibrium description is valid. It is believed that the early universe passed approximately $10\mu s$ after the big bang - when it was cool enough - through this phase transition. Obviously this was a unique 'experiment' and cannot be repeated. But in relativistic heavy ion collisions (RHIC) this phase transition should take place, too, since the conditions for the phase transition, extremely high energy densities, can be reached.

Thus let us review the scenario for an ultra-relativistic heavy ion collision which is shown schematically in Fig. 1.2. Its evolution in space-time is presented in Fig. 1.3. For high beam-energies ($E_{CM} > 50GeV$/nucleon), two Lorentz contracted nuclei pass through each other. Then, shortly after the collision, an energy density of

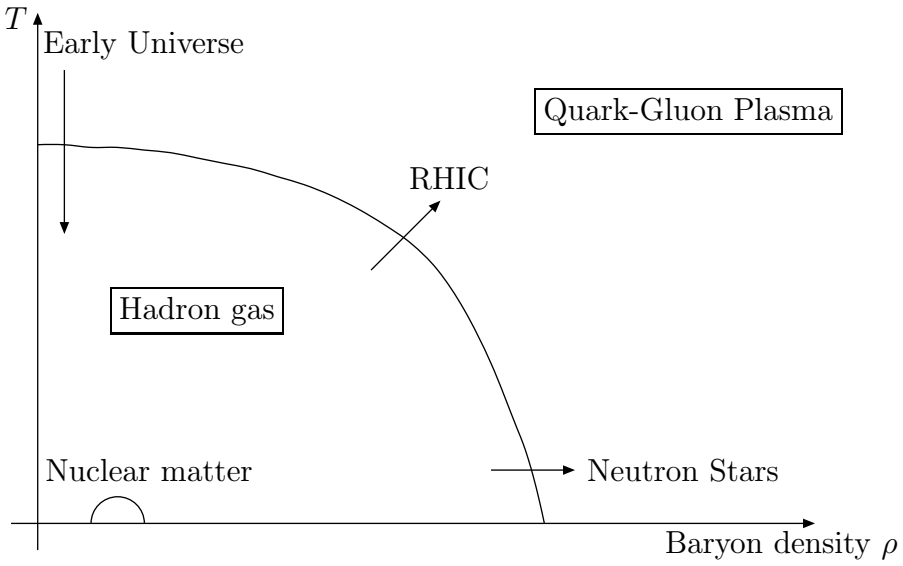

Figure 1.1: Phase diagram for hadronic matter.

one or two orders of magnitude greater than that of ground state nuclear matter ($0.15GeV/fm^3$) is expected to be attained. At this stage, one assumes that the quarks and gluons are no longer confined and form a dense plasma. The excited partons interact with each other, and if the interactions occur frequently enough, the system reaches a local thermodynamic equilibrium, the quark-gluon plasma. Finally the partons hadronize, i.e. hadrons are formed and recede from the collision region. Note that due to the fact that the collision takes place over an extremely small time scale, it is not clear that chemical and thermodynamical equilibrium are reached: this underscores the cartoon like nature of Fig. 1.1.

Thus, in this thesis we address the question as to how the partons evolve after the collision to a point in which thermodynamic equilibrium is possibly reached. This evolution is described by the evolution equations for the distribution function $f_a(x,p)$ in phase space where $f_a(x,p)d^3xd^3p$ gives the probability of finding a parton of type a in d^3x around $\vec{x}$ and with a momentum in d^3p around $\vec{p}$. Now ordinary zero temperature field theory is insufficient for a description of the evolution of the system. One cannot assume that the system passes through a series of equilibrium states, and therefore one needs a description in terms of non-equilibrium field theory. Within this transport theory, the two evolution equations for the distribution function $f_a(x,p)$, the so-called transport and constraint equations can be constructed.

The natural underlying Lagrangian for the description of heavy ion collisions is that of quantum chromodynamics (QCD). Studying this Lagrangian in the context

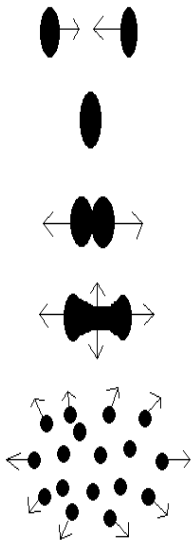

Figure 1.2: Schematic drawing of an heavy ion collision.

of non-equilibrium field theory introduces several difficulties in addition to simply the complexities that non-equilibrium theory gives rise to: these are gauge invariance, renormalization and the non-abelian like nature of the interaction. Clearly to develop a description which can simultaneously account for all these facets, an exact description of the transport equations with all of these facets is required. To the present date, however, each of these facets produces problems of their own. In addition, transport theory per se has only been worked out for few simple interacting systems often assuming contact and abelian interactions and also with the restriction of understanding only the lowest order processes. Consequently the approaches in the literature address one or the other problem in some form. We list some approaches that attempt to develop the relevant equations for QCD:

- Many authors rely on an intuitive extrapolation of the semiclassical Boltzmann equation in their applications (see for example, Geiger and Müller [1, 2] who examine heavy ion collisions in extreme conditions). Here an educated guess at an extended Boltzmann equation is made in order to develop a numerical simulation algorithm. An assumption about which processes should be considered in the collision integral is made on a purely heuristic basis. In such an approach, often the transport equation alone is examined; the constraint equation is simply neglected. In such studies a first attempt at putting this

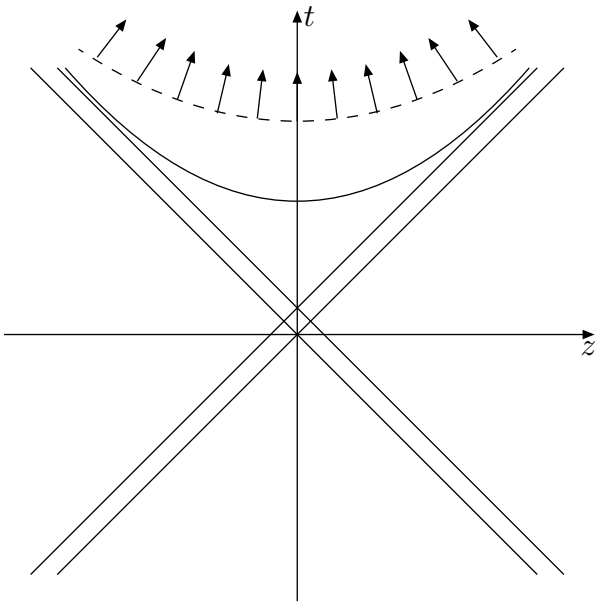

Figure 1.3: Space-time diagram of the evolution of an heavy ion collision.

application on a firm theoretical basis was subsequently made by [3].

- Some authors have centered their investigations on a full quantum treatment of the non-equilibrium Green function equations (see for example [4, 5, 6]). This approach has an aesthetic appeal, but in practice, there is little possibility of its application, as the complexity of solving many (16 or more) coupled integro-differential equations can only be performed under severe physical restrictions, namely that of no collisions.

- Progress in understanding collision theory has been made with the recent developments in real time Green function theory to calculate properties of systems in equilibrium. A theoretical methodology for handling non-equilibrium Green functions was developed by Schwinger and Keldysh [7, 8]. Later, in the 1980's, the development of thermal field theory was initiated by Umezawa [9]. The resulting matrix of real time Green functions has revealed a striking resemblance to the matrix of Green functions that is obtained in the Schwinger-Keldysh formalism. One can in fact quantifiably demonstrate that Schwinger-Keldysh and real time thermal field theory yield the same results in the limit that one considers equilibrium systems. Both formalisms are unwieldy, especially in contrast to the elegant formulation of equilibrium field theory by Matsubara, that was developed in the 60's, and which simply makes

extensive use of function theory. The historically late development of real time Green function theory is due to the fact that several difficulties in this approach are immediately evident: Products of retarded and advanced Green functions occur, so that integration along the real axis becomes problematic as the infinitesimal element $\epsilon \to 0$: the contour is pinched and the function is singular. So called pinch singularities also manifest themselves as products of delta functions when working in a causal / acausal framework. The fact now that two completely different formulations of equilibrium field theory exist has enabled one to understand these apparent difficulties in the real time approach, and this in turn enables one by comparison, to investigate similar situations in the non-equilibrium theory.

Our view in this work is directly to focus on the issue of constructing an exact transport theory in which non-abelian interactions occur and which pushes transport theory into the two-loop level and beyond in constructing an exact solution. In order to do this, the issue of gauge invariance is an unnecessary added degree of complexity, and we therefore do not investigate a gauge theory like QCD per se, but rather a simpler model of QCD which has the properties that it is scalar, and secondly, includes self-interactions in such a fashion that it describes pomeron behavior in elastic quark-quark scattering. The last feature of pomeron behavior is essential in some simulation models [10] that give good descriptions of experimental data for heavy ion collisions at energies attainable today. For the colliders RHIC and especially for LHC, it is unclear whether these pomeron based models will be able to account for the physics, necessitating a deeper understanding of the evolution of the constituents at a parton level.

Within our model of scalar quarks and gluons, we have been successful in building an appropriate transport theory and constructing a collision term exactly for two loop self-energies. This work goes beyond all previous analysis in that the complexity of the interaction introduces a plethora of terms (previously unknown), and the interpretation of which has been clarified. The results are generalized beyond the two loop level and a Boltzmann-like equation is obtained. Multiparticle production and annihilation processes associated with this interaction are seen to occur. Since the quasiparticle approximation is used, the issue of pinch singularities arises, so that it is necessary to check whether and how singular behavior is removed from the transport equations. For consistency, the constraint equation is also examined.

This thesis is structured as follows. In Chapter 2, we introduce our model for scalar quarks and gluons. Furthermore, we show how the pomeron like behavior emerges from elastic quark-quark scattering in the Regge limit. Since the study

of transport theory is similar to equilibrium real time field theory, it is useful to gain knowledge from comparison. Therefore Chapter 3 is devoted to the revision of finite-temperature field theory and the transport and constraint equations are constructed in transport theory. Then the collision term of the transport equation is evaluated for the mean field self-energies in Chapter 4 and for the two loop self-energies in Chapter 5. In Chapter 5, we will in addition address the question as to which propagators should be used for the evaluation of scattering amplitudes - non-equilibrium or $T = 0$ propagators. In Chapter 6, the contributions beyond two loop self-energies to the collision term are considered. We devote Chapter 7 to the cancellation of pinch singularities. First, we demonstrate explicitly their cancellation in equilibrium field theory for several cases. Then we tackle the question whether and how pinch singularities are canceled in non-equilibrium. In Chapter 8, the second evolution equation, the constraint equation, is taken into account. Finally we conclude in Chapter 9. Wigner transforms are listed in Appendix A for completeness. Appendix B shows explicit calculations of color factors for two loop self-energies.

Chapter 2

Model of scalar quarks and gluons

In this chapter, we introduce and discuss the scalar partonic model, and give the equations of motion for quark and gluon fields. We briefly review high energy scattering within this model.

2.1 Scalar partonic model

We study a partonic model of QCD inspired by Polkinghorne [11] and used by Forshaw and Ross [12] that contains scalar partons. Quarks and antiquarks are described by complex scalar fields ϕ, and gluons as the scalar field χ coupled through the Lagrangian

$$\begin{aligned}\mathcal{L} &= \partial^\mu \phi^{\dagger i,l} \partial_\mu \phi_{i,l} + \frac{1}{2}\partial^\mu \chi_{a,r} \partial_\mu \chi^{a,r} - \frac{m^2}{2}\chi_{a,r}\chi^{a,r} \\ &\quad - gm\phi^{\dagger i,l}(T^a)^j_i (T^r)^m_l \phi_{j,m}\chi_{a,r} - \frac{gm}{3!} f_{abc} f_{rst} \chi^{a,r}\chi^{b,s}\chi^{c,t}. \end{aligned} \tag{2.1}$$

The quark fields are regarded as massless, as one generally assumes for high energy processes, while the gluons are usually assigned a mass m *a priori* in order to avoid infra-red divergences. There is an interaction between quarks and gluons as well as a cubic self-interaction between gluons. Since in QCD the quartic interaction between gluons leads in elastic qq scattering to terms which are sub-leading in $\ln s$, such a quartic interaction among gluons is not included within this model.

One notes that both the quark and gluon fields carry two labels. Both of these refer to color groups. The fact that a direct product of two color groups is necessary can be seen on examining the three gluon vertex term. This term must be symmetric under the exchange of two gluons since they are bosons. In addition, one expects that the interaction vertex should be proportional to the (antisymmetric) structure

constants of the color group. A single color group cannot meet these requirements, and the simplest combination which can is a product of two $SU(N_c)$ groups. Thus the gluon field carries two color indices ($a, r = 1...(N_c^2 - 1)$). Since the quark field transforms in the fundamental representation of both of these $SU(N_c)$ groups, it must carry two color indices as well ($i, l = 1...N_c$). The matrices T^a and T^r are the generators and f_{abc} and f_{rst} are the structure constants for the two $SU(N_c)$ groups respectively. Thus they satisfy

$$[T^a, T^b] = if_{abc}T^c, \qquad [T^r, T^s] = if_{rst}T^t. \tag{2.2}$$

Note in Eq.(2.1) that the flavor index of the quark fields is suppressed.

The equations of motion for the fields can be derived from the Euler-Lagrange equations. They are

$$\Box\phi^{(\dagger)i,l} = -gm(T^a)^i_j(T^r)^l_m\phi^{(\dagger)j,m}\chi_{a,r} \tag{2.3}$$

for the (anti-)quarks and

$$(\Box + m^2)\chi^{a,r} = -gm[\phi^{\dagger i,l}(T^a)^i_j(T^r)^m_l\phi_{j,m} + f^{abc}f^{rst}\chi_{b,s}\chi_{c,t}] \tag{2.4}$$

for the gluons.

2.2 Elastic qq scattering at high energies

The main advantage of this simple partonic model is that a calculation of the elastic quark-quark scattering amplitude at high energies at $T = 0$ reflects pomeron behavior. In this section, we simply quote these results, and for details, we refer the reader to [12]. Note that these calculations are performed in equilibrium and at $T = 0$ in contrast to the rest of this thesis.

Quark-quark scattering is calculated via the exchange of a color singlet. It is assumed that the two quarks emerge from the scattering with the same color with which they entered and that they have different flavors. Therefore one has to consider only diagrams with at least two exchanged gluons, and one can neglect diagrams with quarks that are exchanged in the t-channel. The incoming quarks have momenta p_1 and p_2, respectively. To lowest order, this process is shown in Fig. 2.1. Denoting the transferred momentum as $q = p_1 - p_2$, the Mandelstam variables read as $s = (p_1 + p_2)^2$ and $t = q^2$. In the case of Fig. 2.1, it is easy to show that Fig. 2.1 (b) follows from Fig. 2.1 (a) only by a kinematical transformation, so that it is only

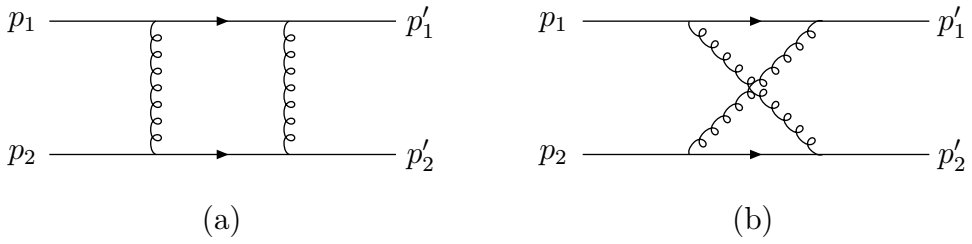

Figure 2.1: Leading order contribution to Pomeron exchange for elastic quark-quark scattering.

necessary to calculate graphs of type (a). The imaginary part of the amplitude can be identified according to the Cutkosky rules [13] to be

$$\Im\mathcal{A}_{2.1(a)} = \frac{1}{2}\int d(P.S.^2)\,\mathcal{A}_0^{(g)}(k)\,\mathcal{A}_0^{(g)\dagger}(k-g), \tag{2.5}$$

where $\mathcal{A}_0^{(g)}$ is the tree amplitude for single gluon exchange and reads as

$$\mathcal{A}_0^{(g)}(k) = -g^2m^2\,\frac{1}{(k^2-m^2)} \tag{2.6}$$

up to a color factor. $\int d(P.S.^2)$ refers to the phase space of the two lines which are cut, i.e.

$$\int d(P.S.^2) = \int \frac{d^4l}{(2\pi)^3}\,\frac{d^4l'}{(2\pi)^3}\,\delta(l^2)\,\delta(l'^2)\,(2\pi)^4\,\delta^4(p_1+p_2-l-l'). \tag{2.7}$$

One integration can be immediately performed, leaving one further integral over the momentum k of the exchanged gluon as

$$\int d(P.S.^2) = \frac{1}{(2\pi)^2}\int d^4k\,\delta((p_1-k)^2)\,\delta((p_2+k)^2). \tag{2.8}$$

The further calculations are now performed in the center-of-mass frame in which the incoming quarks are considered to be along the z-axis, i.e.

$$p_{1/2} = \left(\frac{\sqrt{s}}{2}, \pm\frac{\sqrt{s}}{2}, \mathbf{0}\right). \tag{2.9}$$

Then it is useful to parametrize the integrated momenta k in terms of Sudakov parameters ρ and λ:

$$k = \rho p_1 + \lambda p_2 + k_\perp = \left((\rho+\lambda)\frac{\sqrt{s}}{2}, (\rho-\lambda)\frac{\sqrt{s}}{2}, \mathbf{k}\right), \tag{2.10}$$

where $k_\perp$ is the momentum transverse to p_1 and p_2 and this two-dimensional vector is represented by the boldface $\mathbf{k}$. Then the phase space becomes

$$\int d(P.S.^2) = \frac{s}{8\pi^2} \int d\rho \, d\lambda \, d^2\mathbf{k} \, \delta(-s(1-\rho)\lambda - \mathbf{k}^2) \, \delta(s(1+\lambda)\rho - \mathbf{k}^2) \tag{2.11}$$

where $s = 2p_1p_2$ was used. In the Regge limit $s \gg |t|$ the momentum transferred q is dominated by its transverse component, i.e.

$$t = q^2 \approx -\mathbf{q}^2. \tag{2.12}$$

Similarly one finds

$$k^2 \approx -\mathbf{k}^2 \tag{2.13}$$

and

$$(k-q)^2 \approx -(\mathbf{k}-\mathbf{q})^2. \tag{2.14}$$

Performing the integration over ρ and λ, one finds for the imaginary part of the amplitude

$$\Im\mathcal{A}_{2.1(a)} = \frac{(N_c^2-1)^2}{16N_c^4} \frac{g^4m^4}{16\pi^2 s} \int d^2\mathbf{k} \, \frac{1}{\mathbf{k}^2+m^2} \, \frac{1}{(\mathbf{k}-\mathbf{q})^2+m^2} \tag{2.15}$$

where the color factor has been included.

One expects now to obtain leading $\ln s$ contributions for the scattering amplitude because the calculations are performed in the Regge limit. s/t is negative and therefore the relation

$$\ln\left(\frac{s}{t}\right) = \ln\left(\frac{s}{|t|}\right) - i\pi \tag{2.16}$$

holds. Since $\mathcal{A}_{2.1(a)}$ has an imaginary part, its real part must have a logarithm with equal coefficient but opposite sign. The contribution of Fig. 2.1 (a) is thus proportional to

$$\frac{1}{s}\left(\ln\left(\frac{s}{|t|}\right) - i\pi\right). \tag{2.17}$$

In order to obtain the contribution from Fig. 2.1 (b) the Mandelstam variable s is replaced by u. Since u/t is positive, this diagram has no imaginary part. Therefore its contribution reads

$$\frac{1}{u}\ln\left(\frac{u}{t}\right). \tag{2.18}$$

In the Regge limit $u \approx -s$. Therefore the logarithms in $\mathcal{A}_{2.1} = \mathcal{A}_{2.1(a)} + \mathcal{A}_{2.1(b)}$ cancel and we are left with the imaginary part of $\mathcal{A}_{2.1(a)}$ given in Eq.(2.15).

The higher order calculations are tedious and we therefore state only the results.

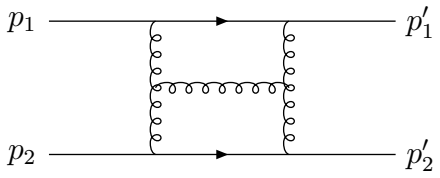

Figure 2.2: One-rung ladder diagram.

The next-to-leading order contribution is given by the so-called one-rung ladder diagram shown in Fig. 2.2. Its contribution is of order $g^2 \ln s$ relative to the leading contribution calculated above. The other three gluon diagrams like vertex correction diagrams or a digram with three exchanged gluons are subleading and therefore neglected.

This result can be generalized. Thus the order $(g^2 \ln s)^n$ correction to the leading order contribution is given by the n-rung uncrossed ladder diagram, $n = 1...\infty$, as shown in Fig. 2.3. The dashed line indicates the cut taken for the direct application

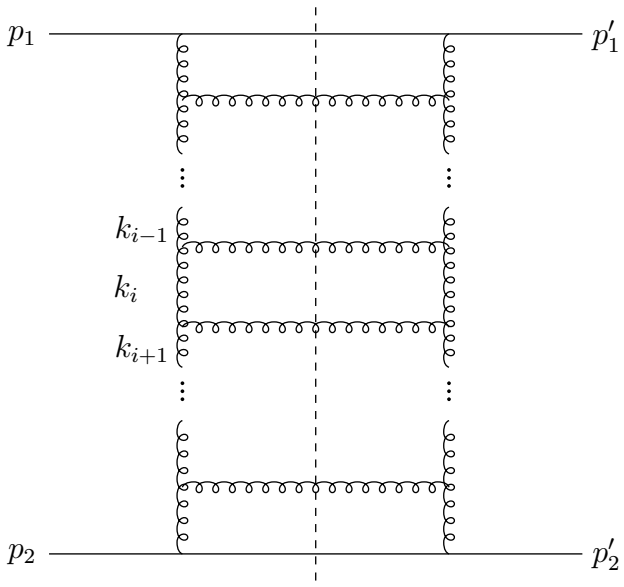

Figure 2.3: n-rung ladder diagram with cut line (dashed line).

of the Cutkosky rules. Applying these rules and keeping only the leading $\ln s$ contributions in evaluating the infinite sum of uncrossed ladder diagrams, one obtains

the following result for the imaginary part of the scattering amplitude

$$\Im\mathcal{A}(s,t) = \frac{(N_c^2-1)^2}{16N_c^4}\frac{g^4m^4}{16\pi^2 s}\int d^2\mathbf{k}\,\frac{1}{(\mathbf{k}^2+m^2)((\mathbf{k}-\mathbf{q})^2+m^2)}\left(\frac{s}{|t|}\right)^{1+\alpha_P(t)}, \quad (2.19)$$

with the trajectory

$$\alpha_P(t) \approx -1 + \frac{g^2N_c^2}{16\pi^2}\left(1+\frac{t}{6m^2}\right). \quad (2.20)$$

In the Regge limit, the real part of $\mathcal{A}(s,t)$ vanishes. Therefore $\mathcal{A}(s,t)$ is purely imaginary and given by Eq.(2.19).

We point out that the selection of ladder diagrams for the evaluation of the scattering amplitude, as indicated in Fig. 2.3 is highly suggestive, particularly with the cut drawn in. One might wish to conclude that (a) gluon production is dominant, and (b) that only ladder type graphs need be considered in constructing gluon emission / absorptive processes. As will be seen in transport theory, however, one finds that (a) is true, having its basis in the $1/N_c$ expansion, but (b) cannot be justified, as it depends on the special kinematical assumptions that are applicable to the quark-quark scattering amplitude, but which do not occur in the self-energy evaluation.

Chapter 3

Field theory in and out of equilibrium

Since processes taking place in heavy ion collisions are most likely to occur out of equilibrium, this chapter is devoted to non-equilibrium field theory, namely to transport theory. As an introduction to and for comparison with non-equilibrium field theory, the first section describes finite-temperature field theory in equilibrium.

3.1 Finite-temperature field theory

In this section, we briefly review the basic ideas of quantum field theory at non-zero temperature in equilibrium (for more details see e.g. [14, 15, 16, 17, 18, 19, 20]). There one can distinguish between two different approaches, the imaginary and the real time formalism (for a comparison of both see e.g. [21]). We will only mention the first one briefly and consider the second one in more detail. The imaginary time formalism was introduced by Matsubara. It provides an elegant and simple way of performing equilibrium calculations via integration in the complex plane. Due to the formal similarities with zero temperature real time field theory, it is simple to identify the correct graphs. This means of calculation is widespread in the theoretical community due to its simplicity. By contrast, development of the real time formalism for finite temperature has been much slower. The reasons for this lie in the technical complexity and difficulties associated with real time formalism that have only recently been resolved or which are currently being addressed. Two famous candidates of the real time formalism are thermo field dynamics and the closed time path method. Especially the latter is important for us since it leads universally to all formalisms and in addition can be generalized to non-equilibrium

cases.

We start now with quantum mechanics: the probability amplitude $F(q',t';q,t)$ of finding a particle at position q' at time t' when it was located at position q at time t is given by

$$F(q',t';q,t) = \langle q' \left| e^{-iH(t'-t)} \right| q \rangle. \tag{3.1}$$

Letting $t \to -i\tau$, we find for the analytical continuation of F to imaginary time

$$F(q',-i\tau';q,-i\tau) = \langle q' \left| e^{-H(\tau'-\tau)} \right| q \rangle. \tag{3.2}$$

In a standard fashion the path integral representation is derived for F as

$$F(q',-i\tau';q,-i\tau) = \int \mathcal{D}q(\tau'') \exp\left\{ -\int_{\tau}^{\tau'} d\tau'' \left[\frac{1}{2} m\dot{q}^2(\tau'') + V(q(\tau'')) \right] \right\} \tag{3.3}$$

with $q(\tau) = q$ and $q(\tau') = q'$. Now we make the connection to quantum statistical mechanics: the partition function is defined as

$$Z(\beta) = \mathrm{Tr} e^{-\beta H} = \int dq \, \langle q \left| e^{-\beta H} \right| q \rangle, \tag{3.4}$$

where $\beta = 1/T$ is the inverse temperature. With the help of Eqs.(3.2) and (3.3), we can express the partition function in terms of a path integral as

$$\begin{aligned} Z(\beta) &= \int dq \, F(q,-i\beta;q,0) \\ &= \int \mathcal{D}q(\tau) \exp\left\{ -\int_0^{\beta} d\tau \left[\frac{1}{2} m\dot{q}^2(\tau) + V(q(\tau)) \right] \right\} \end{aligned} \tag{3.5}$$

with the boundary condition $q(\beta) = q(0)$, i.e. over paths with period β in imaginary time. Now we turn to quantum field theory for a scalar field. The generating functional $Z[\beta;J]$, with $Z(\beta) = Z[\beta;J=0]$, is then given as

$$Z[\beta;J] = \int \mathcal{D}\phi \exp\left\{ i \int_C dt \, \left[\mathcal{L}(\phi) + J(t)\phi(t) \right] \right\}, \tag{3.6}$$

where we have assumed that the Lagrangian does not contain derivative interactions. For simplicity, the spatial coordinates are suppressed in this section. The fields are subject to the (anti-)periodic boundary condition

$$\phi(t - i\beta) = \eta \, e^{\beta\mu} \, \phi(t), \tag{3.7}$$

with the chemical potential μ and $\eta = \pm$ for bosons and fermions respectively. The contour C must end at a point t_f differentiating from the starting point t_i by $-i\beta$:

$$t_f = t_i - i\beta. \tag{3.8}$$

In addition to this requirement, the contour C must have a monotonically decreasing imaginary part. The simplest choice for the contour would be a straight line along the imaginary axis from $t_i = 0$ to $t_f = -i\beta$. This so-called Matsubara contour leads to the imaginary-time formalism (ITF) which we will not consider here any further. Other choices for the contour include the real axis and lead therefore to the real-time formalism. The standard contour is shown in Fig. 3.1. It goes from t_i to $-t_i$ on the

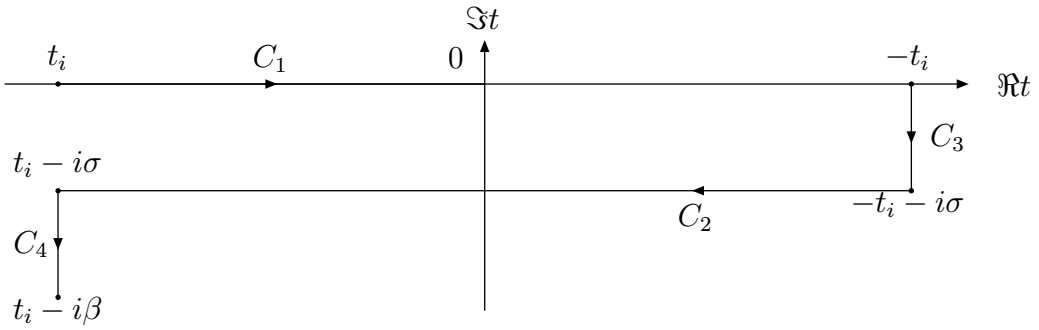

Figure 3.1: Real time contour

real axis, then drops vertically down to $-t_i - i\sigma$, runs parallel to the real axis back to $t_i - i\sigma$ and finally down to $t_i - i\beta$. Here the parameter σ takes a value between 0 and β. One assumes that in the limit $t_i \to -\infty$ the vertical segments of the contour C decouple in the path integral and do not contribute to Green functions with time arguments on the horizontal segments.

Writing the fields on the upper and the lower horizontal segments as functions of real times, $\phi_-(t) = \phi(t)$ and $\phi_+(t) = \phi(t - i\sigma)$, respectively, the generating functional for the Green functions reads as

$$Z[J_-, J_+] = Z[0,0]\langle T_C \exp\left\{ i \int_{-\infty}^{\infty} dt\, \phi_s J_s \right\}\rangle, \tag{3.9}$$

where the sign index s runs over $\{-, +\}$ and $J_-(t)$ is defined to be the source on the upper segment and $J_+(t) = -J(t - i\sigma)$ the source on the lower one. The minus sign in the latter absorbs the minus sign from the opposite direction of the lower contour. Note, that in our notation the '-' sign is associated with the upper branch as in [23] and in contrast to [16]. In the 80's, the '-' fields were termed physical fields according to the idea that physical observables would be expressible in terms of Green functions with only '-' fields on the external legs. The '+' fields were consistently called ghost fields. This is not a valid supposition. As a simple example, the mass term Π^R is made up of both Π^{--} and Π^{-+}, see Eq.(3.45). There are also other interesting physical quantities with '+' fields on their external legs, see e.g. the collision term of Eq.(3.58).

Differentiation with respect to $J_-(t)$ and $J_+(t)$ then gives the real-time Green functions

$$G_\sigma^{s_1\ldots s_N}(t_1,\ldots t_N) := \left.\frac{\delta_{iJ_{s_1}(t_1)}\ldots\delta_{iJ_{s_N}(t_N)}\,Z[J_-,J_+]}{Z[J_-,J_+]}\right|_{J_-=0,J_+=0}. \tag{3.10}$$

The contour ordering T_C implies that this real-time Green function is the thermal average of a product of field operators where the ordering is such that the '-' fields are time-ordered and put on the right hand side and the '+' fields are anti-time-ordered and put on the left hand side. Performing a Fourier transform

$$G_\sigma^{s_1\ldots s_N}(\omega_1,\ldots,\omega_N) := \int dt_1\ldots dt_N\,\exp\left\{i\sum_i \omega_i\,t_i\right\}\,G^\sigma_{s_1\ldots s_N}(t_1,\ldots,t_N) \tag{3.11}$$

yields the relation between Green functions with different values of σ,

$$G_\sigma^{s_1\ldots s_N}(\omega_1,\ldots,\omega_N) = \exp\left\{-\sum_{i|s_i=+}\sigma\,\omega_i\right\}\,G_{\sigma=0}^{s_1\ldots s_N}(\omega_1,\ldots,\omega_N). \tag{3.12}$$

Note that the value $\sigma = 0$ corresponds to a closed time path (CTP) or Schwinger-Keldysh formalism, see Fig. 3.2, while $\sigma = \beta/2$ corresponds to the choice for Thermo Field Dynamics.

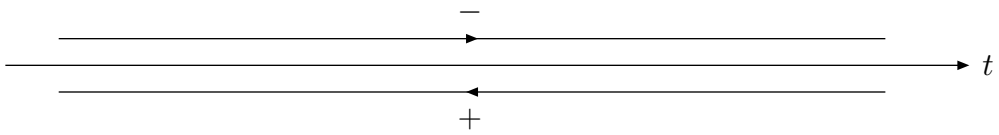

Figure 3.2: Closed time path

There are two important relations which connect the Green functions for a given σ. The first one is the so-called *largest-time relation*. For its derivation we set $\sigma = 0$. Let the time t_j be the largest one, i.e. $t_j > t_i$, $i = 1,\ldots,j-1,j+1,\ldots N$. Then we find

$$\begin{aligned}
&G_{\sigma=0}^{s_1\ldots-\ldots s_N}(t_1,\ldots,t_j,\ldots t_N) - G_{\sigma=0}^{s_1\ldots+\ldots s_N}(t_1,\ldots,t_j,\ldots t_N)\\
&= \mathrm{sgn}P\left\{\langle\tilde{T}(\phi_+\ldots\phi_+)\,[\phi(t_j)T(\phi_-\ldots\phi_-)]\rangle - \langle\left[\tilde{T}(\phi_+\ldots\phi_+)\phi(t_j)\right]T(\phi_-\ldots\phi_-)\rangle\right\}\\
&= 0.
\end{aligned} \tag{3.13}$$

Here $\mathrm{sgn}P$ gives the sign associated with the permutation that is needed to put the fields in the right order. So far, the s_i for $i \neq j$ were arbitrary. Therefore we can

sum over all possibilities for the s_i's with appropriate sign factors to get

$$\sum_{s_1,...,s_N} (-1)^{\#(i|s_i=+)}\, G_{\sigma=0}^{s_1...s_N}(t_1,...,t_N) = 0, \tag{3.14}$$

where $\#(i|s_i=+)$ denotes the number of indices i for which $s_i = +$. This is the largest-time equation although the special role of the largest time t_j is not manifest any more. Fourier transformation and Eq.(3.12) gives a similar relation for arbitrary σ

$$\sum_{s_1,...,s_N} (-1)^{\#(i|s_i=+)} \exp\left\{\sum_{i|s_i=+} \sigma\,\omega_i\right\} G_{\sigma}^{s_1...s_N}(\omega_1,...,\omega_N) = 0. \tag{3.15}$$

It is important to notice that the largest time equation holds true in non-equilibrium situations as well.

Now, the second important relation is the Kubo-Martin-Schwinger (KMS) relation. It is only valid in equilibrium. For its derivation, we consider an alternative contour $\tilde{C}$ which can be obtained form the original one C of Fig. 3.1 with $\sigma = 0$ by flipping it about the $\Im t$-axis. This contour gives rise to different Green functions which satisfy a smallest time equation. These Green functions can be related to the original ones. Fourier transformation and the use of Eq.(3.12) then yields the KMS relation

$$\sum_{s_1,...,s_N} (-1)^{\#(i|s_i=+)} \prod_{i|s_i=+} \eta_i \exp\left\{\sum_{i|s_i=+} -x_i + \sigma\omega_i\right\} G_{\sigma}^{s_1...s_N}(\omega_1,...,\omega_N) = 0, \tag{3.16}$$

where $x_i = \beta(\omega_i - \mu_i)$.

Finally, we state a complex conjugation relation for real-time Green functions

$$[G_{\sigma}^{s_1...s_N}(\omega_1,...,\omega_N)]^* = G_{\sigma}^{\bar{s}_1...\bar{s}_N}(\omega_1,...,\omega_N) \prod_{s_i=+} \eta_i\, e^{x_i - 2\sigma\omega_i}, \tag{3.17}$$

with the conjugate index $\bar{s}_i = +,-$ if $s_i = -,+$.

Since we are ultimately interested in propagators, we consider now the case $N = 2$. The largest-time equation (3.14) then reads

$$D_{\sigma=0}^{--} + D_{\sigma=0}^{++} = D_{\sigma=0}^{-+} + D_{\sigma=0}^{+-}. \tag{3.18}$$

Taking into account momentum conservation ($\omega_1 + \omega_2 = 0$) and charge conservation ($\mu_1 + \mu_2 = 0$), the KMS relation (3.16) gives

$$D_{\sigma=0}^{--} + D_{\sigma=0}^{++} = \eta\, e^{x_1}\, D_{\sigma=0}^{-+} + \eta\, e^{-x_1}\, D_{\sigma=0}^{+-}. \tag{3.19}$$

Subtracting these two equations yields the usual form of the KMS relation for 2-point functions,

$$D_{\sigma=0}^{-+} = \eta\, e^{-x_1}\, D_{\sigma=0}^{+-}. \tag{3.20}$$

From Eq.(3.10) one obtains the real-time propagators as

$$\begin{aligned} iD_\sigma^{--}(t-t') &= \langle T\phi(t)\phi(t')\rangle \\ iD_\sigma^{++}(t-t') &= \langle \tilde{T}\phi(t-i\sigma)\phi(t'-i\sigma)\rangle \\ iD_\sigma^{-+}(t-t') &= \eta\langle\phi(t'-i\sigma)\phi(t)\rangle \\ iD_\sigma^{+-}(t-t') &= \langle\phi(t-i\sigma)\phi(t')\rangle. \end{aligned} \tag{3.21}$$

These four propagators can be written in a compact matrix form as

$$\underline{D}_\sigma = \begin{pmatrix} D_\sigma^{--} & D_\sigma^{-+} \\ D_\sigma^{+-} & D_\sigma^{++} \end{pmatrix}. \tag{3.22}$$

Then performing a Fourier transform yields

$$\begin{aligned} \underline{D}_\sigma(\omega) &= \begin{pmatrix} D_F(\omega) & 0 \\ 0 & -D_F^*(\omega) \end{pmatrix} \\ &+ [D_F(\omega) - D_F^*(\omega)] \begin{pmatrix} \eta n(|\omega|) & e^{\sigma\omega}[\Theta(-\omega)+\eta n(|\omega|)] \\ e^{-\sigma\omega}[\Theta(\omega)+\eta n(|\omega|)] & \eta n(|\omega|) \end{pmatrix}, \end{aligned} \tag{3.23}$$

where iD_F is the zero-temperature Feynman propagator and $n(\omega)$ is the distribution function defined by

$$n(\omega) = \frac{1}{e^{\beta(\omega-\mu)} - \eta}. \tag{3.24}$$

One popular choice is $\sigma = \beta/2$; then the matrix of propagators reads as

$$\begin{aligned} \underline{D}_{\sigma=\beta/2}(\omega) &= \begin{pmatrix} D_F(\omega) & 0 \\ 0 & -D_F^*(\omega) \end{pmatrix} + [D_F(\omega) - D_F^*(\omega)] \\ &\begin{pmatrix} \eta n(|\omega|) & e^{\frac{\beta\mu}{2}}\sqrt{n(|\omega|)}\sqrt{1+\eta n(|\omega|)}[\eta\Theta(\omega)+\Theta(-\omega)] \\ e^{\frac{-\beta\mu}{2}}\sqrt{n(|\omega|)}\sqrt{1+\eta n(|\omega|)}[\Theta(\omega)+\eta\Theta(-\omega)] & \eta n(|\omega|) \end{pmatrix}, \end{aligned} \tag{3.25}$$

where the identity

$$e^{\beta(\omega-\mu)/2} = \Theta(\omega)\sqrt{\frac{1+\eta n(|\omega|)}{n(|\omega|)}} + \Theta(-\omega)\sqrt{\frac{\eta n(|\omega|)}{1+n(|\omega|)}} \tag{3.26}$$

was used. For later use, we give the explicit form of the propagators for bosons ($\eta = +1$) with vanishing chemical potential ($\mu = 0$). With the Feynman propagator for a scalar particle,

$$iD_F(\omega) = \frac{i}{\omega^2 - E^2 + i\epsilon}, \tag{3.27}$$

and the relation

$$\frac{\pm i}{\omega^2 - E^2 \pm i\epsilon} = \mathrm{P}\frac{\pm i}{\omega^2 - E^2} + \pi\delta(\omega^2 - E^2), \tag{3.28}$$

where P denotes the principal value, we find

$$iD_F(\omega) - iD_F^*(\omega) = 2\pi\delta(\omega^2 - E^2) = \frac{\pi}{E}\left[\delta(\omega - E) + \delta(\omega + E)\right]. \tag{3.29}$$

This gives for $\sigma = \beta/2$

$$i\underline{D}_{\sigma=\beta/2}(\omega) = \begin{pmatrix} \frac{i}{\omega^2-E^2+i\epsilon} & 0 \\ 0 & \frac{-i}{\omega^2-E^2-i\epsilon} \end{pmatrix} + \frac{2\pi\delta(\omega^2-E^2)}{e^{\beta|\omega|}-1}\begin{pmatrix} 1 & e^{\beta|\omega|/2} \\ e^{\beta|\omega|/2} & 1 \end{pmatrix}. \tag{3.30}$$

Another popular choice is $\sigma = 0$. For scalar particles with vanishing chemical potential the matrix of propagators reads as

$$\begin{aligned} i\underline{D}_{\sigma=0}(\omega) &= \begin{pmatrix} \frac{i}{\omega^2-E^2+i\epsilon} & 0 \\ 0 & \frac{-i}{\omega^2-E^2-i\epsilon} \end{pmatrix} \\ &+ \begin{pmatrix} 2\pi\delta(\omega^2-E^2)n(|\omega|) & \frac{\pi}{E}\left[\delta(E-\omega)n(|\omega|) + \delta(E+\omega)(1+n(|\omega|))\right] \\ \frac{\pi}{E}\left[\delta(E-\omega)n(|\omega|) + \delta(E+\omega)(1+n(|\omega|))\right] & 2\pi\delta(p^2-m^2)n(|\omega|) \end{pmatrix}. \end{aligned} \tag{3.31}$$

The four propagators are not independent, since they fulfill Eqs.(3.18) and (3.20). Therefore it is possible to transform the matrix such that at least one component is vanishing. For a review of possible transformations see e.g. Ref. [22].

We now return to the general expression of $\underline{D}_\sigma(\omega)$ in Eq.(3.23). In the vacuum limit $\mu \to 0$ and $\beta \to \infty$, the usual zero-temperature field theory should be regained. In this limit, the distribution function $n(|\omega|)$ vanishes and we are left with

$$i\underline{D}_\sigma(\omega) = \begin{pmatrix} iD_F(\omega) & 0 \\ 0 & iD_F^*(\omega) \end{pmatrix} + \left[D_F(\omega) - D_F^*(\omega)\right]\begin{pmatrix} 0 & e^{\sigma\omega}\Theta(-\omega) \\ e^{-\sigma\omega}\Theta(\omega) & 0 \end{pmatrix}. \tag{3.32}$$

In addition to this we perform the limit $\sigma \to \infty$ which is e.g. for the choice $\sigma = \beta/2$ automatically fulfilled. This gives

$$i\underline{D}_\infty(\omega) = \begin{pmatrix} iD_F(\omega) & 0 \\ 0 & iD_F^*(\omega) \end{pmatrix}, \tag{3.33}$$

i.e. one has two identical decoupled copies of zero-temperature field theory as expected.

The real-time Feynman rules are much the same as in zero-temperature field theory. The only difference is that a sign factor $s = -, +$ is assigned to each

vertex. For Green functions and self-energies, the external vertices are fixed, and all internal vertices are summed over (which multiplies the number of graphs, see e.g. Fig. 5.2). A vertex with $s = -$ corresponds to a factor $-igm$ while a vertex with $s = +$ corresponds to a factor $+igm$. (In order to introduce a dimensionless coupling constant g, a mass m is factored out.) A line connecting a vertex s with a vertex s' corresponds to a propagator $D_\sigma^{ss'}$ given in Eq.(3.21).

An example of a scattering amplitude is shown in Fig. 5.5. The external vertices are fixed to be $s = -$ while the internal vertices can be either '-' or '+' and one has to draw all possibilities. The complex conjugate of such an amplitude (*in position space*) is obtained by interchanging all '-' vertices with '+' vertices and vice versa in the original amplitude.

The CTP formalism corresponding to the choice $\sigma = 0$ is now easily generalized for non-equilibrium processes. This is the subject of the next section.

3.2 Transport theory

In this section, we briefly introduce the Schwinger-Keldysh formalism and the quasi-particle approximation. For the purpose of establishing our notation, we give the basic definitions and refer the reader to standard texts [23, 24, 25]. Then we derive the so-called transport and constraint equations following the lines of [26, 27, 28, 4]. While the last section was quite general, we refer in this section only to the cases that are relevant for us, i.e. for scalar quarks and scalar gluons ($\eta = +1$ and $\mu = 0$). The quark Green functions in the Schwinger-Keldysh formalism [7, 8] are defined through their average over operator products,

$$\begin{aligned}
iS^c(x,y) = &\left\langle T\phi^{i,l}(x)\phi^{\dagger j,m}(y)\right\rangle - \left\langle \phi^{i,l}(x)\right\rangle \left\langle \phi^{\dagger j,m}(y)\right\rangle &= iS^{--}(x,y)\\
iS^a(x,y) = &\left\langle \tilde{T}\phi^{i,l}(x)\phi^{\dagger j,m}(y)\right\rangle - \left\langle \phi^{i,l}(x)\right\rangle \left\langle \phi^{\dagger j,m}(y)\right\rangle &= iS^{++}(x,y)\\
iS^>(x,y) = &\left\langle \phi^{i,l}(x)\phi^{\dagger j,m}(y)\right\rangle - \left\langle \phi^{i,l}(x)\right\rangle \left\langle \phi^{\dagger j,m}(y)\right\rangle &= iS^{+-}(x,y)\\
iS^<(x,y) = &\left\langle \phi^{\dagger j,m}(y)\phi^{i,l}(x)\right\rangle - \left\langle \phi^{i,l}(x)\right\rangle \left\langle \phi^{\dagger j,m}(y)\right\rangle &= iS^{-+}(x,y) \quad (3.34)
\end{aligned}$$

and for the gluons as

$$\begin{aligned}
iG^c(x,y) = &\left\langle T\chi^{a,r}(x)\chi^{b,s}(y)\right\rangle - \left\langle \chi^{a,r}(x)\right\rangle \left\langle \chi^{b,s}(y)\right\rangle &= iG^{--}(x,y)\\
iG^a(x,y) = &\left\langle \tilde{T}\chi^{a,r}(x)\chi^{b,s}(y)\right\rangle - \left\langle \chi^{a,r}(x)\right\rangle \left\langle \chi^{b,s}(y)\right\rangle &= iG^{++}(x,y)\\
iG^>(x,y) = &\left\langle \chi^{a,r}(x)\chi^{b,s}(y)\right\rangle - \left\langle \chi^{a,r}(x)\right\rangle \left\langle \chi^{b,s}(y)\right\rangle &= iG^{+-}(x,y)\\
iG^<(x,y) = &\left\langle \chi^{b,s}(y)\chi^{a,r}(x)\right\rangle - \left\langle \chi^{a,r}(x)\right\rangle \left\langle \chi^{b,s}(y)\right\rangle &= iG^{-+}(x,y). \quad (3.35)
\end{aligned}$$

Here T and $\tilde{T}$ are the usual time and anti-time ordering operators respectively. As given, the Green functions fall along the contour designated in Fig. 3.2. Our sign convention follows that of Ref.[23]. Using a generic notation $D = S$ or G as appropriate, we summarize the Green functions in a compact matrix form as

$$\underline{D} = \begin{pmatrix} D^{--} & D^{-+} \\ D^{+-} & D^{++} \end{pmatrix}. \tag{3.36}$$

From the definition of the Green functions follows

$$\left[iD^{--}(x,y)\right]^\dagger = iD^{++}(x,y), \tag{3.37}$$

while $iD^{\pm\mp}$ is hermitian (e.g. $[iD^{-+}(x,y)]^\dagger = iD^{+-}(x,y)$), and the largest time equation (3.14) becomes,

$$D^{--}(x,y) + D^{++}(x,y) = D^{-+}(x,y) + D^{+-}(x,y), \tag{3.38}$$

demonstrating that the four components D^{ij} are not independent. We define the retarded and advanced Green functions in the standard way as

$$\begin{aligned} D^R(x,y) &:= \Theta(x_0 - y_0)[D^{+-}(x,y) - D^{-+}(x,y)] \\ &= D^{--}(x,y) - D^{-+}(x,y) = D^{+-}(x,y) - D^{++}(x,y) \qquad (3.39) \\ D^A(x,y) &:= -\Theta(y_0 - x_0)[D^{+-}(x,y) - D^{-+}(x,y)] \\ &= D^{--}(x,y) - D^{+-}(x,y) = D^{-+}(x,y) - D^{++}(x,y). \qquad (3.40) \end{aligned}$$

The Green functions defined in Eqs.(3.34) and (3.35) satisfy a Dyson equation that introduces the matrix of self-energies for either the quark or gluonic sectors, $\underline{\Sigma}_q$ or $\underline{\Sigma}_g$. Using a generic notation, $\underline{\Pi} = \underline{\Sigma}_q$ or $\underline{\Sigma}_g$ as appropriate, one may write

$$\begin{aligned} \underline{D}(x,y) &= \underline{D}^0(x,y) - \int d^4z d^4w \underline{D}^0(x,w)\underline{\Pi}(w,z)\underline{D}(z,y) \\ &= \underline{D}^0(x,y) - \int d^4z d^4w \underline{D}(x,w)\underline{\Pi}(w,z)\underline{D}^0(z,y), \end{aligned} \tag{3.41}$$

given in terms of the irreducible proper self-energy

$$\underline{\Pi} = \begin{pmatrix} \Pi^{--} & \Pi^{-+} \\ \Pi^{+-} & \Pi^{++} \end{pmatrix}. \tag{3.42}$$

The four components of the self-energy are also not independent. From their definition, the relation

$$\Pi^{--}(x,y) + \Pi^{++}(x,y) = -(\Pi^{+-}(x,y) + \Pi^{-+}(x,y)) \tag{3.43}$$

can be seen to hold. The off-diagonal components are again hermitian, while the diagonal ones fulfill

$$\left[i\Pi^{--}(x,y)\right]^\dagger = i\Pi^{++}(x,y). \tag{3.44}$$

The retarded and advanced self-energies are defined to be

$$\Pi^R(x,y) = \Pi^{--}(x,y) + \Pi^{-+}(x,y) \tag{3.45}$$
$$\Pi^A(x,y) = \Pi^{--}(x,y) + \Pi^{+-}(x,y). \tag{3.46}$$

The equations of motion that the Green functions satisfy are

$$(\Box_x + M^2)\underline{D}(x,y) = -\underline{\sigma}_z\delta^{(4)}(x-y) + \int d^4z\, \underline{\sigma}_z\, \underline{\Pi}(x,z)\underline{D}(z,y), \tag{3.47}$$

where

$$\underline{\sigma}_z = \begin{pmatrix} 1 & 0 \\ 0 & -1 \end{pmatrix} \tag{3.48}$$

and M is a generic parton mass, $M = m$ for gluons and $M = 0$ for quarks. We now consider specifically the equation of motion for D^{-+}. This reads

$$\begin{aligned}(\Box_x + M^2)D^{-+}(x,y) &= \int d^4z\{\Pi^{--}(x,z)D^{-+}(z,y) + \Pi^{-+}(x,z)D^{++}(z,y)\} \\ &= \int d^4z\{\Pi^A(x,z)D^{-+}(z,y) - \Pi^{+-}(x,z)D^{-+}(z,y) \\ &\quad +\Pi^{-+}(x,z)D^{+-}(z,y) - \Pi^{-+}(x,z)D^R(z,y)\}\end{aligned} \tag{3.49}$$

while the conjugate equation is

$$\begin{aligned}(\Box_y + M^2)D^{-+}(x,y) &= -\int d^4z\{D^{-+}(x,z)\Pi^{++}(z,y) + D^{--}(x,z)\Pi^{-+}(z,y)\} \\ &= \int d^4z\{D^{-+}(x,z)\Pi^A(z,y) - D^R(x,z)\Pi^{-+}(z,y)\},\end{aligned} \tag{3.50}$$

where $D^{-+}(x,y)^\dagger = -D^{-+}(y,x)$ was used. In the second step the diagonal elements of the Green functions and the self-energies were replaced via Eq.(3.39) and (3.46). Moving to the center-of-mass variable $X = (x+y)/2$ and the relative variable $u = x-y$, a Fourier transformation with respect to the latter, or Wigner transformation,

$$D(X,p) = \int d^4u\, e^{ipu}\, D\left(X + \frac{u}{2}, X - \frac{u}{2}\right), \tag{3.51}$$

is then performed on the above two equations to yield

$$\begin{aligned}&\left[\frac{1}{4}\Box_X - ip\partial_X - p^2 + M^2\right] D^{-+}(X,p) \\ &= \Pi^A(X,p)\hat{\Lambda}D^{-+}(X,p) - \Pi^{+-}(X,p)\hat{\Lambda}D^{-+}(X,p) \\ &+\Pi^{-+}(X,p)\hat{\Lambda}D^{+-}(X,p) - \Pi^{-+}(X,p)\hat{\Lambda}D^R(X,p)\end{aligned} \tag{3.52}$$

and

$$\left[\frac{1}{4}\Box_X + ip\partial_X - p^2 + M^2\right] D^{-+}(X,p) = D^{-+}(X,p)\hat{\Lambda}\Pi^A(X,p) - D^R(X,p)\hat{\Lambda}\Pi^{-+}(X,p), \tag{3.53}$$

with the differential operator

$$\hat{\Lambda} := \exp\left\{\frac{-i}{2}\left(\overleftarrow{\partial_X}\,\overrightarrow{\partial_p} - \overleftarrow{\partial_p}\,\overrightarrow{\partial_X}\right)\right\}. \tag{3.54}$$

The details of the Wigner transformations are listed in Appendix A. The difference or sum of Eq.(3.52) and Eq.(3.53) gives the so-called transport and constraint equation, respectively,

$$\boxed{\begin{array}{rcll} -2ip\partial_X D^{-+}(X,p) & = & I_- & \text{transport} \\ \left(\frac{1}{2}\Box_X - 2p^2 + 2M^2\right) D^{-+}(X,p) & = & I_+ & \text{constraint} \end{array}} \tag{3.55, 3.56}$$

Here, $I_\mp$ is an abbreviation for the combined functions

$$I_\mp = I_{\rm coll} + I^A_\mp + I^R_\mp, \tag{3.57}$$

and $I_{\rm coll}$ is the collision term,

$$\begin{aligned} I_{\rm coll} &= \Pi^{-+}(X,p)\hat{\Lambda}D^{+-}(X,p) - \Pi^{+-}(X,p)\hat{\Lambda}D^{-+}(X,p) \\ &= I^{\rm gain}_{\rm coll} - I^{\rm loss}_{\rm coll}. \end{aligned} \tag{3.58}$$

$I^R_\mp$ and $I^A_\mp$ are terms containing retarded and advanced components respectively,

$$I^R_\mp = -\Pi^{-+}(X,p)\hat{\Lambda}D^R(X,p) \pm D^R(X,p)\hat{\Lambda}\Pi^{-+}(X,p) \tag{3.59}$$

and

$$I^A_\mp = \Pi^A(X,p)\hat{\Lambda}D^{-+}(X,p) \mp D^{-+}(X,p)\hat{\Lambda}\Pi^A(X,p). \tag{3.60}$$

In order to solve the Eqs.(3.55) and (3.56), we have to calculate the self-energies Π that occur in Eqs.(3.58) to (3.60). The simplest possible approximation is the so-called quasiparticle approximation, in which a *free* scalar parton of mass M is assigned the Green functions

$$iD^{-+}(X,p) = \frac{\pi}{E_p}\{\delta(E_p - p^0)f_a(X,p) + \delta(E_p + p^0)\bar{f}_{\bar{a}}(X,-p)\} \tag{3.61}$$

$$iD^{+-}(X,p) = \frac{\pi}{E_p}\{\delta(E_p - p^0)\bar{f}_a(X,p) + \delta(E_p + p^0)f_{\bar{a}}(X,-p)\} \tag{3.62}$$

$$iD^{--}(X,p) = \frac{i}{p^2 - M^2 + i\epsilon} + \Theta(-p^0)iD^{+-}(X,p) + \Theta(p^0)iD^{-+}(X,p)$$

$$= \frac{i}{p^2 - M^2 + i\epsilon} + \frac{\pi}{E_p}\{\delta(E_p - p^0) f_a(X,p) + \delta(E_p + p^0) f_{\bar{a}}(X,-p)\} \tag{3.63}$$

$$iD^{++}(X,p) = \frac{-i}{p^2 - M^2 - i\epsilon} + \Theta(-p^0) iD^{+-}(X,p) + \Theta(p^0) iD^{-+}(X,p)$$
$$= \frac{-i}{p^2 - M^2 - i\epsilon} + \frac{\pi}{E_p}\{\delta(E_p - p^0) f_a(X,p) + \delta(E_p + p^0) f_{\bar{a}}(X,-p)\} \tag{3.64}$$

with $E_p^2 = p^2 + M^2$, and which are given in terms of the corresponding scalar quark and gluon distribution function, $f_a(X,p)$, and $\bar{f}_a = 1 + f_a$, where a denotes the parton type $a = q, g$ while $\bar{a}$ the antiparton type. These expressions for the Green functions are formally the same as for $\underline{D}_{\sigma=0}$ of Eq.(3.31). The only difference lies in the fact that here f_a and$f_{\bar{a}}$ are unknown functions while in equilibrium both are the Bose-Einstein distribution.

Our task is now to construct an equation for the distribution functions for quarks and gluons $f_a(X,p)$ from Eqs.(3.55) to (3.60), using the quasiparticle Green functions of the form given in Eqs.(3.61) to (3.64). To do so, it is necessary to integrate the entire Eq.(3.55) and Eq.(3.56) over an interval $\Delta_\pm$ which contains $\pm E_p(X)$. To lowest order in the gradient expansion that sets $\hat{\Lambda} = 1$, the terms $I_\pm^{R,A}$ simplify considerably. In particular

$$I_-^{R,A} = 0 \tag{3.65}$$

so that I_- in Eqs.(3.55) and (3.57) becomes

$$I_- = I_{\rm coll}. \tag{3.66}$$

The integration of Eq. (3.55) over $\Delta_\pm$ requires a construction of the form

$$J_{\rm coll} = J_{\rm coll}^{\rm gain} - J_{\rm coll}^{\rm loss}$$
$$= \int_{\Delta^+} dp_0\, I_{\rm coll}^{\rm gain} - \int_{\Delta^+} dp_0\, I_{\rm coll}^{\rm loss} \tag{3.67}$$

for the right hand side. This integral can be easily performed, and one has

$$J_{\rm coll} = \int_{\Delta^+} dp_0\, \Pi^{-+}(X,p)\, D^{+-}(X,p) - \int_{\Delta^+} dp_0\, \Pi^{+-}(X,p)\, D^{-+}(X,p)$$
$$= -i\frac{\pi}{E_p}\, \Pi^{-+}(X, p_0 = E_p, \vec{p})\, \bar{f}_a(X,\vec{p}) + i\frac{\pi}{E_p}\, \Pi^{+-}(X, p_0 = E_p, \vec{p})\, f_a(X,\vec{p}), \tag{3.68}$$

i.e. the off-diagonal quasiparticle self-energies are required to be calculated on-shell. Thus the complete transport equation reads

$$\boxed{2p\partial_X f_a(X,\vec{p}) = i\Pi^{-+}(X,\vec{p})\, \bar{f}_a(X,\vec{p}) - i\Pi^{+-}(X,\vec{p})\, f_a(X,\vec{p})} \tag{3.69}$$

This is the main result in this section and we will evaluate it in the next chapter.

In the same approximation, i.e. setting $\hat{\Lambda} = 1$ and neglecting the term proportional to $\Box_X$, the constraint equation takes the form

$$\begin{aligned}&\left[-2p^2 + 2M^2 - 2\Pi^A(X,p)\right] D^{-+}(X,p) \\ &= \Pi^{-+}(X,p)\, D^{+-}(X,p) - \Pi^{+-}(X,p)\, D^{-+}(X,p) - 2\Pi^{-+}(X,p)\, D^R(X,p). \end{aligned} \tag{3.70}$$

It will be simplified and evaluated in Chapter 8.

Here and throughout this thesis, we work with the Green functions D^{ij} $(i,j = -,+)$ since they are needed to calculate properties like the self-energy in a diagrammatic expansion. But sometimes it is useful to choose another representation for $\underline{D}$. Since the four components of $\underline{D}$ as given in Eq.(3.36) are not independent of each other, it is possible to transform this matrix so that at least one component vanishes. One possible choice is

$$\underline{D}' = U^{-1}\, \underline{D}\, U = \begin{pmatrix} 0 & D^A \\ D^R & F \end{pmatrix} \tag{3.71}$$

with the transformation matrix

$$U = \frac{1}{\sqrt{2}} \begin{pmatrix} 1 & 1 \\ -1 & 1 \end{pmatrix}. \tag{3.72}$$

D^R and D^A are given in Eqs.(3.39) and (3.40), respectively, and F is defined as $F = D^{--} + D^{++}$. The same transformation gives for the self-energy

$$\underline{\Pi}' = U^{-1}\, \underline{\Pi}\, U = \begin{pmatrix} \Omega & \Pi^R \\ \Pi^A & 0 \end{pmatrix}, \tag{3.73}$$

where Π^R and Π^A are defined in Eqs.(3.45) and (3.46), respectively, and Ω is given as $\Omega = \Pi^{--} + \Pi^{++}$. The equation of motion (3.47) transforms to

$$(\Box_x + M^2)\underline{D}'(x,y) = -\underline{\sigma}_x \delta^{(4)}(x-y) + \int d^4z\, \underline{\sigma}_x\, \underline{\Pi}'(x,z)\underline{D}'(z,y), \tag{3.74}$$

with

$$\underline{\sigma}_x = \begin{pmatrix} 0 & 1 \\ 1 & 0 \end{pmatrix}. \tag{3.75}$$

Performing a Wigner transformation as above gives

$$\begin{aligned}&\left[\frac{1}{4}\Box_X - ip\partial_X - p^2 + M^2\right] \begin{pmatrix} 0 & D^A(X,p) \\ D^R(X,p) & F(X,p) \end{pmatrix} \\ &= \begin{pmatrix} 0 & \Pi^A(X,p)\,\hat{\Lambda}\, D^A(X,p) - 1 \\ \Pi^R(X,p)\,\hat{\Lambda}\, D^R(X,p) - 1 & \Omega(X,p)\,\hat{\Lambda}\, D^A(X,p) + \Pi^R(X,p)\,\hat{\Lambda}\, F(X,p) \end{pmatrix}. \end{aligned} \tag{3.76}$$

In a semiclassical expansion, $\hat{\Lambda} = 1$ and the derivatives with respect to X in the bracket on the left hand side are neglected. Then the equation for D^R can be solved easily to yield

$$D^R(X,p) = \frac{1}{p^2 - M^2 + \Pi^R(X,p)}. \tag{3.77}$$

Similar, one finds

$$D^A(X,p) = \frac{1}{p^2 - M^2 + \Pi^A(X,p)}, \tag{3.78}$$

which is just the hermitian conjugate of Eq.(3.77) and therefore contains no additional information. In Chapter 8, these expressions for D^R and D^A will be used.

Chapter 4

The collision integral - mean field self-energies

In the last section, we found in the quasiparticle approximation for the transport equation (3.69)

$$\boxed{2p\partial_X f_a(X,\vec{p}) = i\Pi^{-+}(X,\vec{p})\,\bar{f}_a(X,\vec{p}) - i\Pi^{+-}(X,\vec{p})\,f_a(X,\vec{p}).} \tag{4.1}$$

Let us now examine it further. Since the number of particles can only be changed via collisions, the right hand side of Eq.(4.1) is called collision term. The second term of the right hand side is proportional to f_a and is therefore identified as the loss term [26], while the first one, proportional to $\bar{f}_a = 1 + f_a$, is identified as the gain term. Naturally, one would expect that it should always be possible to express the collision term in terms of differential scattering cross sections as occurs in the Boltzmann equation when only two body processes are present, or alternatively in terms of transition matrix elements.

Several authors have followed this line of thought: for some simple scalar models [29] and the NJL model [6], which contain only a simple form of interaction, it has been shown rigorously that the theoretical generalization of the non-relativistic formalism indeed leads to the relativistic Boltzmann equation with two body scattering. Particularly within QCD and quark-gluon dynamics, however this generalization is far more difficult. Ref. [3] also attempts a formal identification of the Boltzmann equation from quark-gluon dynamics to the two body scattering level in the Keldysh formalism. This derivation is however in itself at the two-body level theoretically incomplete. Furthermore, the two-body level is insufficient for the description of the complex type of processes that can occur in such self-interacting systems, such as multiple gluon production. A precise theoretical understanding of how such a

transport theory should be generalized to include particle production within a non-abelian model has not as yet been addressed. Rather, ad-hoc assumptions for the form of such a generalized collision term have been made on the basis of empirical expectations (see for example [1]). It has been to date unclear what the validity of these assumptions is.

Our task is therefore to investigate the collision term in a non-abelian theory *exactly* at the two-body level and beyond this, and to express, if possible, the self-energies in terms of cross sections or, equivalently, in terms of scattering amplitudes. Due to our particular choice of masses (quarks massless, gluons massive) the lowest order processes that can occur, are the annihilation process $q\bar{q} \to g$ and the decay process $g \to q\bar{q}$. One expects to obtain these processes from the mean field self-energies. Two loop self-energies on the other hand should yield at least $2 \to 2$ scattering processes. These processes, which are far more complex than in a simple model with a static interaction as in [6] for example, are detailed here. This complexity also occurs in the QCD case, and the results here can easily be extrapolated to this, in order to complete the derivations attempted in [3]. We then examine higher order contributions to the aforementioned processes.

Naturally, one has to evaluate the constraint equation (3.70) simultaneously to the transport equation (4.1). But to render the calculations tractable we will first neglect it beyond the Hartree level in the following sections. Its influence will be discussed in Chapter 8.

Now we return to the transport equation Eq.(4.1) and evaluate the self-energies to first order in the interaction strength and illustrate their role in the transport equation in the semi-classical limit.

4.1 Hartree self-energies

For the scalar parton model, two generic kinds of Hartree graphs can be identified in the quark and gluon self-energies. These are depicted in Fig. 4.1.

For Hartree diagrams of any kind, off diagonal self-energies are per definition zero and only diagonal elements can possibly be constructed, *i.e.* Σ_H^{--} or Σ_H^{++}. However, all such diagrams vanish identically in this model. The reason for this lies in the color factors: for the quark self-energy graph in Fig. 4.1 that contains a quark-loop, a single SU(3) color group leads to the associated color factor

$$F_{H,q} = t^a_{ii}\mathrm{tr}(t^a) = 0, \tag{4.2}$$

since $t_a = \lambda^a/2$, where λ^a are the Gell-Mann matrices. In the above expression,

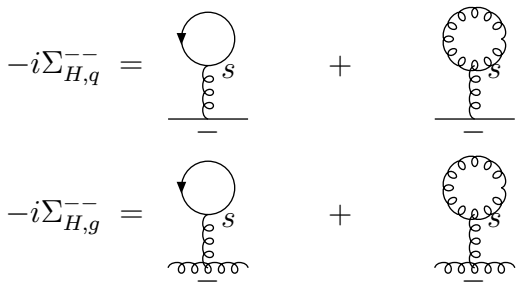

Figure 4.1: Quark and gluon generic Hartree self-energies. Solid lines refer to quarks, wavy lines to gluons. The index s can take the values $+$ or $-$.

i denotes the external quark momentum and is therefore not to be summed over. For the quark self-energy containing a gluon line, the color factor for a single SU(3) group is also vanishing,

$$F_{H,g} = t^a_{ii} T^a_{bb} = -i t^a_{ii} f_{abb} = 0. \tag{4.3}$$

Similar arguments apply to the gluon self-energies. Thus, no mass renormalization occurs due to Hartree terms.

In case of vanishing self-energies, Eq.(4.1) is the equation for free streaming,

$$2p\partial_X f_a(X, \vec{p}) = 0, \tag{4.4}$$

while the constraint equation (3.70) becomes after an integration over Δ_+

$$(E_p^2 - \vec{p}^2 - M^2) f_a(X, \vec{p}) = 0. \tag{4.5}$$

The last equation is the expression of the fact that the partons have to be on mass-shell, and is consistent with the quasiparticle assumption, Eqs.(3.61) to (3.64) made in the first place.

4.2 Fock self-energies

The next type of graph contributing to the mean field expansion is the Fock term. The generic diagrams for the quark and gluon self-energies are shown in Fig. 4.2[1].

[1]Fig. 4.2(b) is strictly speaking a vacuum polarization graph for the gluons

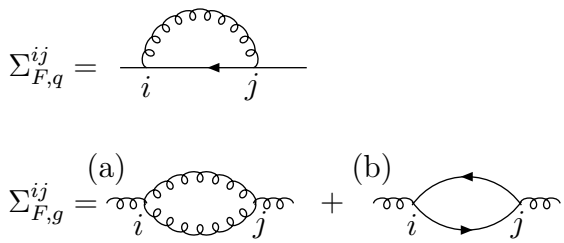

Figure 4.2: Quark and gluon generic one loop self-energies. The quark self-energy plus the first gluon self-energy are Fock diagrams, while (b) of this figure is a polarization insertion.

We start with the quark sector and examine as an example, the gain term generated by the Fock term $\Sigma^{-+}_{F,q}(X,p)$. By inspection, one has

$$i\Sigma^{-+}_{F,q}(X,p) = -g^2 m^2 F^2_{F,q} \int \frac{d^4p_1}{(2\pi)^4} \int \frac{d^4p_2}{(2\pi)^4} S^{-+}(X,p_1) G^{+-}(X,p_2) (2\pi)^4 \delta^{(4)}(p - p_1 + p_2), \tag{4.6}$$

and $F_{F,q}$ is the Fock color factor for a single SU(N_c) group,

$$F_{F,q} = t^a_{ij} t^a_{ji} = \frac{N_c^2 - 1}{2N_c} \delta_{ii}. \tag{4.7}$$

The contribution to the collision term that this makes, using Eq.(3.68) is

$$J^{\rm gain}_{\rm F,coll} = -i \frac{\pi}{E_p} \Sigma^{-+}_{\rm F,q}(X, p_0 = E_p, \vec{p}) \bar{f}_q(X, \vec{p}), \tag{4.8}$$

which, on inserting the explicit expressions for $S^{-+}(X,p)$ and $G^{+-}(X,p)$ from Eqs.(3.61) and (3.62) leads to four distinct terms,

$$J^{\rm gain}_{\rm F,coll} = -g^2 m^2 F^2_F \frac{\pi}{E_p} \int \frac{d^4p_1}{(2\pi)^4} \int \frac{d^4p_2}{(2\pi)^4} (2\pi)^4 \delta^{(4)}(p + p_1 - p_2) \frac{\pi}{E_1} \frac{\pi}{E_2} \sum_{i=1}^{4} T_i, \tag{4.9}$$

where

$$\begin{aligned}
T_1 &= \delta(E_1 - p_1^0)\delta(E_2 - p_2^0) \bar{f}_{\bar{q}}(X,p_1) f_g(X,p_2) \bar{f}_q(X,\vec{p}) \\
T_2 &= \delta(E_1 - p_1^0)\delta(E_2 + p_2^0) \bar{f}_{\bar{q}}(X,p_1) \bar{f}_g(X,-p_2) \bar{f}_q(X,\vec{p}) \\
T_3 &= \delta(E_1 + p_1^0)\delta(E_2 + p_2^0) f_q(X,-p_1) \bar{f}_g(X,-p_2) \bar{f}_q(X,\vec{p}) \\
T_4 &= \delta(E_1 + p_1^0)\delta(E_2 - p_2^0) f_q(X,-p_1) f_g(X,p_2) \bar{f}_q(X,\vec{p}).
\end{aligned} \tag{4.10}$$

By attributing unbarred functions f to incoming particles and barred functions $\bar{f}$ to outgoing ones, one can see that $T_1..T_4$ correspond to the processes $g \to q\bar{q}$, $\emptyset \to q\bar{q}g$,

$q \to qg$ and $qg \to q$. The last three of these are kinematically forbidden, while the former is possible, since the gluons are endowed with a finite mass. Performing the integrals over p_1^0 and p_2^0, Eq.(4.9) becomes

$$\begin{aligned} J^{\rm gain}_{\rm F,coll} &= -\frac{\pi}{E_p}\int \frac{d^3p_1}{(2\pi)^3 2E_1}\frac{d^3p_2}{(2\pi)^3 2E_2}(2\pi)^4\delta^{(4)}(p+p_1-p_2) \\ &\quad \times|\mathcal{M}_{g\to q\bar{q}}|^2 f_g(X,\vec{p}_2)\bar{f}_{\bar{q}}(X,\vec{p}_1)\bar{f}_q(X,\vec{p}). \end{aligned} \tag{4.11}$$

The loss term is obtained in a similar fashion or by exchanging f with $\bar{f}$, since the matrix element is symmetric. Combining both terms, the revised transport equation for quarks is obtained from Eq.(4.1) as

$$\begin{aligned} 2p\partial_X f_q(X,\vec{p}) &= \int \frac{d^3p_1}{(2\pi)^3 2E_1}\frac{d^3p_2}{(2\pi)^3 2E_2}(2\pi)^4\delta^{(4)}(p+p_1-p_2)|\mathcal{M}_{g\to q\bar{q}}|^2 \\ &\quad \times\Big[f_g(X,\vec{p}_2)\bar{f}_{\bar{q}}(X,\vec{p}_1)\bar{f}_q(X,\vec{p}) - \bar{f}_g(X,\vec{p}_2)f_{\bar{q}}(X,\vec{p}_1)f_q(X,\vec{p})\Big]. \end{aligned} \tag{4.12}$$

This is the final expression for the Fock transport equation. One can alternatively introduce a cosmetic recombination or decay rate in which case Eq.(4.12) can be written symbolically as

$$\begin{aligned} 2p\partial_X f_q(X,\vec{p}) &= \int \frac{d^3p_1}{(2\pi)^3 2E_1}\int d\Omega\frac{d\sigma}{d\Omega}\Big|_{q\bar{q}\to g} F \\ &\quad \times\Big[f_g(X,\vec{p}_2)\bar{f}_{\bar{q}}(X,\vec{p}_1)\bar{f}_q(X,\vec{p}) - \bar{f}_g(X,\vec{p}_2)f_{\bar{q}}(X,\vec{p}_1)f_q(X,\vec{p})\Big], \end{aligned} \tag{4.13}$$

where F is the flux factor, and

$$\int d\Omega\frac{d\sigma}{d\Omega} = \int dQ\frac{|\mathcal{M}|^2}{F} \tag{4.14}$$

with the invariant phase space factor dQ given as $dQ = (2\pi)^4\delta^{(4)}(p+p_1-p_2)$ $d^3p_2/((2\pi)^3 2E_2)$.

An analysis of the self-energy graph 3(a) of the gluon sector, $\Sigma^{-+}_{F,g(a)}(X,p)$ along the previous lines leads to processes $g \to gg$, $\emptyset \to ggg$, and $gg \to g$, all of which are kinematically prohibited. One thus obtains

$$(J^{{\rm coll}(a)}_{\rm F,gain/loss})_{\rm gluonic\ graph} = 0. \tag{4.15}$$

This can be attributed to the fact that the self-energies are evaluated on-shell, i.e. we may write

$$\Sigma^{-+}_{F,g(a)}(X,p_0=E_p,\vec{p}) = \Sigma^{+-}_{F,g(a)}(X,p_0=E_p,\vec{p}) = 0, \tag{4.16}$$

which is the statement that an on-shell particle cannot decay into two on-shell particles of the same kind.

The second graph in the gluonic case does not vanish. This self-energy $\Sigma^{-+}_{F,g(b)}$ that enters into the description of the gain in gluons, is precisely that given in Eq.(4.6), but with $G^{+-}(X,p_2)$ replaced by $S^{+-}(X,p_2)$. The color factor in this case is also modified, being $F_{F,g}=1/2\delta^{aa}$. An analysis of the self-energy along the same lines leads to the processes $q\to qg$, $\bar{q}\to\bar{q}g$, $\emptyset\to gq\bar{q}$ and $q\bar{q}\to g$, the last of which is the only term that can contribute. Thus the time evolution of the gluon distribution function is given by

$$\begin{aligned} 2p\partial_X f_g(X,\vec{p}) &= \int \frac{d^3p_1}{(2\pi)^3 2E_1}\frac{d^3p_2}{(2\pi)^3 2E_2}(2\pi)^4\delta^{(4)}(p+p_1-p_2)|\mathcal{M}_{g\to q\bar{q}}|^2 \\ &\quad\times\Big[f_q(X,\vec{p}_2)f_{\bar{q}}(X,\vec{p}_1)\bar{f}_g(X,\vec{p})-\bar{f}_q(X,\vec{p}_2)\bar{f}_{\bar{q}}(X,\vec{p}_1)f_g(X,\vec{p})\Big] \end{aligned} \quad (4.17)$$

We conclude this section by commenting on the result that while the Fock term 3(a) for gluons vanishes identically, the Fock term for the quark self-energy does not. A term of this kind occurs in this model because the quarks are massless, while the gluons are massive. The relevance of this Fock term thus depends on the form of the underlying theory.

Chapter 5

The collision integral - two loop self-energies

To calculate the collision integral beyond the mean field it is necessary to include the two loop self-energies. Their generic diagrams are shown in Fig. 5.1 for the quark

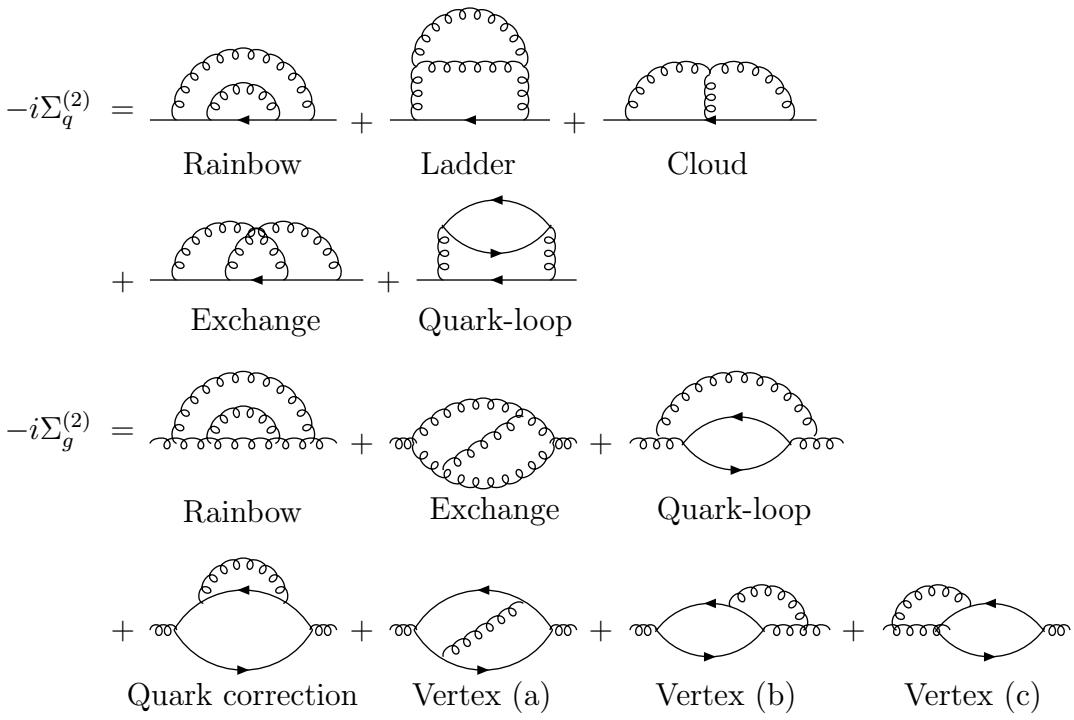

Figure 5.1: Generic diagrams for the quark and gluon self-energies that contain two loops.

and gluon sectors. In the gluonic sector, there are more diagrams, as can be seen in the figure. Note that in this sector, a ladder-like diagram is topologically equivalent to the rainbow kind, and is therefore not included separately.

For clarity, we will consider the quark sector in detail. The calculations for the gluonic sector are similar. To be specific, let us consider first the loss term for which we need $\Sigma^{(2)+-}$. All of its two loop contributions are shown in Fig. 5.2. According to their topology, we denote these graphs as rainbow (R), ladder (L), cloud (C), exchange (E) and quark-loop graphs (QL). In addition to this, one has to sum over the inner vertices. There are four possibilities of arranging the signs at the inner vertices, which yields the diagrams a) to d) for every type of topology.

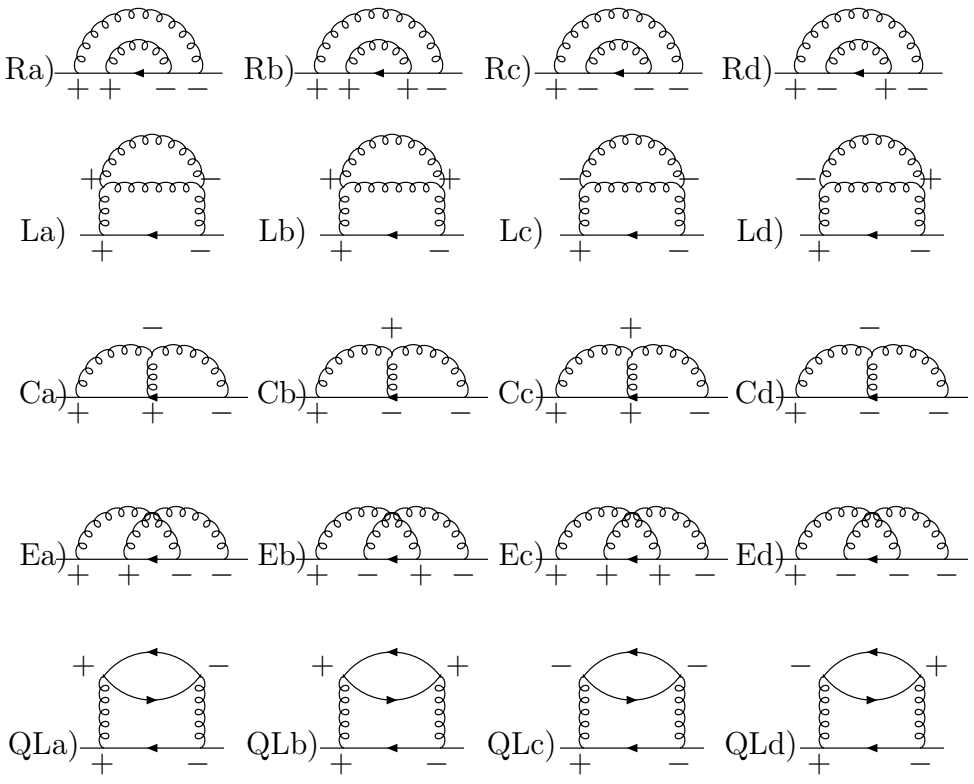

Figure 5.2: All contributions to $\Sigma^{(2)+-}$

5.1 $2 \to 2$ scattering processes

Let us deal first with the diagrams R a), L a), C a), C b), E a), E b) and QL a) of Fig. 5.2. All of these diagrams are necessary to obtain all possible $2 \to 2$ scattering processes as we will now show.

We first note that the diagram E b) is the exchange graph of QL a), because both of these diagrams contain three off-diagonal quark Green functions. The similarly becomes more evident if one redraws the diagram of Fig. 5.2 E b) as shown in Fig. 5.3.

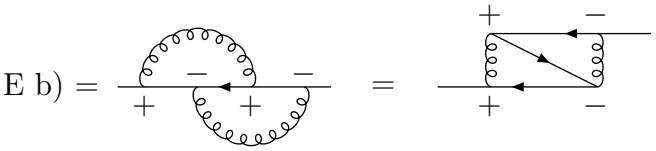

Figure 5.3: Diagram of Fig. 5.2 E b)

We call the sum of the two diagrams QL a) and E b)

$$\Sigma^{(2)+-}_{\text{quark}-\text{quark}}(X,p) = \Sigma^{(2)+-}_{E,b)}(X,p) + \Sigma^{(2)+-}_{\text{QL,a)}}(X,p) \tag{5.1}$$

and collect the remaining five graphs in the construct

$$\begin{aligned}\Sigma^{(2)+-}_{\text{quark}-\text{gluon}}(X,p) &= \Sigma^{(2)+-}_{R,a)}(X,p) + \Sigma^{(2)+-}_{L,a)}(X,p) + \Sigma^{(2)+-}_{C,a)}(X,p) \\ &+ \Sigma^{(2)+-}_{C,b)}(X,p) + \Sigma^{(2)+-}_{E,a)}(X,p).\end{aligned} \tag{5.2}$$

This subdivision in Eqs.(5.1) and (5.2) to $J^{(2)\text{loss}}_{\text{coll}}$ will be handled separately, as the first term will be seen to lead to elastic quark-quark and quark-antiquark differential scattering cross sections in the transport equation, while the $\Sigma_{\text{quark}-\text{gluon}}$ term will be seen to lead to processes involving gluons, such as the processes $q\bar{q} \to gg$ and $qg \to qg$.

5.1.1 Quark-quark and quark-antiquark elastic scattering

Explicit expressions for the quark-loop and its exchange diagram self-energies required in Eq.(5.1) are obtained as

$$\begin{aligned}\Sigma^{(2)+-}_{\text{Ql,a)}}(X,p) &= -g^4 m^4 F^2_{\text{QL}} \int \frac{d^4p_1}{(2\pi)^4}\frac{d^4p_2}{(2\pi)^4}\frac{d^4p_3}{(2\pi)^4}\frac{d^4p_4}{(2\pi)^4}(2\pi)^4\delta^{(4)}(p-p_1-p_2) \\ &\times(2\pi)^4\delta^{(4)}(p_2-p_3+p_4)\, S^{+-}(X,p_1)\, G^{++}(X,p_2) \\ &\times S^{+-}(X,p_3)\, S^{-+}(X,p_4)\, G^{--}(X,p_2)\end{aligned} \tag{5.3}$$

and

$$\begin{aligned}\Sigma^{(2)+-}_{E,b)}(X,p) &= -g^4m^4F_E^2\int\frac{d^4p_1}{(2\pi)^4}\frac{d^4p_2}{(2\pi)^4}\frac{d^4p_3}{(2\pi)^4}\frac{d^4p_4}{(2\pi)^4}(2\pi)^4\delta^{(4)}(p-p_1-p_2)\\ &\quad\times(2\pi)^4\delta^{(4)}(p_2-p_3+p_4)\,S^{+-}(X,p_1)\,G^{--}(X,p_2)\\ &\quad\times S^{+-}(X,p_3)\,S^{-+}(X,p_4)\,G^{++}(X,p-p_3),\end{aligned}\tag{5.4}$$

where $F_{\rm QL}$ and F_E are color factors, that will be given explicitly in Appendix B. Since they do not affect our argument, we suppress them in the following.

The collision integral for loss from Eq.(3.68) can be directly evaluated, to give the quark-loop and exchange contributions

$$\begin{aligned}J^{(2)\rm loss}_{\rm coll,q} &= ig^4m^4\frac{\pi}{E_p}\int\frac{d^4p_1}{(2\pi)^4}\frac{d^4p_2}{(2\pi)^4}\frac{d^4p_3}{(2\pi)^4}\frac{d^4p_4}{(2\pi)^4}(2\pi)^8\delta^{(4)}(p-p_1-p_2)\delta^{(4)}(p_2-p_3+p_4)\\ &\quad\times\left\{G^{++}(X,p_2)G^{--}(X,p_2)+G^{--}(X,p_2)G^{++}(X,p-p_3)\right\}\\ &\quad\times(-i\frac{\pi}{E_1})(-i\frac{\pi}{E_3})(-i\frac{\pi}{E_4})\sum_{i=1}^{8}T_i,\end{aligned}\tag{5.5}$$

where

$$\begin{aligned}T_1 &= \delta(E_1+p_1^0)\,\delta(E_3+p_3^0)\,\delta(E_4+p_4^0)\,f_{\bar q}(-p_1)\,f_{\bar q}(-p_3)\,\bar f_{\bar q}(-p_4)\,f_q(\vec p)\\ T_2 &= \delta(E_1+p_1^0)\,\delta(E_3+p_3^0)\,\delta(E_4-p_4^0)\,f_{\bar q}(-p_1)\,f_{\bar q}(-p_3)\,f_q(p_4)\,f_q(\vec p)\\ T_3 &= \delta(E_1+p_1^0)\,\delta(E_3-p_3^0)\,\delta(E_4+p_4^0)\,f_{\bar q}(-p_1)\,\bar f_q(p_3)\,\bar f_{\bar q}(-p_4)\,f_q(\vec p)\\ T_4 &= \delta(E_1+p_1^0)\,\delta(E_3-p_3^0)\,\delta(E_4-p_4^0)\,f_{\bar q}(-p_1)\,\bar f_q(p_3)\,f_q(p_4)\,f_q(\vec p)\\ T_5 &= \delta(E_1-p_1^0)\,\delta(E_3+p_3^0)\,\delta(E_4+p_4^0)\,\bar f_q(p_1)\,f_{\bar q}(-p_3)\,\bar f_{\bar q}(-p_4)\,f_q(\vec p)\\ T_6 &= \delta(E_1-p_1^0)\,\delta(E_3+p_3^0)\,\delta(E_4-p_4^0)\,\bar f_q(p_1)\,f_{\bar q}(-p_3)\,f_q(p_4)\,f_q(\vec p)\\ T_7 &= \delta(E_1-p_1^0)\,\delta(E_3-p_3^0)\,\delta(E_4+p_4^0)\,\bar f_q(p_1)\,\bar f_q(p_3)\,\bar f_{\bar q}(-p_4)\,f_q(\vec p)\\ T_8 &= \delta(E_1-p_1^0)\,\delta(E_3-p_3^0)\,\delta(E_4-p_4^0)\,\bar f_q(p_1)\,\bar f_q(p_3)\,f_q(p_4)\,f_q(\vec p).\end{aligned}\tag{5.6}$$

One sees that there are eight terms, or eight processes in this expression. However, due to energy-momentum-conservation T_1, T_2, T_4, T_6 and T_7 vanish, leaving only T_3, T_5 and T_8. This is a direct consequence of the on-shell nature of the quasiparticle approximation. Note that if this were relaxed, all terms would necessarily have to be included.

We can reorganize this expression into a recognizable physical form by making some simple manipulations. Letting $p_i \to -p_i$ for the antiquark states and performing the p_1^0, p_3^0, p_4^0 and the p_2 integration by absorbing the appropriate δ-functions, we obtain

$$J^{(2)\rm loss}_{\rm coll,q} = -g^4m^4\frac{\pi}{E_p}\int\frac{d^3p_1}{(2\pi)^3 2E_1}\frac{d^3p_3}{(2\pi)^3 2E_3}\frac{d^3p_4}{(2\pi)^3 2E_4}(2\pi)^4$$

$$
\begin{aligned}
&\times \Big\{\delta^{(4)}(p+p_1-p_3-p_4)\, f_{\bar{q}}(\vec{p}_1)\, \bar{f}_q(\vec{p}_3)\, \bar{f}_{\bar{q}}(\vec{p}_4)\, f_q(\vec{p}) \\
&\quad \times \Big[G^{++}(X,p+p_1)G^{--}(X,p+p_1) + G^{--}(X,p+p_1)G^{++}(X,p-p_3)\Big] \\
&+\delta^{(4)}(p-p_1+p_3-p_4)\, \bar{f}_q(\vec{p}_1)\, f_{\bar{q}}(\vec{p}_3)\, \bar{f}_{\bar{q}}(\vec{p}_4)\, f_q(\vec{p}) \\
&\quad \times \Big[G^{++}(X,p-p_1)G^{--}(X,p-p_1) + G^{--}(X,p-p_1)G^{++}(X,p+p_3)\Big] \\
&+\delta^{(4)}(p-p_1-p_3+p_4)\, \bar{f}_q(\vec{p}_1)\, \bar{f}_q(\vec{p}_3)\, f_q(\vec{p}_4)\, f_q(\vec{p}) \\
&\quad \times \Big[G^{++}(X,p-p_1)G^{--}(X,p-p_1) + G^{--}(X,p-p_1)G^{++}(X,p-p_3)\Big]\Big\}\,.
\end{aligned}
\tag{5.7}
$$

The first two terms of this expression can be combined if one makes the substitution $p_1 \leftrightarrow p_3$ in the second term. The third term has a symmetry in p_1 and p_3 and can be rewritten as one half the sum of two terms with p_1 and p_3 interchanged. The loss term then becomes

$$
\begin{aligned}
J^{(2)\mathrm{loss}}_{\mathrm{coll,q}} = \; & -g^4 m^4 \frac{\pi}{E_p} \int \frac{d^3p_1}{(2\pi)^3 2E_1} \frac{d^3p_3}{(2\pi)^3 2E_3} \frac{d^3p_4}{(2\pi)^3 2E_4} (2\pi)^4 \\
&\times \Big\{\delta^{(4)}(p+p_1-p_3-p_4)\, f_{\bar{q}}(\vec{p}_1)\, \bar{f}_q(\vec{p}_3)\, \bar{f}_{\bar{q}}(\vec{p}_4)\, f_q(\vec{p}) \\
&\quad \times \Big[G^{++}(X,p+p_1)G^{--}(X,p+p_1) + G^{--}(X,p+p_1)G^{++}(X,p-p_3) \\
&\qquad + G^{++}(X,p-p_3)G^{--}(X,p-p_3) + G^{--}(X,p-p_3)G^{++}(X,p+p_1)\Big] \\
&+\delta^{(4)}(p-p_1-p_3+p_4)\, \bar{f}_q(\vec{p}_1)\, \bar{f}_q(\vec{p}_3)\, f_q(\vec{p}_4)\, f_q(\vec{p}) \\
&\quad \times \frac{1}{2}\Big[G^{++}(X,p-p_1)G^{--}(X,p-p_1) + G^{--}(X,p-p_1)G^{++}(X,p-p_3) \\
&\qquad + G^{++}(X,p-p_3)G^{--}(X,p-p_3) + G^{--}(X,p-p_3)G^{++}(X,p-p_1)\Big]\Big\}\,.
\end{aligned}
\tag{5.8}
$$

Using the fact that $[iG^{--}(p)]^\dagger = iG^{++}(p)$ and making the substitution $p_1 \leftrightarrow p_4$ in the second term, one is able to identify the absolute values squared of the Green functions occurring in $J^{(2),\mathrm{loss}}_{\mathrm{coll,q}}$. One has

$$
\begin{aligned}
J^{(2)\mathrm{loss}}_{\mathrm{coll,q}} = \; & g^4 m^4 \frac{\pi}{E_p} \int \frac{d^3p_1}{(2\pi)^3 2E_1} \frac{d^3p_3}{(2\pi)^3 2E_3} \frac{d^3p_4}{(2\pi)^3 2E_4} (2\pi)^4 \delta^{(4)}(p+p_1-p_3-p_4) \\
&\times \Big\{\frac{1}{2}\Big|iG^{--}(X,p-p_3) + iG^{--}(X,p-p_4)\Big|^2\, f_q(\vec{p})\, f_q(\vec{p}_1)\, \bar{f}_q(\vec{p}_3)\, \bar{f}_q(\vec{p}_4) \\
&\quad + \Big|iG^{--}(X,p+p_1) + iG^{--}(X,p-p_3)\Big|^2\, f_q(\vec{p})\, f_{\bar{q}}(\vec{p}_1)\, \bar{f}_q(\vec{p}_3)\, \bar{f}_{\bar{q}}(\vec{p}_4)\Big\}\,.
\end{aligned}
\tag{5.9}
$$

Now one may recognize the scattering amplitude for elastic quark-quark scattering,

$$
-i\mathcal{M}_{qq\to qq}(p1 \to 34) = (-igm)^2 \Big[iG^{--}(p-p_3) + iG^{--}(p-p_4)\Big]\,, \tag{5.10}
$$

and the scattering amplitude for quark-antiquark scattering,

$$-i\mathcal{M}_{q\bar{q}\to q\bar{q}}(p1\to 34) = (-igm)^2\left[iG^{--}(p+p_1)+iG^{--}(p-p_3)\right], \tag{5.11}$$

occurring in Eq.(5.9), which may be concisely written as to give the final result

$$\begin{aligned} J^{(2)\text{loss}}_{\text{coll,q}} &= \frac{\pi}{E_p}\int\frac{d^3p_1}{(2\pi)^3 2E_1}\frac{d^3p_3}{(2\pi)^3 2E_3}\frac{d^3p_4}{(2\pi)^3 2E_4}(2\pi)^4\delta^{(4)}(p+p_1-p_3-p_4) \\ &\times\Big\{\frac{1}{2}\left|\mathcal{M}_{qq\to qq}(p1\to 34)\right|^2 f_q(\vec{p})\, f_q(\vec{p_1})\, \bar{f}_q(\vec{p_3})\, \bar{f}_q(\vec{p_4}) \\ &+\left|\mathcal{M}_{q\bar{q}\to q\bar{q}}(p1\to 34)\right|^2 f_q(\vec{p})\, f_{\bar{q}}(\vec{p_1})\, \bar{f}_q(\vec{p_3})\, \bar{f}_{\bar{q}}(\vec{p_4})\Big\}. \end{aligned} \tag{5.12}$$

The Feynman graphs corresponding to these processes are shown in Fig. 5.4 a) and b) respectively.

5.1.2 Scattering cross sections involving quarks and gluons

We now turn our attention to the graphs of $\Sigma^{(2)+-}_{\text{quark}-\text{gluon}}$ of Eq.(5.2), which will lead to scattering processes that involve gluonic degrees of freedom. As in the previous section, the Feynman rules for non-equilibrium processes can be applied to these diagrams and the result Wigner transformed. This results in the following expressions for the self-energies,

$$\begin{aligned} \Sigma^{(2)+-}_{R,a)}(X,p) &= -g^4m^4F_R^2\int\frac{d^4p_1}{(2\pi)^4}\frac{d^4p_2}{(2\pi)^4}\frac{d^4p_3}{(2\pi)^4}\frac{d^4p_4}{(2\pi)^4}(2\pi)^4\delta^{(4)}(p-p_1-p_2) \\ &\times(2\pi)^4\delta^{(4)}(p_2-p_3-p_4)\, G^{+-}(X,p_1)\, S^{++}(X,p-p_3) \\ &\times G^{+-}(X,p_3)\, S^{+-}(X,p_4)\, S^{--}(X,p-p_3) \end{aligned} \tag{5.13}$$

for the rainbow diagram,

$$\begin{aligned} \Sigma^{(2)+-}_{L,a)}(X,p) &= -\frac{1}{2}g^4m^4F_L^2\int\frac{d^4p_1}{(2\pi)^4}\frac{d^4p_2}{(2\pi)^4}\frac{d^4p_3}{(2\pi)^4}\frac{d^4p_4}{(2\pi)^4}(2\pi)^4\delta^{(4)}(p-p_1-p_2) \\ &\times(2\pi)^4\delta^{(4)}(p_2-p_3-p_4)\, G^{+-}(X,p_1)\, G^{++}(X,p_2) \\ &\times G^{+-}(X,p_3)\, S^{+-}(X,p_4)\, G^{--}(X,p_2) \end{aligned} \tag{5.14}$$

for the ladder graph,

$$\begin{aligned} \Sigma^{(2)+-}_{C,a)/b)}(X,p) &= -g^4m^4F_C^2\int\frac{d^4p_1}{(2\pi)^4}\frac{d^4p_2}{(2\pi)^4}\frac{d^4p_3}{(2\pi)^4}\frac{d^4p_4}{(2\pi)^4}(2\pi)^4\delta^{(4)}(p-p_1-p_2) \\ &\times(2\pi)^4\delta^{(4)}(p_2-p_3-p_4)\, G^{+-}(X,p_1)\, G^{\pm\pm}(X,p_2) \\ &\times G^{+-}(X,p_3)\, S^{+-}(X,p_4)\, S^{\mp\mp}(X,p-p_3) \end{aligned} \tag{5.15}$$

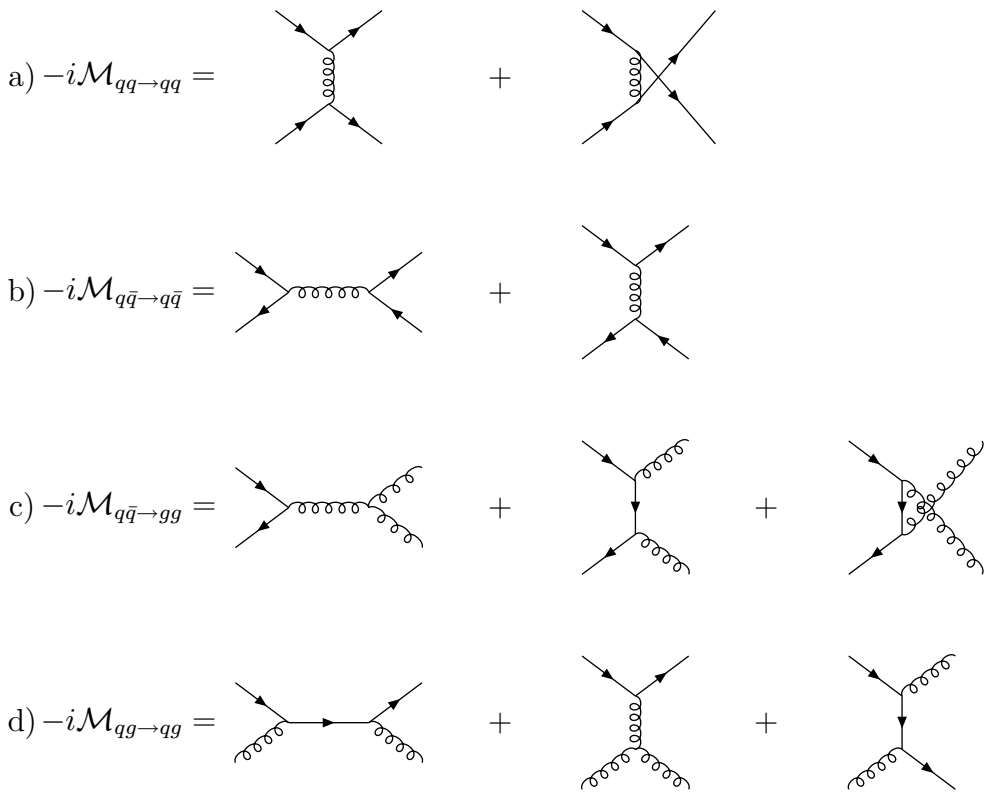

Figure 5.4: Feynman diagrams for the matrix element for elastic quark-quark scattering, elastic quark-antiquark scattering, for the process $q\bar{q} \to gg$, and for the process $qg \to qg$.

for the two cloud diagrams, and

$$\begin{aligned}\Sigma^{(2)+-}_{E,a)}(X,p) &= -g^4 m^4 F_E^2 \int \frac{d^4p_1}{(2\pi)^4}\frac{d^4p_2}{(2\pi)^4}\frac{d^4p_3}{(2\pi)^4}\frac{d^4p_4}{(2\pi)^4}(2\pi)^4\delta^{(4)}(p-p_1-p_2) \\ &\quad \times(2\pi)^4\delta^{(4)}(p_2-p_3-p_4)\, G^{+-}(X,p_1)\, S^{++}(X,p-p_4) \\ &\quad \times G^{+-}(X,p_3)\, S^{+-}(X,p_4)\, S^{--}(X,p-p_3) \qquad (5.16)\end{aligned}$$

for the first exchange diagram. F_R, F_L, F_C and F_E are appropriate color factors, that will be discussed in detail in Appendix B, but which will be suppressed here. Note that a factor $1/2$ occurs in the expression for the ladder diagram because of the gluon loop. The expressions for $\Sigma^{(2)-+}$ are obtained from the ones for $\Sigma^{(2)+-}$ by exchanging $-$ and $+$. The loss term of Eq.(3.68) incorporating $\Sigma^{(2)+-}_{\text{quark}-\text{gluon}}$, is given

as

$$
\begin{aligned}
J^{(2)\mathrm{loss}}_{\mathrm{coll,g}} = \; & ig^4m^4\frac{\pi}{E_p}\int\frac{d^4p_1}{(2\pi)^4}\frac{d^4p_2}{(2\pi)^4}\frac{d^4p_3}{(2\pi)^4}\frac{d^4p_4}{(2\pi)^4}(2\pi)^8\delta^{(4)}(p-p_1-p_2)\delta^{(4)}(p_2-p_3-p_4) \\
& \times\Big\{S^{++}(X,p-p_3)S^{--}(X,p-p_3)+\frac{1}{2}G^{++}(X,p_2)G^{--}(X,p_2) \\
& +G^{++}(X,p_2)S^{--}(X,p-p_3)+G^{--}(X,p_2)S^{++}(X,p-p_3) \\
& +S^{++}(X,p-p_4)S^{--}(X,p-p_3)\Big\}(-i\frac{\pi}{E_1})(-i\frac{\pi}{E_3})(-i\frac{\pi}{E_4})\sum_{i=1}^{8}T_i, \quad (5.17)
\end{aligned}
$$

where

$$
\begin{aligned}
T_1 &= \delta(E_1+p_1^0)\,\delta(E_3+p_3^0)\,\delta(E_4+p_4^0)\,f_{\bar q}(-p_1)\,f_{\bar g}(-p_3)\,f_{\bar g}(-p_4)\,f_q(\vec p) \\
T_2 &= \delta(E_1+p_1^0)\,\delta(E_3+p_3^0)\,\delta(E_4-p_4^0)\,f_{\bar q}(-p_1)\,f_{\bar g}(-p_3)\,\bar f_g(p_4)\,f_q(\vec p) \\
T_3 &= \delta(E_1+p_1^0)\,\delta(E_3-p_3^0)\,\delta(E_4+p_4^0)\,f_{\bar q}(-p_1)\,\bar f_g(p_3)\,f_{\bar g}(-p_4)\,f_q(\vec p) \\
T_4 &= \delta(E_1+p_1^0)\,\delta(E_3-p_3^0)\,\delta(E_4-p_4^0)\,f_{\bar q}(-p_1)\,\bar f_g(p_3)\,\bar f_g(p_4)\,f_q(\vec p) \\
T_5 &= \delta(E_1-p_1^0)\,\delta(E_3+p_3^0)\,\delta(E_4+p_4^0)\,\bar f_q(p_1)\,f_{\bar g}(-p_3)\,f_{\bar g}(-p_4)\,f_q(\vec p) \\
T_6 &= \delta(E_1-p_1^0)\,\delta(E_3+p_3^0)\,\delta(E_4-p_4^0)\,\bar f_q(p_1)\,f_{\bar g}(-p_3)\,\bar f_g(p_4)\,f_q(\vec p) \\
T_7 &= \delta(E_1-p_1^0)\,\delta(E_3-p_3^0)\,\delta(E_4+p_4^0)\,\bar f_q(p_1)\,\bar f_g(p_3)\,f_{\bar g}(-p_4)\,f_q(\vec p) \\
T_8 &= \delta(E_1-p_1^0)\,\delta(E_3-p_3^0)\,\delta(E_4-p_4^0)\,\bar f_q(p_1)\,\bar f_g(p_3)\,\bar f_g(p_4)\,f_q(\vec p). \quad (5.18)
\end{aligned}
$$

Once again, eight terms result from this multiplication. Now, again due to energy-momentum-conservation, T_1, T_2, T_3, T_5 and T_8 vanish, and we are left with three non-vanishing terms, T_4, T_6 and T_7.

Applying the same procedure as for $J^{(2)\mathrm{loss}}_{\mathrm{coll,q}}$ as in the previous section, one can regroup the remaining terms to read

$$
\begin{aligned}
J^{(2)\mathrm{loss}}_{\mathrm{coll,g}} = \; & g^4m^4\frac{\pi}{E_p}\int\frac{d^3p_1}{(2\pi)^3 2E_1}\frac{d^3p_3}{(2\pi)^3 2E_3}\frac{d^3p_4}{(2\pi)^3 2E_4}(2\pi)^4\delta^{(4)}(p+p_1-p_3-p_4) \\
& \times\Big\{\frac{1}{2}\Big|iG^{--}(X,p+p_1)+iS^{--}(X,p-p_3)+iS^{--}(X,p-p_4)\Big|^2 \\
& \times f_q(\vec p)\,f_{\bar q}(\vec p_1)\,\bar f_g(\vec p_3)\,\bar f_g(\vec p_4) \\
& +\Big|iS^{--}(X,p+p_1)+iG^{--}(X,p-p_3)+iS^{--}(X,p-p_4)\Big|^2 \\
& \times f_q(\vec p)\,f_g(\vec p_1)\,\bar f_q(\vec p_3)\,\bar f_g(\vec p_4)\Big\}. \quad (5.19)
\end{aligned}
$$

In order to identify the physical processes that give rise to these terms, we examine first all possible contributions to the annihilation process $q\bar q \to gg$. The Feynman graphs for this within this model are shown in Fig. 5.4 c). The scattering amplitude

associated therewith is

$$-i\mathcal{M}_{q\bar{q}\to gg}(p1 \to 34) = (-igm)^2 \left[iG^{--}(p+p_1) + iS^{--}(p-p_3) + iS^{--}(p-p_4)\right]. \tag{5.20}$$

In a similar manner, the elastic scattering process $qg \to qg$, which is shown in Fig. 5.4 d), has the scattering amplitude

$$-i\mathcal{M}_{qg\to qg}(p1 \to 34) = (-igm)^2 \left[iS^{--}(p+p_1) + iG^{--}(p-p_3) + iS^{--}(p-p_4)\right]. \tag{5.21}$$

One can identify the absolute value squared of Eqs.(5.20) and (5.21) in Eq.(5.19) and therefore $J^{(2)\text{loss}}_{\text{coll,g}}$ can be written as

$$\begin{aligned} J^{(2)\text{loss}}_{\text{coll,g}} &= \frac{\pi}{E_p}\int \frac{d^3p_1}{(2\pi)^3 2E_1}\frac{d^3p_3}{(2\pi)^3 2E_3}\frac{d^3p_4}{(2\pi)^3 2E_4}(2\pi)^4\delta^{(4)}(p+p_1-p_3-p_4) \\ &\quad\times\left\{\frac{1}{2}\left|\mathcal{M}_{q\bar{q}\to gg}(p1\to 34)\right|^2 f_q(\vec{p})\, f_{\bar{q}}(\vec{p}_1)\, \bar{f}_g(\vec{p}_3)\, \bar{f}_g(\vec{p}_4)\right. \\ &\quad\left. + \left|\mathcal{M}_{qg\to qg}(p1\to 34)\right|^2 f_q(\vec{p})\, f_g(\vec{p}_1)\, \bar{f}_q(\vec{p}_3)\, \bar{f}_g(\vec{p}_4)\right\}. \end{aligned} \tag{5.22}$$

The complete loss term is obtained by adding Eq.(5.12) and (5.22),

$$J^{(2)\text{loss}}_{\text{coll}} = J^{(2)\text{loss}}_{\text{coll,q}} + J^{(2)\text{loss}}_{\text{coll,g}}. \tag{5.23}$$

The gain term can be constructed by replacing $f \leftrightarrow \bar{f}$ in the complete loss term. With the relation

$$\frac{d\sigma}{d\Omega} = \frac{|\mathcal{M}|^2}{|\vec{v}_p - \vec{v}_1|2E_p 2E_1}\frac{dQ}{d\Omega} \tag{5.24}$$

and the phase space factor

$$Q = (2\pi)^4\delta^{(4)}(p+p_1-p_3-p_4)\frac{d^3p_3}{(2\pi)^3 2E_3}\frac{d^3p_4}{(2\pi)^3 2E_4}, \tag{5.25}$$

the final form for the transport equation, calculated for two loop self-energy graphs, is for quarks ($a = q$)

$$\begin{aligned} 2p\partial_X f_a(X,\vec{p}) &= \int d\Omega \frac{d^3p_1}{(2\pi)^3 2E_1}|\vec{v}_p - \vec{v}_1|2E_p 2E_1 \\ &\times\sum_{j=1}^{4} s_j \frac{d\sigma_j}{d\Omega}\Big|_{ab\to cd}\left[\bar{f}_a(\vec{p})\bar{f}_b(\vec{p}_1)f_c(\vec{p}_3)f_d(\vec{p}_4) - f_a(\vec{p})f_b(\vec{p}_1)\bar{f}_c(\vec{p}_3)\bar{f}_d(\vec{p}_4)\right], \end{aligned} \tag{5.26}$$

where partons b, c, and d can be a quark, antiquark or gluon, and j labels the four processes $j = 1...4$ corresponding to $q\bar{q} \to gg$, $qg \to qg$, $qq \to qq$ and $q\bar{q} \to q\bar{q}$. The s_j are symmetry factors $s_1 = s_3 = 1/2$ and $s_2 = s_4 = 1$.

The transport equation for gluons can be obtained in an analogous way and calculated for two loops, it takes the same form as Eq.(5.26) with $a = g$. Then j labels the four processes $j = 1...4$ corresponding to $gg \to gg$, $gg \to q\bar{q}$, $gq \to gq$ and $g\bar{q} \to g\bar{q}$. The appropriate symmetry factors are $s_1 = 1/2$ and $s_2 = s_3 = s_4 = 1$.

5.2 Higher order corrections to the process $q\bar{q} \to g$

Now, we wish to demonstrate precisely that the remaining two loop graphs contribute to corrections of order g^3m^3 to the lower order process $q\bar{q} \to g$. To demonstrate this, we arbitrarily examine the set of quark-loop diagrams. The QL a) graph of Fig. 5.2 leads directly to the qq and $q\bar{q}$ cross sections of Fig. 5.4 a) and b), while the three graphs, QL b)-d) of Fig. 5.2 were *not* required for the evaluation of these cross sections. We notice that the quark-loop self-energy graphs contain a self-energy insertion which is just the gluonic Fock self-energy shown in Fig. 4.2 (b). To simplify our notations, we call it in the following $\Pi^{ij}(X,k)$ and it reads as

$$-i\Pi^{ij}(X,k) := (-)^{i+j}(igm)^2 \int \frac{d^4l}{(2\pi)^4} iS^{ij}(X,k+l)\, iS^{ji}(X,l) \tag{5.27}$$

where the color factor is suppressed. Here $i,j = +,-$ and $(-)^{i+j} = +1$ (-1) for $i = j$ $(i \neq j)$.

We commence now with the diagram QL b) of Fig. 5.2 which is given by

$$\begin{aligned} -i\Sigma^{(2)+-}_{\rm QL,b)}(X,p) &= g^2m^2F^2_{\rm QL} \int \frac{d^4p_1}{(2\pi)^4}\frac{d^4p_2}{(2\pi)^4}(2\pi)^4\delta^{(4)}(p-p_1-p_2)\, iS^{+-}(X,p_1) \\ &\quad \times iG^{+-}(X,p_2)\,(-i\Pi^{++}(X,p_2))iG^{++}(X,p_2), \end{aligned} \tag{5.28}$$

where $F^2_{\rm QL}$ is again the color factor given in Eq.(B.12). The corresponding loss term of the collision integral of Eq.(3.68) to this self-energy reads as

$$J^{(2)\rm loss}_{\rm coll,QL,b)} = -i\frac{\pi}{E_p}\Sigma^{(2)+-}_{\rm QL,b)}(X,p^0=E_p,\vec{p})f_q(X,\vec{p}). \tag{5.29}$$

In this expression, the product $iS^{+-}(X,p_1)iG^{+-}(X,p_2)f_q(X,\vec{p})$ occurs. Inserting the quasiparticle approximation for the Green functions of Eqs.(3.61) and (3.62), we obtain for this product the sum of four terms:

$$\begin{aligned} T_1 &= \frac{\pi}{E_1}\frac{\pi}{E_2}\delta(E_1-p_1^0)\delta(E_2-p_2^0)\bar{f}_q(X,p_1)\bar{f}_g(X,p_2)f_q(X,\vec{p}) \\ T_2 &= \frac{\pi}{E_1}\frac{\pi}{E_2}\delta(E_1-p_1^0)\delta(E_2+p_2^0)\bar{f}_q(X,p_1)f_g(X,-p_2)f_q(X,\vec{p}) \\ T_3 &= \frac{\pi}{E_1}\frac{\pi}{E_2}\delta(E_1+p_1^0)\delta(E_2-p_2^0)f_{\bar{q}}(X,-p_1)\bar{f}_g(X,p_2)f_q(X,\vec{p}) \\ T_4 &= \frac{\pi}{E_1}\frac{\pi}{E_2}\delta(E_1+p_1^0)\delta(E_2+p_2^0)f_{\bar{q}}(X,-p_1)f_g(X,-p_2)f_q(X,\vec{p}). \end{aligned} \tag{5.30}$$

By attributing again f to incoming particles and $\bar{f}$ to outgoing ones, we see that $T_1 ... T_4$ correspond to the processes $q \to qg$, $qg \to q$, $q\bar{q} \to g$ and $q\bar{q}g \to \emptyset$. Since the quarks are massless while the gluons are endowed with a finite mass, the processes

corresponding to T_1, T_2 and T_4 are kinematically forbidden as also occurred in the discussion of the Fock term in Sec. 4.2. One thus has one remaining non-vanishing contribution $iS^{+-}(X,p_1)iG^{+-}(X,p_2)f_q(X,\vec{p}) = T_3$. This product is now inserted into Eq.(5.29). In the resulting expression, we interchange p_1 with $-p_1$ and on performing the p_1^0 and p_2^0 integrations, we find the result

$$\begin{aligned} J^{(2)\mathrm{loss}}_{\mathrm{coll,QL,b)}} &= -\frac{\pi}{E_p} g^2 m^2 F^2_{\mathrm{QL}} \int \frac{d^3p_1}{(2\pi)^3 2E_1} \frac{d^3p_2}{(2\pi)^3 2E_2} (2\pi)^4 \delta^{(4)}(p+p_1-p_2) \\ &\quad \times G^{++}(X,p_2)\,\Pi^{++}(X,p_2) f_{\bar{q}}(X,\vec{p}_1) \bar{f}_g(X,\vec{p}_2) f_q(X,\vec{p}) \end{aligned} \tag{5.31}$$

as the remaining contribution of the QL b) graph to the collision integral.

Since T_3 corresponds to the process $q\bar{q} \to g$ which has also come to the fare in Section 4.2, we would like to take a closer look at this process. In Fig. 5.5, all Feynman diagrams for this process are shown up to order g^3m^3. As mentioned in

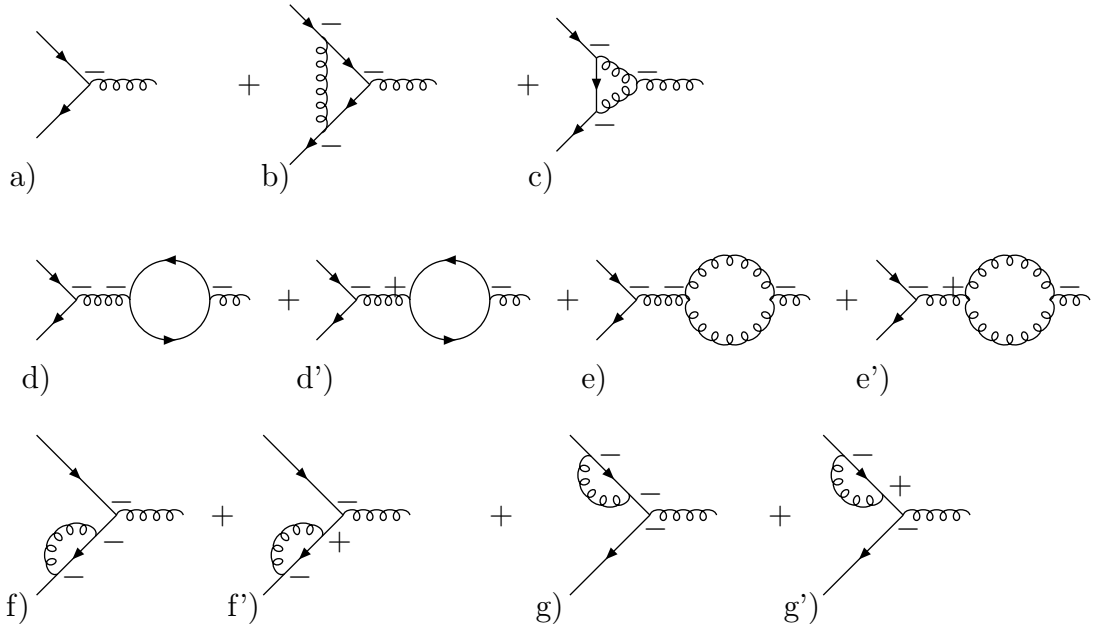

Figure 5.5: The process $q\bar{q} \to g$ up to order $(gm)^3$.

Sec. 3.1, the vertices linked to external lines are $s = -$ ("physical fields"), while the inner vertices can be of type $-$ or $+$ and one has to include all possibilities. That leads to a doubling of the diagrams with inner vertices and we obtain, in addition to the diagrams which one has in T=0 equilibrium field theory, i.e. diagrams with only $-$ vertices, (in our case graph a), b), c), d), e), f) and g)), also diagrams with one $+$ vertex, i.e. in our case graph d'), e'), f') and g').

The scattering amplitude associated with Fig. 5.5 a) has purely a point-like structure with color groups occurring:

$$-i\mathcal{M}^{a)}_{q\bar{q}\to g} = -igm\, t^a_{ij} \otimes t^r_{lm} \tag{5.32}$$

while from Fig. 5.5 d), one has

$$-i\mathcal{M}^{d)}_{q\bar{q}\to g} = -igm[t^b_{ji}\mathrm{tr}(t^b t^a)] \otimes [t^s_{ml}\mathrm{tr}(t^s t^r)]\, G^{--}(X,p_2)\,\Pi^{--}(X,p_2), \tag{5.33}$$

where t^a_{ij} is the matrix of the color group in the representation of the quarks. Now note that using the fact that $[iG^{--}]^\dagger = iG^{++}$ and $F_{\mathrm{QL}} = t^a_{ij}t^b_{ji}\mathrm{tr}(t^b t^a)$, one can rewrite Eq.(5.31) in terms of these matrix elements, i.e.

$$\begin{aligned} J^{(2)\mathrm{loss}}_{\mathrm{coll,QL,b)}} &= \frac{\pi}{E_p}\int \frac{d^3p_1}{(2\pi)^3 2E_1}\frac{d^3p_2}{(2\pi)^3 2E_2}(2\pi)^4\delta^{(4)}(p+p_1-p_2) \\ &\quad \times \mathcal{M}^{a)}_{q\bar{q}\to g}[\mathcal{M}^{d)}_{q\bar{q}\to g}]^\dagger f_q(X,\vec{p}) f_{\bar{q}}(X,\vec{p}_1)\bar{f}_g(X,\vec{p}_2), \end{aligned} \tag{5.34}$$

illustrating that the cross term between these two processes, denoted symbolically as $ad^\dagger$, is derived from the self-energy diagram QL b) of Fig. 5.2. The gain term can be obtained by replacing f with $\bar{f}$ and vice versa in Eq.(5.34).

In a similar fashion, the collision integral can be constructed from the quark-loop diagram QL c) in Fig. 5.2. One obtains an expression for the loss term as in Eq.(5.31) with $G^{++}\,\Pi^{++}$ replaced by the combination $G^{--}\,\Pi^{--}$. Again $J^{(2)\mathrm{loss}}_{\mathrm{coll,QL,c)}}$ can be expressed by the scattering amplitudes of Eq.(5.32) and (5.33):

$$\begin{aligned} J^{(2)\mathrm{loss}}_{\mathrm{coll,QL,c)}} &= \frac{\pi}{E_p}\int \frac{d^3p_1}{(2\pi)^3 2E_1}\frac{d^3p_2}{(2\pi)^3 2E_2}(2\pi)^4\delta^{(4)}(p+p_1-p_2) \\ &\quad \times [\mathcal{M}^{a)}_{q\bar{q}\to g}]^\dagger \mathcal{M}^{d)}_{q\bar{q}\to g} f_q(X,\vec{p}) f_{\bar{q}}(X,\vec{p}_1)\bar{f}_g(X,\vec{p}_2), \end{aligned} \tag{5.35}$$

i.e. the second cross term $a^\dagger d$ required in building a cross section of the basic component a) and d) of Fig. 5.5 is obtained.

In an analogous fashion, one can show that the rainbow diagrams R b) and c) lead to a collision integral containing $\mathcal{M}^{a)}_{q\bar{q}\to g}[\mathcal{M}^{f)}_{q\bar{q}\to g}]^\dagger$ and the hermitian conjugate of this product, the ladder diagrams Lb) and c) to a collision integral containing $\mathcal{M}^{a)}_{q\bar{q}\to g}[\mathcal{M}^{e)}_{q\bar{q}\to g}]^\dagger$ and its hermitian conjugate, the cloud diagrams C c) and d) to a collision integral containing $\mathcal{M}^{a)}_{q\bar{q}\to g}[\mathcal{M}^{c)}_{q\bar{q}\to g}]^\dagger$ and its hermitian conjugate, and finally the exchange diagrams E c) and d) to a collision integral containing $\mathcal{M}^{a)}_{q\bar{q}\to g}[\mathcal{M}^{b)}_{q\bar{q}\to g}]^\dagger$ and its hermitian conjugate.

Note that if we would have only "physical" fields, i.e. only $-$ vertices, then we would be able to account for all mixed diagrams that would occur in the construction

of the $|\mathcal{M}_{q\bar{q}\to g}|^2$ up to order g^4m^4, with the exception of the diagram g) of Fig. 5.5. This graph does not enter into the collision integral, as it is a renormalization diagram for the *incoming* quark, for which the momentum p is fixed externally.

Returning to our explicit example of the quark-loop self-energy of Fig. 5.2, one sees that a simple graphical interpretation can be applied to each figure which we have considered so far. A rule in which all lines that are connected by $\pm$ and $\mp$ are cut in a single path, separates the graphs QL a) to c) into their component matrix elements. This is illustrated in Fig. 5.6.

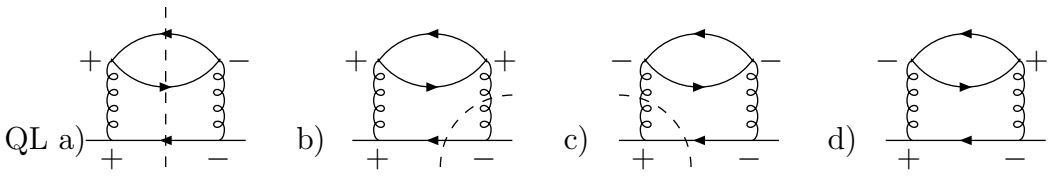

Figure 5.6: Quark-loop self-energy diagrams with cut lines (dashed lines).

This procedure, however, cannot be applied uniquely to the graph QL d), nor for that matter to the remaining graphs which are not required for construction of the mixed terms or direct contributions to the cross sections, i.e. the graphs R d) and L d). We are thus now left with the three graphs QL d), R d) and L d) which at first sight fit into no apparent scheme, and which therefore may present difficulties.

We commence with the investigation of L d). To each of the three gluon vertices are associated three off-diagonal gluonic Green functions. Due to the quasiparticle approximation, they have to be on-shell. Therefore each three gluon vertex corresponds to a on-shell process of a (massive) gluon decaying into two (massive) gluons which is forbidden. For this reason, the diagram L d) vanishes.

For the graphs QL d) and R d), the situation is different. For QL d) we obtain an expression as in Eq.(5.28) with the product of the five Green functions replaced by $S^{+-}(X,p_1)[G^{+-}(X,p_2)]^2S^{-+}(X,p_3)S^{+-}(X,p_4)$. In the quasiparticle approximation the off-diagonal Green functions are on mass shell:

$$p_1^2 = p_3^2 = p_4^2 = 0 \tag{5.36}$$

$$p_2^2 = m^2 \tag{5.37}$$

In addition to this, the two δ-functions for the energy-momentum conservation of Eq.(5.28) have to be fulfilled. Therefore we can write for example

$$0 = p_3^2 = (p_2 + p_4)^2 = 2p_2p_4 + m^2. \tag{5.38}$$

One possible choice which fulfills these equations is

$$p_2 = (m, 0) \quad \text{and} \quad p_4 = (-m/2, m/2). \tag{5.39}$$

Here and in the following, the first component denotes the energy and the second one the value of the three momentum leaving its direction arbitrary. From this one obtains $m_3 = m_2 + m_4 = (m/2, m/2)$ which is on its mass shell.

Thus we are left with the two graphs QL d) and R d). Our task is now to rewrite these self-energies in terms of a scattering product. We were able to express all other self-energy graphs of Fig. 5.2 in terms of scattering amplitudes and saw afterwards, that this corresponds to the cutting of all off-diagonal propagators. But for the graphs QL d) and R d) we cannot use this cutting rule, since each graph consists of five off-diagonal propagators and therefore cannot be cut in an obvious and unique way.[1]

On the other hand, to obtain $|\mathcal{M}_{q\bar{q}\to g}|^2$ up to order g^4m^4 correctly, we still have to consider the scattering amplitudes shown in Fig. 5.5 d'), e') and f'). Since g') is again a renormalization graph for the incoming quark with fixed momentum, we do not have to consider it. Let us first note that diagram e') vanishes for the same reason as the self-energy graph L d): the inner vertex corresponds to the (on-shell) decay of a massive particle into two (on-shell) particles of the same species which is forbidden. For this reason, we still need the products $\mathcal{M}^{a)}_{q\bar{q}\to g}[\mathcal{M}^{d')}_{q\bar{q}\to g}]^\dagger$, $\mathcal{M}^{a)}_{q\bar{q}\to g}[\mathcal{M}^{f')}_{q\bar{q}\to g}]^\dagger$ and their hermitian conjugates.

As mentioned in Sec. 3.1, to obtain the absolute square of a scattering amplitude, one needs the scattering amplitude times its hermitian conjugate in *position* space. The latter is obtained from the original scattering amplitude by interchanging $-$ with $+$ vertices and vice versa [17]. So far, we have considered only scattering amplitudes containing $-$ vertices only, for which the hermitian conjugate in position space, i.e. the same amplitude but all vertices are $+$, is also the hermitian conjugate in momentum space, since $[iD^{--}]^\dagger = iD^{++}$ and $(-igm)^\dagger = +igm$. But now we have to consider scattering amplitudes containing both types of vertices, and the difference between hermitian conjugation in position and momentum space therefore matters.

After we have now clarified the meaning of hermitian conjugation, we take a closer look at the diagram QL d) of Fig. 5.2.

As before, we obtain an expression for the loss term as in Eq.(5.31) with $G^{++}\,\Pi^{++}$

[1]Note that the cutting rule must be derived as a consequence of a calculation and serves in hindsight as an aid.

replaced by $G^{+-}\,\Pi^{-+}$ to read as

$$-i\Sigma^{(2)+-}_{\rm QL,d)}(X,p) = g^2m^2F^2_{\rm QL}\int\frac{d^4p_1}{(2\pi)^4}\frac{d^4p_2}{(2\pi)^4}(2\pi)^4\delta^{(4)}(p-p_1-p_2)\,iS^{+-}(X,p_1) \times iG^{+-}(X,p_2)\,(-i\Pi^{-+}(X,p_2))iG^{+-}(X,p_2). \quad (5.40)$$

On the other hand, the scattering amplitude of Fig. 5.5 d') is given by

$$-i\mathcal{M}^{d')}_{q\bar{q}\to g} = -igm[t^b_{ji}{\rm tr}(t^bt^a)]\otimes[t^s_{ml}{\rm tr}(t^st^r)]\,G^{+-}(X,p_2)\,\Pi^{-+}(X,p_2). \quad (5.41)$$

Therefore one can express $J^{(2)\rm loss}_{\rm coll,QLd)}$ by the scattering amplitudes of Eq.(5.32) and (5.41):

$$J^{(2)\rm loss}_{\rm coll,QL,d)} = \frac{\pi}{E_p}\int\frac{d^3p_1}{(2\pi)^32E_1}\frac{d^3p_2}{(2\pi)^32E_2}(2\pi)^4\delta^{(4)}(p+p_1-p_2) \times[\mathcal{M}^{a)}_{q\bar{q}\to g}]^\dagger\mathcal{M}^{d')}_{q\bar{q}\to g}f_q(X,\vec{p})f_{\bar{q}}(X,\vec{p}_1)\bar{f}_g(X,\vec{p}_2). \quad (5.42)$$

Note that it is *not* possible to express $J^{(2)\rm loss}_{\rm coll,QL,d)}$ in terms of $\mathcal{M}^{a)}_{q\bar{q}\to g}\,[\mathcal{M}^{d')}_{q\bar{q}\to g}]^\dagger$. The latter amplitude is obtained from the graph in Fig. 5.5 d') by replacing all $-$ vertices with $+$ vertices and vice versa. It reads

$$[-i\mathcal{M}^{d')}_{q\bar{q}\to g}]^\dagger = igm[t^b_{ji}{\rm tr}(t^bt^a)]\otimes[t^s_{ml}{\rm tr}(t^st^r)]\,G^{-+}(X,p_2)\,\Pi^{+-}(X,p_2). \quad (5.43)$$

Since in Eq.(5.40) p_2 is integrated over, we are free to replace p_2 by $-p_2$. Noting that $G^{+-}(X,-p_2) = G^{-+}(X,p_2)$ and $\Pi^{-+}(X,-p_2) = \Pi^{+-}(X,p_2)$, we obtain an expression which superficially resembles the one in Eq.(5.43). However, on the other hand, the second $G^{+-}(X,-p_2)$ yields a factor $\bar{f}_g(X,-p_2)$ which does not correspond to the process $[-i\mathcal{M}^{d')}_{q\bar{q}\to g}]^\dagger$, for which a gluon with momentum $+p_2$ is outgoing.

In a similar fashion, one can show that the remaining rainbow graph R d) of Fig. 5.2 leads to a collision integral containing $[\mathcal{M}^{a)}_{q\bar{q}\to g}]^\dagger\,\mathcal{M}^{f')}_{q\bar{q}\to g}$. A collision integral containing the hermitian conjugate term $\mathcal{M}^{a)}_{q\bar{q}\to g}\,\mathcal{M}^{f')}_{q\bar{q}\to g}]^\dagger$ is not obvious, but is in fact present. This is discussed in the following section.

We compare this result with real time thermal field theory for which cutting rules were derived in the 1980's by Kobes and Semenoff [30, 31] and in the 1990's by Bedaque, Das, and Naik [32] (for a comparison of these two approaches see [33]). Kobes and Semenoff investigated in [31] self-energy graphs with one type of particles. For the two loop self-energy graph containing a self-energy insertion (corresponding e.g. to our quark-loop graph with only one type of particles) they found that three graphs can be cut as shown in Fig. 5.6 and can be interpreted in terms of products of scattering amplitudes, while the last graph (in our case $\Sigma^{+-}_{QL,d)}$) cannot be cut, but

corresponds to a product of scattering amplitudes of which one contains a + vertex (in our case this is the product $a^\dagger d'$). To this extent, their result is similar to ours. They concluded that decay amplitudes with only $-$ vertices correspond directly to specific cuts of the associated self-energy graph while decay amplitudes containing some + vertices correspond to self-energy graphs which are not cuttable. They did not state that one product (i.e. in our case $a\, d'^\dagger$) is missing nor is an explanation given for this.

For the derivation of the cutting rules of Bedaque et al., the KMS relation was used and can therefore not be generalized directly for non-equilibrium systems. In their approach all "uncuttable" graphs cancel when a summation over the internal vertices ($s = -, +$) is performed. The discrepancy with the approach of Kobes and Semenoff lies in the difference in definition of the propagators which are to be cut. A closer analysis of Gelis [33] has revealed that uncuttable graphs in the sense of Kobes and Semenoff are hidden in the cuttable graphs of Bedaque et al. As an example, they have investigated the two loop self-energy graphs with a vertex correction (these graphs correspond to our cloud graphs with only one type of particles). But these graphs are problem-free anyway and they have found the same products of scattering amplitudes as we have.

For a further review of the different approaches for thermal cutting rules we refer the reader to Ref. [34] while for cutting rules in the imaginary time formalism to Ref. [35].

Let us conclude this section by commenting that the collision integral constructed from a first set of two loop self-energy diagrams, i.e. the graphs R a), L a), C a) and b), E a) and b), and QL a) of Fig. 5.2, was expressed in terms of all possible $2 \to 2$ cross sections. The collision integral constructed from the remaining self-energy diagrams of Fig. 5.2 was rewritten in terms of products of scattering amplitudes of the process $q\bar{q} \to g$. In this fashion, however, it is not possible to obtain an absolute square of the sum of amplitudes a) to f') shown in Fig. 5.5 up to order $g^4 m^4$ since two products, i.e. $\mathcal{M}^{a)}_{q\bar{q}\to g}\,[\mathcal{M}^{d')}_{q\bar{q}\to g}]^\dagger$ and $\mathcal{M}^{a)}_{q\bar{q}\to g}\,[\mathcal{M}^{f')}_{q\bar{q}\to g}]^\dagger$ are still missing. We will tackle this issue in the next section.

5.3 Another approach

We found in the last section that it was not possible to obtain an absolute square of the sum of the amplitudes a) - f') shown in Fig. 5.5 up to order $g^4 m^4$ since two products, i.e. $\mathcal{M}^{a)}_{q\bar{q}\to g}\,[\mathcal{M}^{d')}_{q\bar{q}\to g}]^\dagger$ and $\mathcal{M}^{a)}_{q\bar{q}\to g}\,[\mathcal{M}^{f')}_{q\bar{q}\to g}]^\dagger$ are still missing.

For the first product, one requires $[\mathcal{M}^{d')}_{q\bar{q}\to g}]^\dagger$ given in Eq.(5.43). This amplitude

contains the self-energy insertion $\Pi^{+-}(X,p_2)$ which cannot be obtained from the self-energy graph $\Sigma^{(2)+-}_{QLd)}$ as explained in the last section after Eq.(5.43). The only other self-energy graph which could possibly supply this self-energy insertion is obviously $\Sigma^{(2)+-}_{QLa)}$ of Fig. 5.2. Thus let us look at this graph again in more detail: its contribution to the collision integral reads

$$\begin{aligned} J^{(2)\mathrm{loss}}_{\mathrm{coll,QLa)}} &= g^2m^2\frac{\pi}{E_p}\int\frac{d^4p_1}{(2\pi)^4}\,\frac{d^4p_2}{(2\pi)^4}\,(2\pi)^4\,\delta^{(4)}(p-p_1-p_2)\,iS^{+-}(X,p_1) \\ &\quad\times iG^{--}(X,p_2)\,\Big[-i\Pi^{+-}(X,p_2)\Big]\,iG^{++}(X,p_2)\,f_q(X,\vec{p}). \end{aligned} \tag{5.44}$$

Here and in the following we suppress the color factors for simplicity. Inserting the quasiparticle approximation $iS^{+-}(X,p_1)=\pi/E_1\{\delta(E_1-p_1^0)\bar{f}_q(X,p_1)+\delta(E_1+p_1^0)f_{\bar{q}}(X,-p_1)\}$ yields two contributions. The first one is proportional to $\bar{f}_q(X,p_1)$ and is considered later. The second one is proportional to $f_{\bar{q}}(X,-p_1)$ and gives

$$\begin{aligned} J^{(2)\mathrm{loss\ 2^{nd}}}_{\mathrm{coll,QLa)}} &= g^2m^2\frac{\pi}{E_p}\int\frac{d^3p_1}{2E_1(2\pi)^3}\,\frac{d^4p_2}{(2\pi)^4}\,(2\pi)^4\,\delta^{(3)}(\vec{p}+\vec{p}_1-\vec{p}_2)\,\delta(E_p+E_1-p_2^0) \\ &\quad\times iG^{--}(X,p_2)\,\Big[-i\Pi^{+-}(X,p_2)\Big]\,iG^{++}(X,p_2)\,f_{\bar{q}}(X,\vec{p}_1)\,f_q(X,\vec{p}), \end{aligned} \tag{5.45}$$

where p_1 was substituted by $-p_1$ and the p_1^0-integration was performed. Now we insert the quasiparticle approximation of Eqs.(3.63) and (3.64) for $G^{\mp\mp}(X,p_2)$. Using the relation

$$\frac{\pm i}{p_2^2-m^2\pm i\epsilon}=\mathrm{P}\frac{\pm i}{p_2^2-m^2}+\pi\delta(p_2^2-m^2) \tag{5.46}$$

and the fact that

$$\int dp_2^0\;\mathrm{P}\frac{1}{p_2^2-m^2}\;\delta(E_2\pm p_2^0)=0, \tag{5.47}$$

where P denotes the principal value, we find

$$\begin{aligned} J^{(2)\mathrm{loss\ 2^{nd}}}_{\mathrm{coll,QLa)}} &= g^2m^2\frac{\pi}{E_p}\int\frac{d^3p_1}{2E_1(2\pi)^3}\,\frac{d^4p_2}{(2\pi)^4}\,(2\pi)^4\,\delta^{(3)}(\vec{p}+\vec{p}_1-\vec{p}_2)\,\delta(E_p+E_1-p_2^0) \\ &\quad\times\Big[-i\Pi^{+-}(X,p_2)\Big]\left\{\left|\mathrm{P}\frac{i}{p_2^2-m^2}\right|^2+\left[\frac{\pi}{E_2}\delta(E_2-p_2^0)\left(f_g(X,p_2)+\frac{1}{2}\right)\right.\right. \\ &\quad\left.\left.+\frac{\pi}{E_2}\delta(E_2+p_2^0)\left(f_g(X,-p_2)+\frac{1}{2}\right)\right]^2\right\}\,f_{\bar{q}}(X,\vec{p}_1)\,f_q(X,\vec{p}). \end{aligned} \tag{5.48}$$

The energy conserving δ-function yields $p_2^0=E_p+E_1>0$. Therefore the term proportional to $\delta(E_2+p_2^0)$ cannot contribute and the term in the curly bracket reads

$$\left\{\left|\mathrm{P}\frac{i}{p_2^2-m^2}\right|^2+\left[\frac{\pi}{E_2}\delta(E_2-p_2^0)\left(f_g(X,p_2)+\frac{1}{2}\right)\right]^2\right\}$$

$$
\begin{aligned}
&= \left|\mathrm{P}\frac{i}{p_2^2-m^2}\right|^2 + \frac{\pi^2}{E_2^2}\delta^2(E_2-p_2^0)\left(f_g(X,p_2)\bar{f}_g(X,p_2)+\frac{1}{4}\right)\\
&= \left|\mathrm{P}\frac{i}{p_2^2-m^2}\right|^2 + \frac{\pi}{E_2}\delta(E_2-p_2^0)\bar{f}_g(X,p_2)\frac{\pi}{E_2}\delta(E_2-p_2^0)f_g(X,p_2) + \left[\frac{\pi}{2E_2}\delta(E_2-p_2^0)\right]^2\\
&= \left|\mathrm{P}\frac{i}{p_2^2-m^2}\right|^2 + \frac{\pi}{E_2}\delta(E_2-p_2^0)\bar{f}_g(X,p_2)\;\Theta(p_2^0)iG^{-+}(X,p_2) + \left[\pi\Theta(p_2^0)\delta(p_2-m^2)\right]^2\\
&= \left|\frac{i}{p_2^2-m^2+i\epsilon}\right|^2 + \frac{\pi}{E_2}\delta(E_2-p_2^0)\bar{f}_g(X,p_2)\;iG^{-+}(X,p_2). \qquad (5.49)
\end{aligned}
$$

In the last step we have used $p_2^0 > 0$ and Eqs.(5.46) and (5.47). Inserting this expression in Eq.(5.48) gives

$$
\begin{aligned}
J^{(2)\text{loss }2^{\text{nd}}}_{\text{coll,QLa)}} &= g^2m^2\frac{\pi}{E_p}\int\frac{d^3p_1}{2E_1(2\pi)^3}\,\frac{d^4p_2}{(2\pi)^4}\,(2\pi)^4\,\delta^{(4)}(p+p_1-p_2)\,\left[-i\Pi^{+-}(X,p_2)\right]\\
&\quad\times\left\{\left|\frac{i}{p_2^2-m^2+i\epsilon}\right|^2 + \frac{\pi}{E_2}\delta(E_2-p_2^0)\bar{f}_g(X,p_2)\;iG^{-+}(X,p_2)\right\}\\
&\quad\times f_{\bar{q}}(X,\vec{p}_1)\,f_q(X,\vec{p}). \qquad (5.50)
\end{aligned}
$$

We can express the second term in terms of the scattering amplitude $[-i\mathcal{M}^{d')}_{q\bar{q}\to g}]^\dagger$ of Eq.(5.43) to obtain

$$
\begin{aligned}
J^{(2)\text{loss }2^{\text{nd}}}_{\text{coll,QLa)}} &= g^2m^2\frac{\pi}{E_p}\int\frac{d^3p_1}{2E_1(2\pi)^3}\,\frac{d^4p_2}{(2\pi)^4}\,(2\pi)^4\,\delta^{(4)}(p+p_1-p_2)\,\left[-i\Pi^{+-}(X,p_2)\right]\\
&\quad\times\left|\frac{i}{p_2^2-m^2+i\epsilon}\right|^2\; f_{\bar{q}}(X,\vec{p}_1)\,f_q(X,\vec{p})\\
&\quad+\frac{\pi}{E_p}\int\frac{d^3p_1}{2E_1(2\pi)^3}\,\frac{d^3p_2}{2E_2(2\pi)^3}\,(2\pi)^4\,\delta^{(4)}(p+p_1-p_2)\\
&\quad\times\mathcal{M}^{a)}_{q\bar{q}\to g}\,[\mathcal{M}^{d')}_{q\bar{q}\to g}]^\dagger\,f_q(X,\vec{p})\,f_{\bar{q}}(X,\vec{p}_1)\,\bar{f}_g(X,\vec{p}_2). \qquad (5.51)
\end{aligned}
$$

Let us comment on this result. The second term gives precisely the contribution we were looking for, i.e. the missing product of the scattering amplitudes $\mathcal{M}^{a)}_{q\bar{q}\to g}\,[\mathcal{M}^{d')}_{q\bar{q}\to g}]^\dagger$! The first term however gives the same contribution as Eq.(5.45) with the non-equilibrium propagators $G^{\mp\mp}(X,p_2)$ replaced by the $T=0$ Feynman propagators $G_F^{(*)}(p_2) = (-)i/(p_2^2-m^2\pm i\epsilon)$. Therefore we can make the same manipulations with this term as we did with the first term of Eq.(5.5) in Sec.5.1.1. There, we found that only one term proportional to $f_{\bar{q}}(X,\vec{p}_1)$ contributed to $J^{(2)\text{loss}}_{\text{coll,QLa)}}$, i.e. T_3 of Eq.(5.6). We showed that this term corresponds to the s-channel of the process $q\bar{q}\to q\bar{q}$. Thus, we can rewrite the first term of Eq.(5.51) in a similar fashion to

Eq.(5.12) and obtain for Eq.(5.51)

$$
\begin{aligned}
J^{(2)\text{loss } 2^{\text{nd}}}_{\text{coll,QLa)}} &= \frac{\pi}{E_p}\int \frac{d^3p_1}{2E_1(2\pi)^3}\,\frac{d^3p_3}{2E_3(2\pi)^3}\,\frac{d^3p_4}{2E_4(2\pi)^3}\,(2\pi)^4\,\delta^{(4)}(p+p_1-p_3-p_4) \\
&\quad\times\left|\mathcal{M}^{s-\text{channel}}_{q\bar{q}\to q\bar{q}}\right|^2\, f_q(X,\vec{p})\,f_{\bar{q}}(X,\vec{p}_1)\,\bar{f}_q(X,\vec{p}_3)\,\bar{f}_{\bar{q}}(X,\vec{p}_4) \\
&\quad+\frac{\pi}{E_p}\int \frac{d^3p_1}{2E_1(2\pi)^3}\,\frac{d^3p_2}{2E_2(2\pi)^3}\,(2\pi)^4\,\delta^{(4)}(p+p_1-p_2) \\
&\quad\times\mathcal{M}^{a)}_{q\bar{q}\to g}\,[\mathcal{M}^{d')}_{q\bar{q}\to g}]^\dagger\, f_q(X,\vec{p})\,f_{\bar{q}}(X,\vec{p}_1)\,\bar{f}_g(X,\vec{p}_2), \qquad (5.52)
\end{aligned}
$$

where for $\left|\mathcal{M}^{s-\text{channel}}_{q\bar{q}\to q\bar{q}}\right|^2$ the Feynman propagator G_F is used. Here, the gluon propagator can be on-mass shell, and the difference between the non-equilibrium propagator G^{--} and the Feynman propagator G_F matters.

We consider now the contribution to $J^{(2)\text{loss}}_{\text{coll,QLa)}}$ of Eq.(5.44) given by the first term of iS^{+-} proportional to $\bar{f}_q(X,p_1)$. We have already evaluated this contribution in Sec.5.1.1. It gives the terms T_5 - T_8 of Eq.(5.6). We showed that only T_5 and T_8 were non-vanishing and lead to the t-channel of quark-antiquark scattering and to the t- and u-channel of quark-quark scattering shown in Fig. 5.4 a) and b). In each of these channels the gluonic propagator cannot be on-mass shell. Therefore the on-shell part of G^{--} does not contribute and we can replace the non-equilibrium propagator G^{--} by the Feynman propagator G_F.

In Sec.5.1.1, we derived the mixed terms for quark-quark and quark-antiquark scattering from the exchange graph $\Sigma^{(2)+-}_{Eb)}$ given in Eq.(5.4). We investigate now the question whether it is possible to replace the gluonic non-equilibrium propagators $G^{\mp\mp}$ by the Feynman propagators again. This difference only matters for the s-channel where the gluonic propagator can be on-shell. Therefore we investigate now the mixed term from the s- and t-channel of quark-antiquark scattering. This mixed term is given in the first term of Eq.(5.8) and the contribution of the gluonic propagators reads $G^{--}(X,p+p_1)\,G^{++}(X,p-p_3)+G^{--}(X,p-p_3)\,G^{++}(X,p+p_1)$. Setting $G^{\mp\mp}=G^{(*)}_F+G_{n.e.}$, where $G_{n.e.}$ denotes the on-shell non-equilibrium part of the diagonal propagators, and using the fact that the gluon propagator of the t-channel is off-shell, we find

$$
\begin{aligned}
& G^{--}(X,p+p_1)\,G^{++}(X,p-p_3)+G^{--}(X,p-p_3)\,G^{++}(X,p+p_1) \\
= \;& [G_F(X,p+p_1)+G_{n.e.}(X,p+p_1)]\,\mathrm{P}\frac{-i}{(p-p_3)^2-m^2} \\
& +\mathrm{P}\frac{i}{(p-p_3)^2-m^2}\,[G^*_F(X,p+p_1)+G_{n.e.}(X,p+p_1)] \\
= \;& G_F(X,p+p_1)\,\mathrm{P}\frac{-i}{(p-p_3)^2-m^2}+\mathrm{P}\frac{i}{(p-p_3)^2-m^2}\,G^*_F(X,p+p_1). \qquad (5.53)
\end{aligned}
$$

Thus the non-equilibrium part of the gluonic propagator of the s-channel does not contribute and one can replace the non-equilibrium propagators by their Feynman counterparts. To summarize, the contributions of $\Sigma^{(2)+-}_{QLa)}$ and $\Sigma^{(2)+-}_{Eb)}$ to the collision integral read

$$\begin{aligned} J^{(2)\text{loss}}_{\text{coll,q}} &= \frac{\pi}{E_p}\int \frac{d^3p_1}{2E_1(2\pi)^3}\,\frac{d^3p_3}{2E_3(2\pi)^3}\,\frac{d^3p_4}{2E_4(2\pi)^3}\,(2\pi)^4\,\delta^{(4)}(p+p_1-p_3-p_4) \\ &\times\Big\{\frac{1}{2}\,|\mathcal{M}_{qq\to qq}|^2\;\; f_q(X,\vec{p})\,f_q(X,\vec{p}_1)\,\bar{f}_q(X,\vec{p}_3)\,\bar{f}_q(X,\vec{p}_4) \\ &\quad + |\mathcal{M}_{q\bar{q}\to q\bar{q}}|^2\;\; f_q(X,\vec{p})\,f_{\bar{q}}(X,\vec{p}_1)\,\bar{f}_q(X,\vec{p}_3)\,\bar{f}_{\bar{q}}(X,\vec{p}_4)\Big\} \\ &+\frac{\pi}{E_p}\int \frac{d^3p_1}{2E_1(2\pi)^3}\,\frac{d^3p_2}{2E_2(2\pi)^3}\,(2\pi)^4\,\delta^{(4)}(p+p_1-p_2) \\ &\times\mathcal{M}^{a)}_{q\bar{q}\to g}\,[\mathcal{M}^{d')}_{q\bar{q}\to g}]^\dagger\,f_q(X,\vec{p})\,f_{\bar{q}}(X,\vec{p}_1)\,\bar{f}_g(X,\vec{p}_2), \end{aligned} \tag{5.54}$$

where for the quark-quark and quark-antiquark scattering amplitudes $T=0$ Feynman propagators are used.

As was stated at the beginning of this section, the product $\mathcal{M}^{a)}_{q\bar{q}\to g}\,[\mathcal{M}^{f')}_{q\bar{q}\to g}]^\dagger$ is still missing. Obviously it can only emerge from the self-energy graph $\Sigma^{(2)+-}_{Ra)}$. Since the rainbow and the quark-loop graphs have similar topologies, this product can be derived in an analogous way. In Sec.5.1.2, we showed that $\Sigma^{(2)+-}_{Ra)}$ yield the t- and u-channel of the process $q\bar{q}\to gg$ and the s- and u-channel of the process $qg\to qg$ shown in Fig. 5.4. Due to our choice of masses, none of the propagators of these channels can be on-mass shell, i.e. only the principal values of the propagators contribute. Therefore it makes no difference if one uses the non-equilibrium or the (temperature independent) Feynman propagators! We emphasize that the self-energy graph $\Sigma^{(2)+-}_{Ra)}$ not only yields the above mentioned absolute squares of scattering channels but also the "missing" product $\mathcal{M}^{a)}_{q\bar{q}\to g}\,[\mathcal{M}^{f')}_{q\bar{q}\to g}]^\dagger$ without any change of propagators! This result is quite surprising and could not be derived by any "cutting rules".

We comment that also the gluonic propagator is off-shell for the s-channel of the process $q\bar{q}\to gg$. Otherwise it could not decay into two on-shell gluons.

We conclude that only the exchange propagator of the s-channel of $q\bar{q}$ scattering can be on-mass shell, and only in this case the substitution of the non-equilibrium propagator by the Feynman propagator matters.

We summarize the result of this section. Collecting all contributions of the Fock and the two loop self-energies to the collision integral, the transport equation reads

$$2p\partial_X f_q(X,p) = \int \frac{d^3p_1}{(2\pi)^3 2E_1}\frac{d^3p_2}{(2\pi)^3 2E_2}(2\pi)^4\delta^{(4)}(p+p_1-p_2)|\mathcal{M}_{g\to q\bar{q}}|^2$$

$$\times[f_g(X,p_2)\bar{f}_{\bar{q}}(X,p_1)\bar{f}_q(X,p) - \bar{f}_g(X,p_2)f_{\bar{q}}(X,p_1)f_q(X,p)]$$
$$+\int d\Omega \frac{d^3p_1}{(2\pi)^3 2E_1}\,|\vec{v}_p - \vec{v}_1|\,2E_p\,2E_1$$
$$\times\left\{\sum_{j=1}^{4} s_j \frac{d\sigma_j}{d\Omega}\,|_{qa\to bc}\,\left[\bar{f}_q(X,\vec{p})\,\bar{f}_a(X,\vec{p}_1)\,f_b(X,\vec{p}_3)\,f_c(X,\vec{p}_4)\right.\right.$$
$$\left.\left.-f_q(X,\vec{p})\,f_a(X,\vec{p}_1)\,\bar{f}_b(X,\vec{p}_3)\,\bar{f}_c(X,\vec{p}_4)\right]\right\}, \qquad (5.55)$$

where j denotes the four processes $j = 1...4$ corresponding to $q\bar{q} \to gg$, $qg \to qg$, $qq \to qq$ and $q\bar{q} \to q\bar{q}$. The s_j are symmetry factors $s_1 = s_3 = 1/2$ and $s_2 = s_4 = 1$. This equation is correct up to order g^4m^4.

For the evaluation of the $2 \to 2$ cross sections, the Feynman propagators, i.e. the $T = 0$ equilibrium propagators were used, while for the evaluation of the process $q\bar{q} \to g$ up to order g^4m^4 the non-equilibrium propagators of Eqs.(3.61) to (3.64) were used.

One last comment is in order: for this derivation we evaluated the self-energy graphs directly with the help of Feynman rules. We were able to rewrite each self-energy graph in terms of one or several products of scattering amplitudes. It is not possible to find "cutting rules" from which the same result could be obtained.

Let us now compare our work with results found by other authors. Blaizot and Iancu [36] found a collision term containing the absolute square of a matrix element corresponding to the t-channel of particle-particle scattering, and to the s- and t-channel of particle-antiparticle scattering. The u-channel of particle-particle scattering nor the mixed terms between the channels are included. For the evaluation of the scattering amplitudes the *equilibrium retarded* propagator is used and not the causal propagator as we have.

Baier, Dirks, and Redlich [37] study the production of thermal dileptons in a hot pion gas, examining the two loop diagrams that can occur within the theory. In their approach, these graphs are subdivided as giving rise to real and virtual processes, and in doing so, the exchanged meson is represented accordingly by its principal or thermal parts respectively.

Chapter 6

Three and more loop self-energies

Up to this point, we have made a semiclassical expansion that involves keeping only the leading term in expanding the exponential in Eq.(3.54) (here the factor $\hbar$ has been set to one.) In addition, we have examined sets of diagrams organized according to the number of interaction lines, i.e. according to the coupling strength. We have found that all generic types of graphs are required in order to build up the cross sections that ultimately occur in a Boltzmann-like equation. However, at the level of two exchanged gluons, we are already faced with five types of graphs, and this number increases rapidly with the number of exchanged gluons. One possible simplifying assumption is the additional imposition of an expansion in the inverse number of colors. According to such a criterion, the ladder, the rainbow and the cloud diagrams are leading, since their color factors for one color group are of order $O(N_c^2)$ while for the quark-loop diagram it goes as N_c and for the exchange diagram only as N_c^0 (see Appendix B).

Since the ladder and the rainbow diagram lead to cross sections involving gluons while the quark-loop diagram leads to elastic quark-(anti)quark cross sections, one can conclude that the quark degrees of freedom are suppressed in comparison with the gluon degrees of freedom. This is in agreement with the results of an evaluation of the quark-quark scattering amplitude within this model [12], in which the quark degrees of freedom are neglected, however due to kinematical reasons. Although the ladder and the rainbow diagram are both of order $O(N_c^2)$, the ratio of their color factors for one color group is not one, but

$$\frac{F_R}{F_L} = \frac{C_F}{C_A}, \tag{6.1}$$

which is $4/9 \approx 1/2$ for $N_c = 3$. Since in the rainbow diagram the second gluon couples at the quark-line while in the ladder diagram it couples at the first gluon,

two quark-quark-gluon vertices are suppressed by a factor 4/9 per color group in comparison with two 3-gluon vertices. Thus, there is no *strict* ordering of the gluon graphs according to a single class of diagrams, in an expansion in $1/N_c$. Although the ladder graphs and the processes that they lead to appear largest, one should note that the symmetry factors of the other graphs compensate for this. A numerical study is essential to determine the actual order of magnitude of each graph.

Note that an expansion in color also incorporates the coupling strength. Assuming that $g \sim 1/N_c$, we find that the Fock term $\sim g^2 N_c^2$ and the ladder diagram $\sim g^4 N_c^4$ are of the same order.

Note also that the result here stands in apposition to the naive expectations from the scalar quark-gluon model that was discussed in Chapter 2. Here, the fact that the ladder diagrams dominate the elastic scattering process could lead one to heuristically develop a transport theory that favors only these types of graphs. We have however found no reason to justify such an assumption.

6.1 Three loop self-energies

In the case of the two loop self-energy for quarks, we found five generic types of diagrams. For the three loop self-energy however the number of generic types of diagrams is much larger. To reduce this we make an expansion in $1/N_c$ as explained above and omit all graphs containing quark-loops. The number of the remaining self-energy diagrams is still enormous. Therefore we will not perform the calculations in any detail but rather outline it. We start with the three loop rainbow and ladder diagram and all possible mixtures between them shown in Fig. 6.1. To be specific,

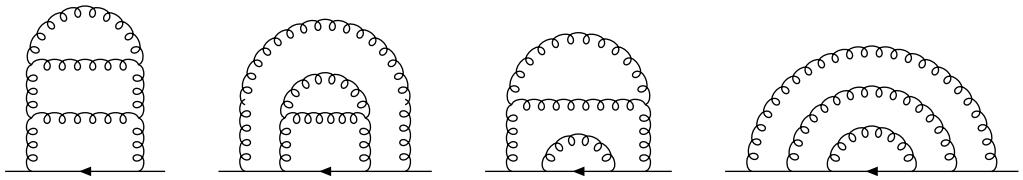

Figure 6.1: Generic three loop ladder, rainbow and mixed diagrams.

we consider $\Sigma^{(3)+-}$ which is needed for the construction of the loss term. Then there are 16 possibilities of arranging the $-$ or $+$ indices at the remaining four vertices. Let us first choose the possibility where only $+$ vertices on the left hand side of each diagram are placed and only $-$ vertices on the right hand side. This gives the diagrams shown in Fig. 6.2. These four graphs then lead to the squared

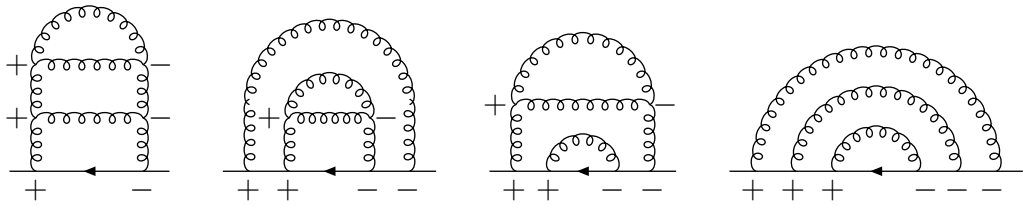

Figure 6.2: One possible index arrangement for $\Sigma^{(3)+-}$.

scattering amplitudes of *individual* channels of processes containing three gluons. For kinematical reasons only processes with at least two partons in the initial and final state are involved. Since we are considering the loss term, one quark must be in the initial state. This gives us the four processes $q\bar{q} \to ggg$, $qg \to qgg$, $q\bar{q}g \to gg$ and $qgg \to qg$. Calculations analogous to the ones in Sec. 5.1 prove this. For the first two processes the generic Feynman diagrams are shown in Fig. 6.3.

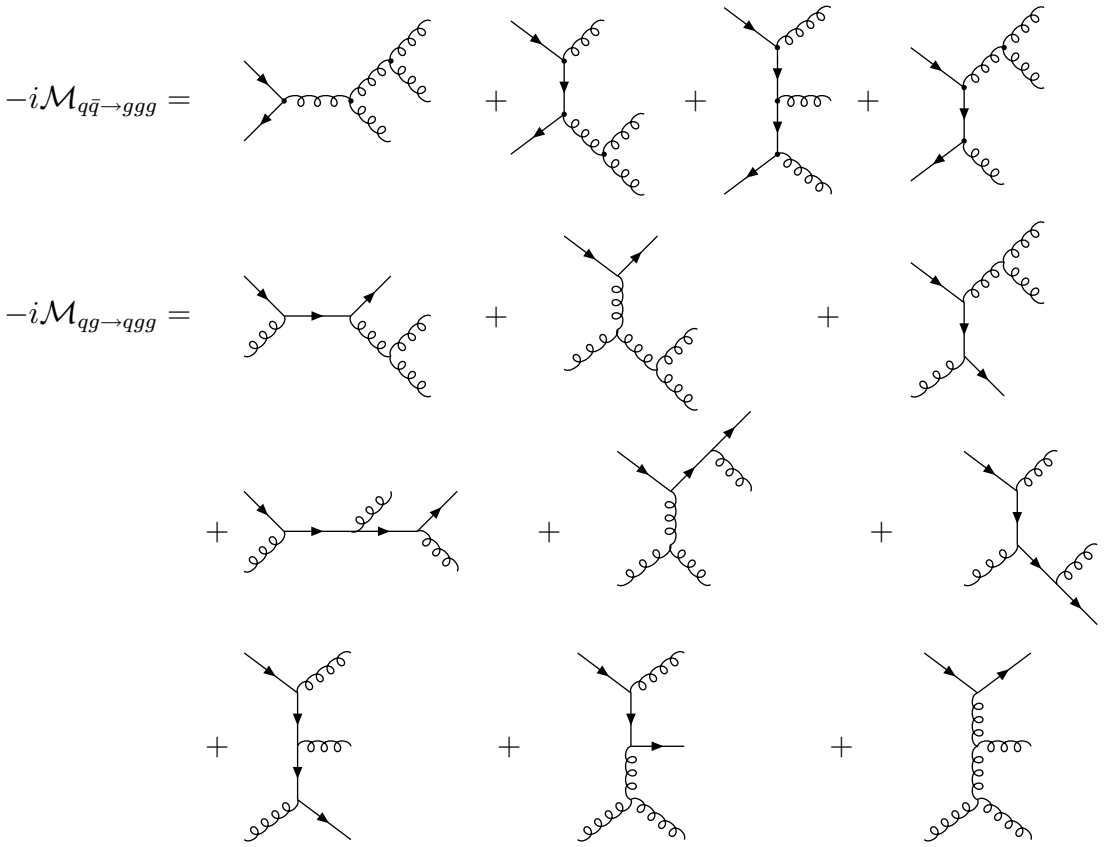

Figure 6.3: Generic Feynman diagrams for the processes $q\bar{q} \to ggg$ and $qg \to qgg$.

The mixed terms between single channels are provided by the self-energy diagrams shown in Fig. 6.4 as we have checked.

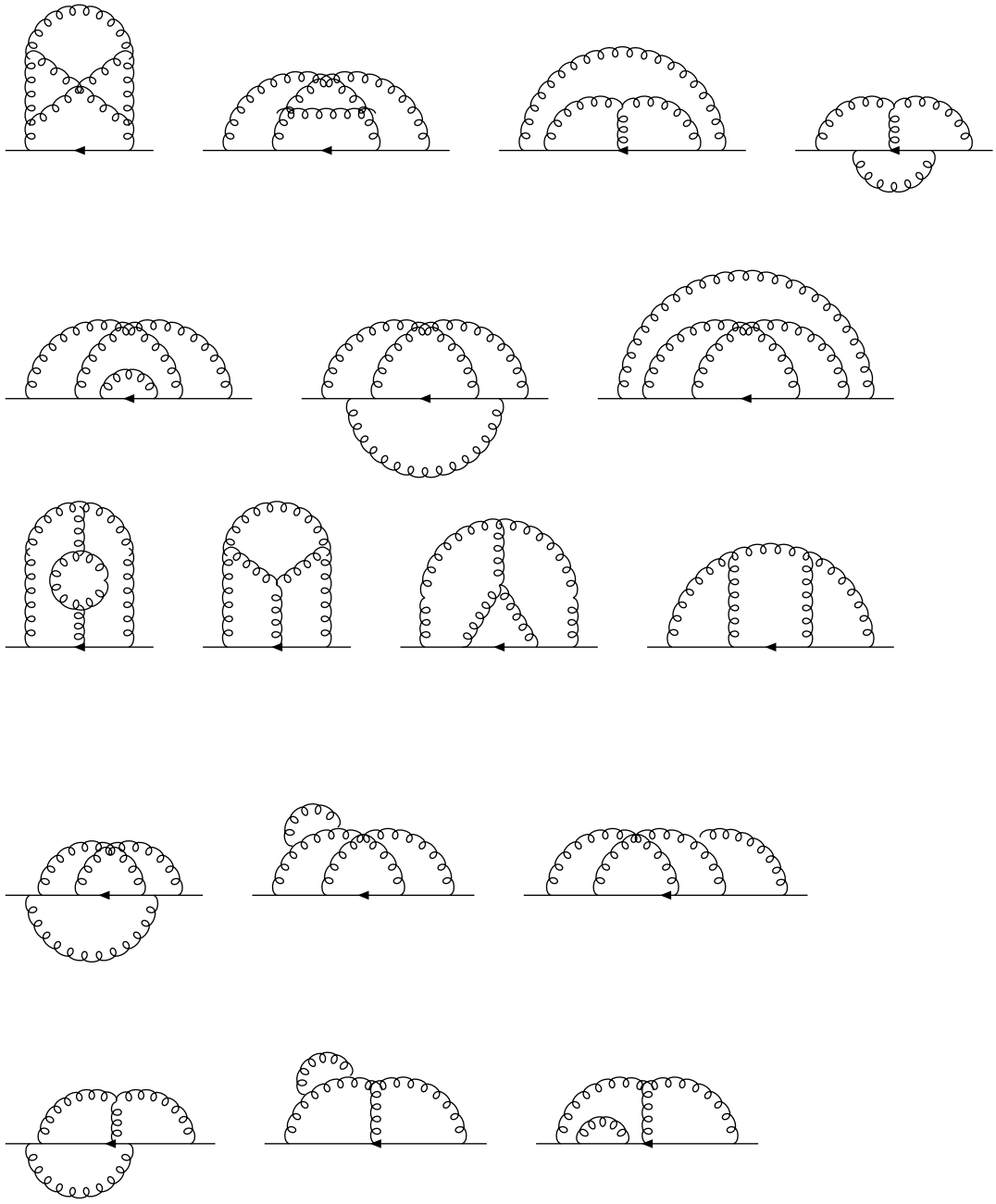

Figure 6.4: Generic three loop self-energy diagrams leading to mixed terms between single channels of scattering processes involving three gluons.

The last six diagrams of Fig. 6.4 are not symmetric, and it is to be understood that the mirror reflected diagrams must also be taken into account. Note that our expansion in $1/N_c$ is not rigorous since we are keeping non-planar diagrams which can be of lower order in $1/N_c$ than diagrams containing quark-loops. For comparison see the case of two loop self-energies where the exchange diagram is subleading compared to the quark-loop graph.

We saw in Sec. 5.2 that the two loop self-energies not only lead to $2 \to 2$ cross sections but also to corrections to processes of lower order, i.e. to the annihilation process $q\bar{q} \to g$. Similarly we expect the three loop self-energies to provide corrections of order g^6m^6 to all $2 \to 2$ processes obtained in Sec. 5.1 and also to $q\bar{q} \to g$. Since the derivation of these corrections follows the one given in Sec. 5.2 and above, we will not list them here but give only one final example: The process $q\bar{q} \to g$ is shown in Fig. 5.5 up to order g^3m^3. Hence, the product of two amplitudes among b) to g') of Fig. 5.5 is of order g^6m^6. The three loop self-energy diagrams which give the squared amplitudes $bb^\dagger$, $cc^\dagger$, $ee^\dagger$ and $ff^\dagger$ are shown in Fig. 6.5. Since self-energy graphs containing quark-loops are neglected, the product $dd^\dagger$ cannot be obtained in this approximation.

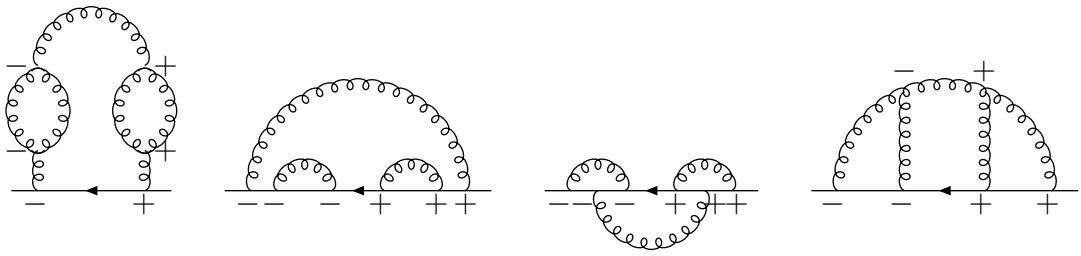

Figure 6.5: Generic three loop diagrams leading to corrections of order g^6m^6 of the process $q\bar{q} \to g$.

6.2 n to m processes

Of the self-energy diagrams of order $O(g^{2n})$, we take again only the diagrams which are leading in an expansion in $1/N_c$. On evaluation, the ladder diagram, the rainbow diagram and all possible mixtures between these two lead to the scattering process $q\bar{q} \to ng$ and all possible crossed processes, such as $q\bar{q}g \to (n-1)g$, $qg \to q(n-1)g$, ... in which at least two partons occur both in the initial and final states. In addition to this, the leading self-energy diagrams provide corrections of order $O(g^{2n})$ to lower

order processes. The transport equation for quarks then reads

$$
\begin{aligned}
2p\partial_X f_q(X,\vec{p}) &= \int \frac{d^3k}{(2\pi)^3 2E_k}\frac{d^3p_1}{(2\pi)^3 2E_1}(2\pi)^4\delta^{(4)}(p+k-p_1)|\mathcal{M}_{q\bar{q}\to g}|^2 \\
&\times \left[\bar{f}_q(X,\vec{p})\bar{f}_{\bar{q}}(X,\vec{k})f_g(X,\vec{p}_1) - f_q(X,\vec{p})f_{\bar{q}}(X,\vec{k})\bar{f}_g(X,\vec{p}_1)\right] \\
&+ \sum_{m,n=1}^{\infty}\int \frac{d^3k}{(2\pi)^3 2E_k}\frac{d^3p_1}{(2\pi)^3 2E_1}\cdots\frac{d^3p_{m+n}}{(2\pi)^3 2E_{m+n}}(2\pi)^4 \\
&\times \Big\{\delta^{(4)}(p+k+p_1+...+p_{m-1}-p_m-...-p_{m+n}) \\
&\quad \times s_{m-1}s_{n+1}\ |\mathcal{M}(q\bar{q}\,(m-1)g\to(n+1)g)|^2 \\
&\quad \times \left[\bar{f}_q(\vec{p})\bar{f}_{\bar{q}}(\vec{k})\bar{f}_g(\vec{p}_1)...\bar{f}_g(\vec{p}_{m-1})f_g(\vec{p}_m)...f_g(\vec{p}_{m+n})\right. \\
&\quad \left. -f_q(\vec{p})f_{\bar{q}}(\vec{k})f_g(\vec{p}_1)...f_g(\vec{p}_{m-1})\bar{f}_g(\vec{p}_m)...\bar{f}_g(\vec{p}_{m+n})\right] \\
&+ \delta^{(4)}(p+p_1+...+p_m-k-p_{m+1}-...-p_{m+n})s_m s_n\ |\mathcal{M}(q\,mg\to q\,ng)|^2 \\
&\quad \times \left[\bar{f}_q(\vec{p})\bar{f}_g(\vec{p}_1)...\bar{f}_g(\vec{p}_m)f_q(\vec{k})f_g(\vec{p}_{m+1})...f_g(\vec{p}_{m+n})\right. \\
&\quad \left. -f_q(\vec{p})f_g(\vec{p}_1)...f_g(\vec{p}_m)\bar{f}_q(\vec{k})\bar{f}_g(\vec{p}_{m+1})...\bar{f}_g(\vec{p}_{m+n})\right]\Big\}
\end{aligned}
\tag{6.2}
$$

with the symmetry factors $s_n = 1/(n!)$. This is our final result for the transport equation and its resemblance to the Boltzmann equation is obvious.

Chapter 7

Pinch singularities

When dealing with transport theory, and in particular when applying the quasi-particle assumption to processes of higher order, it becomes mandatory to examine another possible problem which can arise, the issue of so-called pinch singularities. To elucidate this, let us look again at the quark-loop self-energy diagrams shown in Fig. 5.2. We can write the sum of these four self-energy graphs as

$$\begin{aligned}\Sigma^{(2)+-}_{QL}(X,p) &\equiv \Sigma^{(2)+-}_{QLa)}(X,p) + \Sigma^{(2)+-}_{QLb)}(X,p) + \Sigma^{(2)+-}_{QLc)}(X,p) + \Sigma^{(2)+-}_{QLd)}(X,p) \\ &= ig^2m^2 \int \frac{d^4k}{(2\pi)^4}\, iS^{+-}(X,p-k)\, iF^{+-}_{QL}(X,k) \end{aligned} \tag{7.1}$$

with

$$\begin{aligned}F^{+-}_{QL}(X,k) \equiv\ & G^{++}(X,k)\,\Pi^{+-}(X,k)\,G^{--}(X,k) + G^{++}(X,k)\,\Pi^{++}(X,k)\,G^{+-}(X,k) \\ & + G^{+-}(X,k)\,\Pi^{--}(X,k)\,G^{--}(X,k) + G^{+-}(X,k)\,\Pi^{-+}(X,k)\,G^{+-}(X,k)\end{aligned} \tag{7.2}$$

where Π^{ij} is defined in Eq.(5.27) and all color factors are suppressed for simplicity.

We see that in Eq.(7.2) each term contains two gluonic propagators with the same argument. Since the off-diagonal propagators are on-shell and also the diagonal propagator contain on-shell parts, seen in the δ-functions in k that are present, we obtain for each term a product of two δ-functions, which is clearly divergent.

This is a manifestation of so-called pinch singularities. The etymology is made evident if we express F^{+-}_{QL} in terms of the retarded and advanced components given in Eqs.(3.39), (3.40), (3.45) and (3.46):

$$\begin{aligned}F^{+-}_{QL}(X,k) \equiv\ & G^{R}(X,k)\,\Pi^{R}(X,k)\,G^{+-}(X,k) + G^{+-}(X,k)\,\Pi^{A}(X,k)\,G^{A}(X,k) \\ & - G^{R}(X,k)\,\Pi^{+-}(X,k)\,G^{A}(X,k).\end{aligned} \tag{7.3}$$

In the last term, the product

$$G^R(X,k)\,G^A(X,k) = \frac{1}{k^2 - m^2 + i\epsilon}\,\frac{1}{k^2 - m^2 - i\epsilon} \tag{7.4}$$

has a pinch singularity, since an integration contour running along the real k_0 axis is "pinched" between the two poles for $\epsilon \to 0$. For the rainbow and ladder self-energy graphs of Fig. 5.2, the situation is similar as for the quark-loop graph: each graph contains two propagators with the same argument. Therefore pinch singularities may occur in these terms, too.

In *equilibrium*, however, studies over the last decade show that pinch singularities vanish in the calculations of physical quantities [14, 38] in a well-defined theory (such as thermal field theory). Therefore we start our investigation in equilibrium.

7.1 Cancellation of pinch singularities in equilibrium

To get a feeling of how the cancellation of pinch singularities happens, we investigate a couple of cases in equilibrium.

7.1.1 Model with one type of particle

We start with a simplified model that contains only one type of particle. Therefore the number of generic two loop self-energy diagrams reduces drastically. Then the rainbow, ladder and quark-loop graphs are topically equivalent as well as the cloud and exchange graphs; i.e. the number of generic graphs reduces to two, see Fig. 7.1.

Self-energy with zero momentum

It is useful now to make another simplifying assumption: we calculate the self-energies at zero momentum. For this case, the labeling of momenta is shown in Fig. 7.1. Note that the cloud diagram has two pairs of propagators with the same argument while the rainbow diagram has in fact three propagators with the same argument. Thus both are possible candidates that might display pinch singularities. We start now with the investigation of the rainbow diagrams which are shown for Σ_R^{--} and Σ_R^{-+} in more detail in Fig. 7.2. From these two self-energies, the retarded self-energy can be constructed as

$$\Sigma_R^r = \Sigma_R^{--} + \Sigma_R^{-+}. \tag{7.5}$$

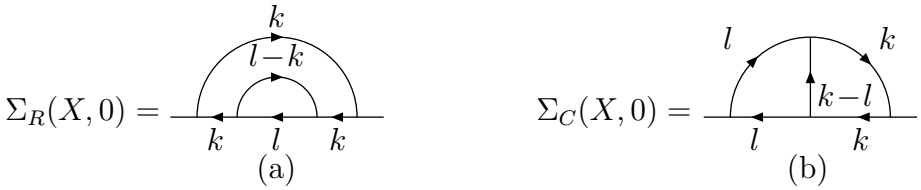

Figure 7.1: Generic two loop self-energy diagrams for one parton type and vanishing momentum.

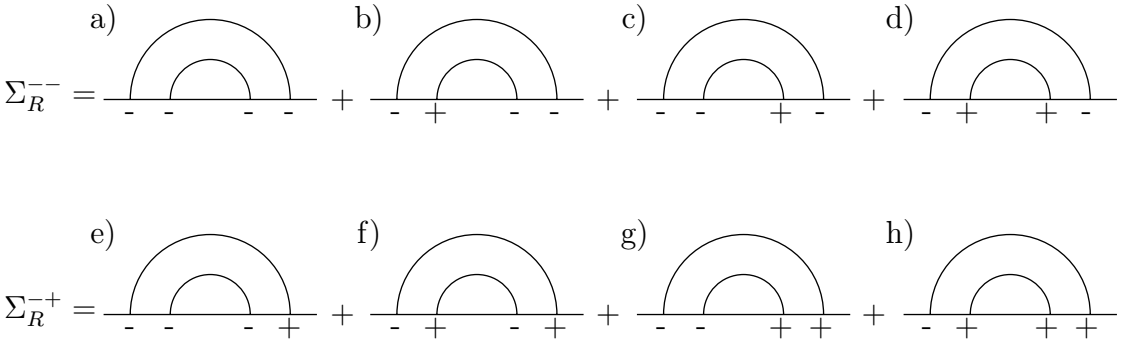

Figure 7.2: Rainbow self-energy diagrams for Σ_R^{--} and Σ_R^{-+}.

Since the retarded self-energy is a physically relevant property, that enters, for example, into the constraint equation Eq.(3.56), we would like to investigate the diagrams of Fig. 7.2 in more detail. In each of the diagrams b), c) and f) of Fig. 7.2, it is possible to identify an internal vertex to which lines three off-diagonal Green functions are attached. Since these Green functions are on mass shell, this corresponds to a decay of an on-shell particle into two on-shell particles of the same species. This is a forbidden process, and therefore these three diagrams vanish. We now take a closer look at Fig. 7.2 g). The propagator of the larger bow has an on-shell momentum. Since the self-energy is calculated for vanishing momentum, the two propagators D^{--} and D^{++} have to be on-shell too. Thus each of the inner vertices corresponds to a decay of an on-shell particle into on-shell particles and this graph is therefore also vanishing. Consequently, Σ_R^r is the sum of the remaining diagrams a), d), e) and h):

$$\Sigma_R^r(X,0) \;=\; (-igm)^4 \int \frac{d^4k}{(2\pi)^4}\frac{d^4l}{(2\pi)^4}\left\{[D^{--}(k)]^3 D^{--}(l-k)D^{--}(l)\right.$$

$$
\begin{aligned}
&+D^{--}(k)[D^{-+}(k)]^2 D^{++}(l-k)D^{++}(l) \\
&-D^{--}(k)[D^{-+}(k)]^2 D^{--}(l-k)D^{--}(l) \\
&-D^{++}(k)[D^{-+}(k)]^2 D^{++}(l-k)D^{++}(l)\Big\}. \quad (7.6)
\end{aligned}
$$

This construction appears to contain pinch singularities, evidenced by the fact that products of $D(k)$ occur, and it is imperative to show that while the individual graphs diverge, their combination leads to the fact that the apparent divergence vanishes through cancellation.

Since physical quantities should be independent of the choice of σ we are free to choose to take $\sigma = \beta/2$ as e.g. in [39, 40]. Then the propagators given in Eq.(3.30) read

$$
\begin{aligned}
i\underline{D}_{\sigma=\beta/2}(\omega) &= \begin{pmatrix} \frac{i}{\omega^2-E^2+i\epsilon} & 0 \\ 0 & \frac{-i}{\omega^2-E^2-i\epsilon} \end{pmatrix} + \frac{2\pi\delta(\omega^2-E^2)}{e^{\beta|\omega|}-1}\begin{pmatrix} 1 & e^{\beta|\omega|/2} \\ e^{\beta|\omega|/2} & 1 \end{pmatrix} \\
&= \begin{pmatrix} D_1+D_\beta & D'_\beta \\ D'_\beta & D_2+D_\beta \end{pmatrix} \quad (7.7)
\end{aligned}
$$

so defining D_1, D_2, D_β and D'_β[1]. Clearly, D_1 is just the Feynman propagator for a scalar particle, iD_F defined in Eq.(3.27). For this subsection, we stay with above notation, corresponding to that of Ref. [39].

Now consider the last term of the retarded self-energy in Eq.(7.6):

$$
\begin{aligned}
\int\frac{d^4l}{(2\pi)^4}D^{++}(l-k)D^{++}(l) &= \int\frac{d^4l}{(2\pi)^4}\{D_2(l-k)D_2(l)+D_2(l-k)D_\beta(l) \\
&\quad +D_\beta(l-k)D_2(l)+D_\beta(l-k)D_\beta(l)\} \\
&= \int\frac{d^4l}{(2\pi)^4}\{-D_1(l-k)D_1(l)-D_1(l-k)D_\beta(l) \\
&\quad -D_\beta(l-k)D_1(l)+D_\beta(l-k)D_\beta(l)\} \\
&= -\int\frac{d^4l}{(2\pi)^4}D^{--}(l-k)D^{--}(l). \quad (7.8)
\end{aligned}
$$

In the first step, we have made use of the relations [39]

$$
\int\frac{d^4l}{(2\pi)^4}D_1(l-k)D_1(l) = -\int\frac{d^4l}{(2\pi)^4}D_2(l-k)D_2(l) \quad (7.9)
$$

and

$$
\int\frac{d^4l}{(2\pi)^4}D_1(l-k)D_\beta(l) = -\int\frac{d^4l}{(2\pi)^4}D_2(l-k)D_\beta(l). \quad (7.10)
$$

[1]Our notation leaves out a factor i in the last matrix, in order to establish consistency with the standard use of thermo field theory users [39].

In the second step, we have made use of the fact that the fourth term, $D_\beta(l-k)D_\beta(l)$, has to vanish, since together with $D'_\beta(k)$ of Eq.(7.6) it corresponds again to the decay of an on-shell particle into two on-shell particles. With Eq.(7.8), we can rewrite Eq.(7.6) for the retarded self-energy as

$$\begin{aligned}\Sigma^r_R(X,0) &= (gm)^4 \int \frac{d^4k}{(2\pi)^4}\frac{d^4l}{(2\pi)^4} D^{--}(l-k)D^{--}(l) \\ &\quad \times \left\{[D^{--}(k)]^3 - 2D^{--}(k)[D^{-+}(k)]^2 + D^{++}(k)[D^{-+}(k)]^2\right\}. \end{aligned} \tag{7.11}$$

It is now convenient to make use of the following representation of δ-function,

$$2\pi\delta(k^2-m^2) = \frac{i}{k^2-m^2+i\epsilon} - \frac{i}{k^2-m^2-i\epsilon} = D_1(k) + D_2(k). \tag{7.12}$$

Expressing D_β and D'_β in terms of D_1 and D_2 as

$$\begin{aligned} D_\beta(k) &= [D_1(k) + D_2(k)]\, f_B \\ D'_\beta(k) &= [D_1(k) + D_2(k)]\, g_B \end{aligned} \tag{7.13}$$

with the Bose-Einstein distribution $f_B = 1/(e^{\beta|k_0|}-1)$ and $g_B = e^{\beta|k_0|/2}/(e^{\beta|k_0|}-1)$, possible pinch singularities will manifest themselves no longer as products of δ functions but rather as products of D_1D_2. Then the term in curly brackets of Eq.(7.11) is evaluated to give

$$\begin{aligned}\{...\} &= [D_1 + (D_1+D)f_B]^3 + [D_2 + (D_1+D_2)f_B](D_1+D_2)^2 g_B^2 \\ &\quad -2[D_1 + (D_1+D_2)f_B](D_1+D_2)^2 g_B^2. \end{aligned} \tag{7.14}$$

Using the fact that $f_B^2 - g_B^2 = -f_B$, we find

$$\{...\} = (D_1)^3 + [(D_1)^3 + (D_2)^3]f_B. \tag{7.15}$$

This expression is well defined, since no products of D_1D_2 occur any longer. With the relation

$$\begin{aligned}[D_1(k)]^3 + [D_2(k)]^3 &= -\frac{1}{2}\left(\frac{\partial}{\partial m^2}\right)^2 [D_1(k) + D_2(k)] \\ &= -\frac{1}{2}\left(\frac{\partial}{\partial m^2}\right)^2 2\pi\delta(k^2-m^2), \end{aligned} \tag{7.16}$$

we can write the retarded self-energy as

$$\begin{aligned}\Sigma^r_R(X,0) &= (gm)^4 \int \frac{d^4k}{(2\pi)^4}\frac{d^4l}{(2\pi)^4} D^{--}(l-k)D^{--}(l) \\ &\quad \times \left\{[D_1(k)]^3 - \frac{1}{2}\left(\frac{\partial}{\partial m^2}\right)^2 2\pi\delta(k^2-m^2) f_B\right\}. \end{aligned} \tag{7.17}$$

We conclude that for the retarded rainbow self-energy Σ^r_R, no pinch singularities occur.

We now have to consider the cloud self-energy of Fig. 7.1 (b). The retarded self-energy is constructed in a similar way as for the rainbow diagram. The calculation of such a diagram within the framework of ϕ^3 theory has been performed in [39]. This result can be simply taken over for our purposes, and we quote the final expression here:

$$\begin{aligned}\Sigma^r_C(X,0) &= (gm)^4 \int \frac{d^4k}{(2\pi)^4}\frac{d^4l}{(2\pi)^4}\left[(D_1(k))^2+\chi(k)\right] \\ &\quad \times [D_1(l-k)+D_\beta(l-k)]\left[(D_1(l))^2+\chi(l)\right], \end{aligned} \tag{7.18}$$

where the function

$$\begin{aligned}\chi(k) &= 2D_1(k)D_\beta(k)+[D_\beta(k)]^2-[D'_\beta(k)]^2 \\ &= 2P\frac{i}{k^2-m^2}2\pi\delta(k^2-m^2)f_B \\ &= i\frac{\partial}{\partial m^2}2\pi\delta(k^2-m^2)f_B \end{aligned} \tag{7.19}$$

is free of singularities. Thus we conclude that in equilibrium, the two loop retarded self-energies $\Sigma^r_{R/C}$ have no pinch singularities for vanishing momentum. Note that it was necessary to consider the retarded self-energies which are the sum of $\Sigma^{(2)--}_{R/C}$ and $\Sigma^{(2)-+}_{R/C}$ since only the sum of both terms is free of pinching and not each term in itself. The reason for this lies in the fact that the rainbow diagram contains not only two propagators with the same argument but three.

Self-energy with non-zero momentum

As a next step, we now consider the case for self-energies with non-vanishing momentum but still with only one particle type. In order to establish our labeling of momenta, the generic rainbow and cloud diagram are shown in Fig. 7.3 for finite momentum. One notices immediately that the cloud self-energy in Fig. 7.3 has no pair of propagators with the same argument. Therefore no pinch singularities can arise in this case and we only have to examine the rainbow self-energy further. We start with Σ^{--}_R shown in Fig. 7.2 a) to d). For the same reason a mentioned above the diagrams b) and c) vanish. The remaining two graphs give

$$\begin{aligned}\Sigma^{--}_R(X,p) &= (-igm)^4 \int \frac{d^4k}{(2\pi)^4}\frac{d^4l}{(2\pi)^4}\, D^{--}(k-p)\,\Big\{D^{--}(l-k)\,D^{--}(l)[D^{--}(k)]^2 \\ &\quad + D^{++}(l-k)\,D^{++}(l)[D^{-+}(k)]^2\Big\}. \end{aligned} \tag{7.20}$$

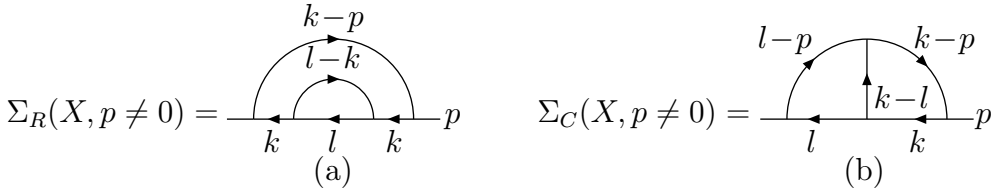

Figure 7.3: Generic two loop self-energy diagrams with non-zero momentum.

Pinch singularities can only occur for k on-shell. In this case we are allowed to use Eq.(7.8) and find

$$\begin{aligned}\Sigma_R^{--(PS)}(X,p) &= (-igm)^4 \int \frac{d^4k}{(2\pi)^4}\frac{d^4l}{(2\pi)^4}\, D^{--}(k-p)\, D^{--}(l-k)\, D^{--}(l) \\ &\quad \times \left\{ [D^{--}(k)]^2 - [D^{-+}(k)]^2 \right\}. \end{aligned} \tag{7.21}$$

With the help of Eqs.(7.7) and (7.13), we can express the term in curly brackets in terms of D_1 and D_2 as

$$\{...\} = D_1^2 + 2(D_1^2 + D_1 D_2) f_B + (D_1 + D_2)^2 (f_B^2 - g_B^2). \tag{7.22}$$

Using again the fact that $f_B^2 - g_B^2 = -f_B$, we obtain

$$\begin{aligned}\Sigma_R^{--(PS)}(X,p) &= (gm)^4 \int \frac{d^4k}{(2\pi)^4}\frac{d^4l}{(2\pi)^4}\, D^{--}(k-p)\, D^{--}(l-k)\, D^{--}(l) \\ &\quad \times \left\{ [D_1(k)]^2 + \left([D_1(k)]^2 - [D_2(k)]^2 \right) f_B \right\}, \end{aligned} \tag{7.23}$$

which is free of pinch singularities.

Now we turn to Σ_R^{-+} shown in Fig. 7.2 e) to h). Diagram f) vanishes as explained above while for diagram g) the above given argumentation does not hold true any more and it gives a finite contribution. On the other hand pinch singularities can only arise if the momentum k is on-shell. For this particular choice of k the inner two vertices of graph g) contribute to the forbidden process of an on-shell particle decaying into two on-shell particles of the same species. Therefore only graphs e) and h) can possible display pinch singularities:

$$\begin{aligned}\Sigma_R^{-+(PS)}(X,p) &= -(-igm)^4 \int \frac{d^4k}{(2\pi)^4}\frac{d^4l}{(2\pi)^4}\, D^{+-}(k-p)\, D^{--}(l-k)\, D^{--}(l) \\ &\quad \times \left\{ D^{-+}(k) \left[D^{--}(k) - D^{++}(k) \right] \right\}. \end{aligned} \tag{7.24}$$

Since $D^{-+}(k)$ is on-shell we are allowed to use Eq.(7.8) again. Using Eqs.(7.7) and (7.13) the term in curly brackets reads

$$\{...\} = (D_1 + D_2) g_B \, (D_1 - D_2) \tag{7.25}$$

and we therefore obtain

$$\Sigma_R^{-+(PS)}(X,p) = (gm)^4 \int \frac{d^4k}{(2\pi)^4}\frac{d^4l}{(2\pi)^4}\, D^{+-}(k-p)\, D^{--}(l-k)\, D^{--}(l) \times \Big([D_2(k)]^2 - [D_1(k)]^2\Big)\, g_B, \tag{7.26}$$

where no products of $D_1 D_2$ occur any longer.

We summarize our result found in this subsection: for only one particle type, the two loop self-energies are given as $\Sigma^{--} = \Sigma_R^{--} + \Sigma_C^{--}$ and $\Sigma^{-+} = \Sigma_R^{-+} + \Sigma_C^{-+}$. Then for finite momentum p both, $\Sigma^{--}(X,p)$ and $\Sigma^{-+}(X,p)$, are free of pinch singularities while for vanishing momentum only the sum of both, i.e. the retarded self-energy $\Sigma^r(X,p)$ is free from pinching.

7.1.2 Model with two particle types

In this subsection, we consider the inclusion of different kinds of particles interacting with each other as in our model introduced in Chapter 2. Our task is now to show that the pinch singularities vanish in equilibrium. Since we want to generalize later on our results for systems in non-equilibrium if possible we choose this time the $\sigma = 0$ representation. For our purpose, it is helpful to use following relations,

$$\Pi^{--}(p) = -\Pi^{++}(p)^* \tag{7.27}$$

$$\Im\Pi^{--}(p) = \frac{i}{2}\Big[\Pi^{-+}(p) + \Pi^{+-}(p)\Big] \tag{7.28}$$

$$\Pi^{+-}(p) = e^{\beta p_0}\,\Pi^{-+}(p). \tag{7.29}$$

The first two are valid in general (see Eq.(3.43) and (3.44)) while the last one is the KMS relation of Eq.(3.16) and holds only in equilibrium.

We consider only $\Sigma^{(2)+-}$ shown in Fig. 5.2. The calculations for $\Sigma^{(2)--}$ can then be performed in a similar way. Only rainbow, ladder and quark-loop graphs are possible candidates for pinch singularities since they contain a pair of propagators with the same argument. We start with the sum of the four quark-loop graphs QL a) to QL d) of Fig. 5.2 and given in Eq.(7.1). With the help of the above relations F_{QL}^{+-} defined in Eq.(7.2) can be written as

$$F_{QL}^{+-} = \Re\Pi^{--}\Big[-G^{++}\,G^{+-} + G^{+-}\,G^{--}\Big] + i\Im\Pi^{--}\left[G^{++}\,G^{+-} + G^{+-}\,G^{--} - \frac{2e^{\beta p_0}}{e^{\beta p_0}+1}\,G^{++}\,G^{--} - \frac{2}{e^{\beta p_0}+1}\,G^{+-}\,G^{+-}\right] \tag{7.30}$$

where the arguments (X,k) are suppressed. The propagators of Eq.(3.23) read for $\sigma = 0$ as

$$\begin{aligned}\underline{D}_{\sigma=0}(k) &= \begin{pmatrix} D_F(k) & 0 \\ 0 & -D_F^*(k) \end{pmatrix} \\ &\quad + [D_F(k) - D_F^*(k)] \begin{pmatrix} n(|k|) & [\Theta(-k_0) + n(|k|)] \\ [\Theta(k_0) + n(|k|)] & n(|\omega|) \end{pmatrix}. \end{aligned} \tag{7.31}$$

Inserting these expressions for the propagators, one can express F_{QL}^{+-} in terms of G_F and G_F^*. After some algebra, one finds

$$\begin{aligned} F_{QL}^{+-}(X,k) &= \Re\Pi^{--}(X,k) \left[G_F^2(X,k) - G_F^{*2}(X,k)\right] [\Theta(k_0) + n(|k|)] \\ &\quad + i\Im\Pi^{--}(X,k) \left[G_F^2(X,k) + G_F^{*2}(X,k)\right] \frac{1}{e^{-\beta k_0}+1}. \end{aligned} \tag{7.32}$$

No products of the form $G_F\, G_F^*$ occur, and therefore one may conclude that this expression is also free of pinch singularities.

For the sum of the four rainbow graphs shown in Fig. 5.2 R a) to R d), one obtains a similar expression by replacing the gluonic propagators by quark propagators and the self-energy insertion Π by the quark Fock self-energy $\Sigma_{F,q}$ shown in Fig. 4.2. One finds

$$\begin{aligned} F_R^{+-}(X,k) &= \Re\Sigma_{F,q}^{--}(X,k) \left[S_F^2(X,k) - S_F^{*2}(X,k)\right] [\Theta(k_0) + n(|k|)] \\ &\quad + i\Im\Sigma_{F,q}^{--}(X,k) \left[S_F^2(X,k) + S_F^{*2}(X,k)\right] \frac{1}{e^{-\beta k_0}+1}, \end{aligned} \tag{7.33}$$

which is also free of pinch singularities.

For the sum of the four ladder graphs shown in Fig. 5.2 L a) to L d) one cannot perform an analogous calculation since the graph $\Sigma_{Ld)}^{+-}$ vanishes due to the vertices with three on-shell gluons. One finds the expression for $F_L^{+-}(X,k)$ to be

$$F_L^{+-} = G^{++}\,\tilde{\Pi}^{+-}\,G^{--} + G^{++}\,\tilde{\Pi}^{++}\,G^{+-} + G^{+-}\,\tilde{\Pi}^{--}\,G^{--}, \tag{7.34}$$

where $\tilde{\Pi}$ is the gluonic Fock self-energy $\Sigma_{F,g(a)}^{-+}$ shown in Fig. 4.2 (a). Since pinch singularities can only occur on-shell, we consider now the self-energy insertions on-shell and find

$$\tilde{\Pi}^{+-}(X;E_k,\vec{k}) = \tilde{\Pi}^{-+}(X;E_k,\vec{k}) = \Im\tilde{\Pi}^{--}(X;E_k,\vec{k}) = 0 \tag{7.35}$$

$$\tilde{\Pi}^{--}(X;E_k,\vec{k}) = -\tilde{\Pi}^{++}(X;E_k,\vec{k}) = \Re\tilde{\Pi}^{--}(X;E_k,\vec{k}). \tag{7.36}$$

Inserting this into Eq.(7.34) yields

$$F_L^{+-}(X;E_k,\vec{k}) = \Re\tilde{\Pi}^{--}(X;E_k,\vec{k}) \left[G_F^2(X;E_k,\vec{k}) - G_F^{*2}(X;E_k,\vec{k})\right] \left[\Theta(k^0) + n(|k|)\right]. \tag{7.37}$$

This expression is also free from pinching, and therefore $F_L^{+-}(X,k)$ for arbitrary k has no pinch singularities.

We summarize that in equilibrium in single two loop self-energy graphs pinch singularities can occur, but the sum of the graphs a) to d) of one generic type (i.e. rainbow, ladder or quark-loop graphs) is free of pinching.

7.2 Pinch singularities in non-equilibrium

Our task is now to investigate if and how the pinch singularities cancel in non-equilibrium. We start with the ladder diagrams of Fig. 5.2 for which we showed in the last section that the pinch singularities vanish. For this derivation only relations (7.27) and (7.28) were used. Hence it holds also in non-equilibrium, and we conclude that even for arbitrary distribution functions $f_g(X,p)$ the ladder diagrams have no pinch singularities.

Unfortunately, the calculations for the rainbow and quark-loop diagrams of Fig. 5.2 performed in the last section in equilibrium cannot be generalized for the case of non-equilibrium field theory since the use of the KMS relation which is only valid in equilibrium was crucial in this derivation.

A similar result was found by Altherr and Seibert [41]. They investigated a scalar self-energy diagram with an inserted self-energy like our rainbow, ladder or quark-loop diagram. They found that a cancellation of pinch singularities only occurs if the condition

$$[\Theta(p_0)\, n(p) - \Theta(-p_0)\ (1+n(p))]\, \Sigma^{+-}(P) = \epsilon(p_0)\, [\Theta(p_0) + n(p)]\, \Sigma^{-+}(P) \tag{7.38}$$

is fulfilled. For $p_0 > 0$ this gives

$$n(p)\Sigma^{+-}(P) = [1+n(p)]\, \Sigma^{-+}(P) \tag{7.39}$$

and if $n(p)$ is the Bose-Einstein distribution this condition reduces to the KMS relation (7.29). The time evolution of the particle number density reads

$$-2ip_0 \frac{dn(p,t)}{dt} = [1+n(p)]\, \Sigma^{-+}(P) - n(p)\Sigma^{+-}(P). \tag{7.40}$$

If condition (7.39) it fulfilled, one is left with

$$\frac{dn(p,t)}{dt} = 0. \tag{7.41}$$

On first sight, this is very unsatisfactory for a non-equilibrium field theory. But on the other hand, the time variation of the density matrix has to be slow compared to

the typical time scale of the particle interactions. Otherwise the Fourier transformation of the propagators does not make sense. Although there is reversibility at the microscopic level, one can impose the condition of irreversibility at the macroscopic level. Even if a slow variation of the density matrix is assumed, the condition (7.39) is not guaranteed to hold. The micro-reversibility conditions are only satisfied by *equilibrium* distributions. The only alternative would be to give up energy conservation at the vertices.

Note that relation (7.39) implies that the collision term of Eq.(4.1) vanishes. Then clearly the system is in equilibrium and therefore no pinch singularities arise.

Although Altherr and Seibert found that only for systems in thermal and chemical equilibrium the pinch singularities cancel, there are several attempts to find solutions to this problem for systems out of equilibrium.

We start with a subsequent paper of Altherr [42]. There, the propagators are expressed in terms of the retarded and advanced propagators

$$\Delta_{R/A}(K) = \frac{\pm i}{K^2 - m^2 \pm i\gamma k_0}, \tag{7.42}$$

where γ is an arbitrary finite width. Due to this width the pathologies associated with multiple products of delta-functions are regularized. The width is introduced here heuristically "by hand", but it can in fact be calculated perturbatively. We will come to this point again in the next chapter.

A couple of years later, Dadić developed two mechanisms for the elimination of pinch singularities in non-equilibrium field theory [43]. The first one is based on the vanishing of phase space at the singular point, and it can be applied e.g. to QED with massive electrons and massless photons. This however does unfortunately not apply to our theory, since we have massless quarks and massive gluons. In massless QCD, this method fails, too. But here the second mechanism holds: the pinch singularities cancel due to the spinor/tensor structure of the single self-energy insertion. Since we consider scalar particles, this mechanism does not work in our case either.

Bedaque [44] argued that pinch singularities are an artifact of an infinite interaction time. If the interaction is switched on at a finite time then the integration range over time becomes limited. In this bounded domain the functions are well behaved. In momentum space, the limited range of integration over time produces fractions of the form $i/(\alpha + i\eta)$ instead of delta-functions. Clearly this fraction is related via Eq.(3.28) to delta-functions but the singularities produced from multiple products of delta-functions cancel with the singularities from the principal value. Therefore for a finite interaction time, no pinch singularities can occur. Should on the other hand the fields have interacted since $t = -\infty$, then they should have attained equilibrium

by any finite time and pinch singularities would cancel anyway.

Greiner and Leupold [45] have also argued that the pinch singularities are due to the infinite duration time of the interaction and can be regulated by a finite duration time. In addition they pointed out the relation of pinch singularities to Fermi's golden rule known from elementary scattering theory.

We conclude by commenting that in out of equilibrium field theory the pinch singularities in our rainbow and quark-loop diagrams do not cancel. But in a more realistic model with massless vector gluons and scalar or spinor quarks (either massless or massive) the pinch singularities would in fact cancel [43]. Another possibility is to use propagators with a finite width instead of the quasiparticle approximation. We will tackle this issue in the next chapter.

We present now another attempt to solve the problem with pinch singularities in the rainbow and quark-loop diagrams of Fig. 5.2: we use dressed gluons instead of the bare ones. A dressed gluon is the sum of the bare gluon plus all possible self-energy insertions in the bare gluon. This is shown in Fig. 7.4 up to the Fock level where a dressed gluon propagator is denoted by a thick gluon line. One could

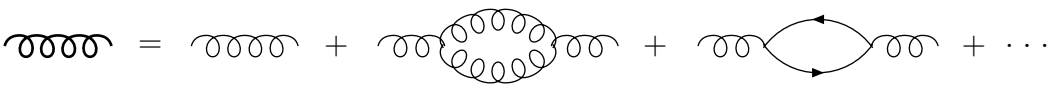

Figure 7.4: Full gluon propagator.

dress the quark propagator as well but this must be done with caution. Using now the dressed gluon propagators, the number of generic quark self-energy graphs reduces and they are shown up to the two loop level in Fig. 7.5. The rainbow and

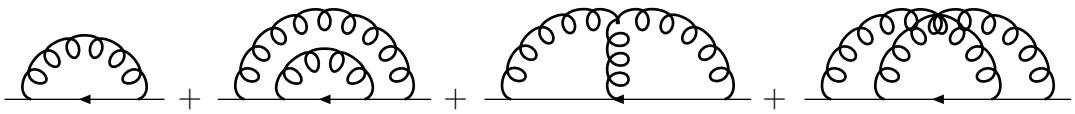

Figure 7.5: Generic self-energy diagrams up to two loops with dressed gluons.

ladder diagrams of Fig. 5.2 are now included in the Fock diagram of Fig. 7.5. We assume that the resumed gluon propagator is free from singularities, in particular from pinch singularities, since multiple self-energy insertions can be summed over as in the random phase approximation. As an example this is shown graphically in

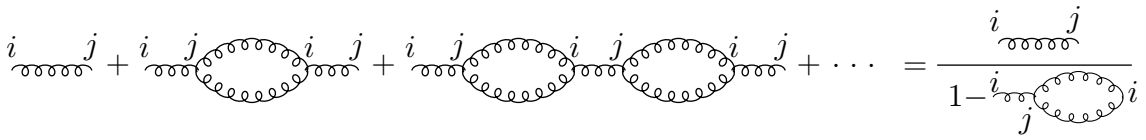

Figure 7.6: Summation of propagators with gluon-loop insertions

Fig. 7.6 for the case of multiple gluon-loop insertions with indices i and j.

Hence, the pinch singularities of the quark-loop diagram of Fig. 5.1 have disappeared. Nevertheless, this approach is not very satisfactory: The pinch singularities displayed in the rainbow diagram are still present. Furthermore, without the ladder and quark-loop diagrams it is not possible to construct the squared scattering amplitudes of all $2 \to 2$ processes shown in Fig. 5.4 since squared amplitudes of single channels are missing. Additional problems in obtaining a Boltzmann-like equation are also generated when moving away from δ-function distributions.

Chapter 8

The constraint equation

So far we have treated only the transport equation (4.1) as an isolated equation. As we have seen, this in itself has a complexity in deriving an extended Boltzmann equation. The main assumption that has been made is the quasiparticle approximation, and this has been inserted into every level of calculation of the self-energy. In principle, however, the transport equation does not stand alone, but must be solved simultaneously with the constraint equation, which in practice must be newly evaluated for each additional term in the expansion (here in the coupling constant and of the self-energy) that has been used. In Section 4.1, we demonstrated explicitly that the constraint equation gives rise to the quasiparticle approximation for free streaming. Here this corresponds to the Hartree approximation for the self-energy. In general, however, this is not so. We thus take a closer look at the constraint equation (3.70). Using the relations (3.37), (3.38) and (3.43), we can rewrite the constraint equation in a simpler form as

$$\left[p^2 - M^2 + \Re\Pi^{--}(X,p)\right] D^{-+}(X,p) = \Pi^{-+}(X,p)\,\Re D^{--}(X,p). \tag{8.1}$$

With the aid of Eqs.(3.37), (3.39), (3.40), (3.77) and (3.78), we can express the real part of D^{--} as

$$\begin{aligned} 2\Re D^{--}(X,p) &= D^{--}(X,p) - D^{++}(X,p) = D^R(X,p) + D^A(X,p) \\ &= \frac{1}{p^2 - M^2 + \Pi^R(X,p)} + \frac{1}{p^2 - M^2 + \Pi^A(X,p)}. \end{aligned} \tag{8.2}$$

Using Eqs.(3.44) to (3.46), one finds

$$\Re\Pi^R(X,p) = \Re\Pi^A(X,p) = \Re\Pi^{--}(X,p) \tag{8.3}$$

$$\Im\Pi^R(X,p) = -\Im\Pi^A(X,p) = p_0\,\Gamma(X,p), \tag{8.4}$$

where the width Γ is defined as

$$\Gamma(X,p) = \frac{i}{2p_0}(\Pi^{+-} - \Pi^{-+}). \tag{8.5}$$

Inserting Eqs.(8.3) and (8.4) into Eq.(8.2) leads to

$$\Re D^{--}(X,p) = \frac{p^2 - M^2 + \Re\Pi^{--}(X,p)}{\left[p^2 - M^2 + \Re\Pi^{--}(X,p)\right]^2 + \left[p_0\,\Gamma(X,p)\right]^2}. \tag{8.6}$$

Substituting p with $-p$ in Eq.(8.1) yields the relation

$$\left[p^2 - M^2 + \Re\Pi^{--}(X,p)\right] D^{+-}(X,p) = \Pi^{+-}(X,p)\,\Re D^{--}(X,p). \tag{8.7}$$

Subtracting (8.1) from (8.7) gives

$$\begin{aligned}&\left[p^2 - M^2 + \Re\Pi^{--}(X,p)\right] \mathcal{A}(X,p)\\ &= 2p_0\,\Gamma(X,p)\,\frac{p^2 - M^2 + \Re\Pi^{--}(X,p)}{\left[p^2 - M^2 + \Re\Pi^{--}(X,p)\right]^2 + \left[p_0\,\Gamma(X,p)\right]^2},\end{aligned} \tag{8.8}$$

where the spectral density $\mathcal{A}$ is defined through the combination

$$\mathcal{A}(X,p) = iD^{+-}(X,p) - iD^{-+}(X,p). \tag{8.9}$$

For $p^2 - M^2 + \Re\Pi^{--}(X,p) \neq 0$, Eq.(8.8) gives

$$\mathcal{A}(X,p) = \frac{2p_0\,\Gamma(X,p)}{\left[p^2 - M^2 + \Re\Pi^{--}(X,p)\right]^2 + \left[p_0\,\Gamma(X,p)\right]^2}. \tag{8.10}$$

If $\mathcal{A}$ is calculated, one can immediately find expressions for the off-diagonal Green functions via

$$iD^{-+}(X,p) = \Theta(p_0)\,\mathcal{A}(X,p)\,f_a(X,p) - \Theta(-p_0)\,\mathcal{A}(X,p)\,\bar{f}_{\bar{a}}(X,-p) \tag{8.11}$$

$$iD^{+-}(X,p) = \Theta(p_0)\,\mathcal{A}(X,p)\,\bar{f}_a(X,p) - \Theta(-p_0)\,\mathcal{A}(X,p)\,f_{\bar{a}}(X,-p) \tag{8.12}$$

and subsequently for the diagonal Green functions with the help of Eqs.(3.63) and (3.64). In the limit of vanishing self-energies (and therefore vanishing width Γ) $\mathcal{A}$ simplifies to

$$\mathcal{A}(X,p) \longrightarrow 2\pi\delta(p^2 - M^2)\,\mathrm{sign}(p_0) \tag{8.13}$$

and for the Green functions one regains the quasiparticle approximation Eqs.(3.61) to (3.64) as it should be.

One thus finds the situation that higher order corrections to the transport equation should, strictly speaking, be evaluated with propagators that contain a finite

width Γ. This has both advantages and disadvantages. The main advantage is that no pinch singularities can possibly occur with the use of a finite width by definition (see also Ref. [42]). Thus, one may definitively state that non-equilibrium theory is non-singular; any apparent singularities are a result of using an inconsistent approximation and these may be removed by the introduction of a cutoff related to a width.

The disadvantages of using a finite width are manifold: Firstly the presence of a finite width automatically admits all possible processes: for example, the first exchange and quark-loop diagrams led to a sum of eight terms Eq.(5.6). These in turn led to two possible types of scattering processes that were admissible, with the restriction being directly due to the quasiparticle assumption. In the presence of a finite width, all eight terms would be non-vanishing. In this sense, the theory is expanded well over the Boltzmann approach. Furthermore, an additional complexity arises. The transition from Green functions to the more physical quantities, the distribution functions, in terms of which the Boltzmann equation is expressed, no longer becomes possible. Thus the evaluation of physical entities becomes more distanced from our knowledge of the Boltzmann equation. It is our point of view that research in both directions is interesting. While it is more easily conceivable to do physics in extending the Boltzmann equation, it is equally necessary to attempt to solve the exact equations, and determine the difference between these two approaches. From an analytic point of view, it is not simple to extract this difference. Rather numerical calculations should prove interesting and insightful.

Chapter 9

Summary and conclusions

In this work, we have derived the transport and constraint equations for a theory of scalar quarks and gluons. Special care has been taken in particular in understanding how the transport equation, taken on its own, leads to a Boltzmann-like equation when considered in the quasiparticle approximation. Thus, our aim has been to express the collision integral of the transport equation in terms of cross sections or, more generally, in terms of squared scattering amplitudes. For this purpose, the self-energy diagrams are organized according to their order in the coupling strength and built into the collision term. We have examined this systematically. Most facets of this study show the following:

1. We have been successful in expressing the collision integral up to the two loop level in terms of products of scattering amplitudes using non-equilibrium propagators. The differential cross sections of all possible $2 \to 2$ processes are obtained. However, for the absolute square of the complete amplitude of the process $q\bar{q} \to g$ up to order g^3m^3 two products of single amplitudes are missing.

2. By the use of $T = 0$ Feynman propagators instead of non-equilibrium ones in the evaluation of the $2 \to 2$ scattering amplitudes the two missing products could be gained. Hence the complete absolute square of the process $q\bar{q} \to g$ up to order g^3m^3 evaluated with non-equilibrium propagators is obtained.

3. Thus, taking the transport equation on its own in the quasiparticle approximation, a generalized Boltzmann equation is found. This applies to all orders.

4. No leading class of diagrams like the ladder graphs in elastic quark-quark scattering has been found. But an expansion in $1/N_c$ reduces the number of self-energy graphs and favors gluon production.

5. The quasiparticle approximation causes artificial difficulties - pinch singularities occur as a consequence of products of delta-functions. Within the scope of these calculations they do not cancel in non-equilibrium.

6. A simultaneous consideration of the constraint equation leads to a finite width in the propagators. On one hand, this prevents the appearance of pinch singularities, but on the other hand, added complexities arise which make it impossible to cast the transport equation into a Boltzmann-like form.

7. The study shows a definite association of non-equilibrium self-energy graphs with Feynman graphs of scattering and particle production / annihilation processes. The association of several graphs with standard two body scattering is clear. Not obvious, however, is the renormalization of lower order diagrams by the remaining self-energy graphs of higher order. In addition to this there are some diagrams that cannot be easily classified anywhere. We have clarified which graphs lead to which processes.

8. It is not possible to define universal non-equilibrium cutting rules which give in a simple way the relation between self-energy diagrams and products of scattering amplitudes.

There are many interesting applications and challenges which have to be investigated in the future. The most natural continuations of this work are

- To calculate the transport equation consistently with the constraint equation, i.e. with propagators containing a finite width.

- To evaluate the transport and constraint equations up to higher orders in the gradient expansion.

- To check with the help of numerical studies whether a class of self-energy diagrams is leading. Then the calculations including higher order loop diagrams could be simplified.

- To use massless vector gluons and/or spinor quarks (massless or massive) instead of scalar partons, to finally extend these results to real QCD.

- Generally numerical simulations, in conjunction with existing pomeron theories.

The applications of transport theory are manifold: it describes not only heavy ion collisions but also the evolution of the early universe and in general of every system

in non-equilibrium. Therefore it is essential to put the existent approaches on a solid footing and derive the evolution equations from first principles. We believe that with this work an important step has been made in this direction.

Appendix A

Wigner transforms

For completeness, we list the Wigner transforms which were necessary to obtain Eqs.(3.52) and (3.53):

$$\partial_x^\mu f(x,y) \longrightarrow \left(-ip^\mu + \frac{1}{2}\partial_X^\mu\right) f(X,p) \tag{A.1}$$

$$\partial_y^\mu f(x,y) \longrightarrow \left(ip^\mu + \frac{1}{2}\partial_X^\mu\right) f(X,p) \tag{A.2}$$

$$\Box_x f(x,y) \longrightarrow \left(\frac{1}{4}\Box_X - \frac{i}{\hbar}p\partial_X - \frac{1}{\hbar^2}p^2\right) f(X,p) \tag{A.3}$$

$$\Box_y f(x,y) \longrightarrow \left(\frac{1}{4}\Box_X + \frac{i}{\hbar}p\partial_X - \frac{1}{\hbar^2}p^2\right) f(X,p) \tag{A.4}$$

$$\int d^4z\, f(x,z)\, g(z,y) \longrightarrow f(X,p)\,\hat{\Lambda}\, g(X,p) \tag{A.5}$$

with the differential operator

$$\hat{\Lambda} = \exp\left\{-\frac{i\hbar}{2}\left(\overleftarrow{\partial_X}\,\overrightarrow{\partial_p} - \overleftarrow{\partial_p}\,\overrightarrow{\partial_X}\right)\right\}. \tag{A.6}$$

These relations can be derived simply from the definition of the Wigner transform in Eq.(3.51) (a proof of the last relation is given for example in Ref. [46]).

The Green functions and self-energies are now assumed to vary slowly with X as it is the case for weakly inhomogeneous systems. In addition, it is assumed that they are strongly peaked near $u = 0$. These assumptions are equivalent to the requirement

$$|f(X,p)| \gg |\partial_X\partial_p\, f(X,p)| \gg \left|(\partial_X\partial_p)^2\, f(X,p)\right|, \tag{A.7}$$

where $f(X,p)$ is a Green function or a self-energy respectively. This condition justifies the expansion of $\hat{\Lambda}$ in gradients which was used in Sec. 3.2 where $\hat{\Lambda}$ was set to 1 in lowest order.

Appendix B

Color factors

In this Appendix, we deal with the color factors which were neglected so far. We calculate them for *one* $SU(N)$ color group. The overall color factor for both color groups is then obtained by squaring it.

The matrices $(t^a)_{ij}$ are the matrices of the color group in the representation of the quarks, while $(T^a)_{bc} = -if_{abc}$ are the color matrices in the adjoint representation and f_{abc} are the structure constants of the color group, see Eq.(2.2). The t^a's are normalized to

$$\mathrm{tr}(t^a t^b) = \frac{1}{2}\delta_{ab}. \tag{B.1}$$

The "square" of the generator in some representation must be proportional to the unit operator (Schur's Lemma). Therefore

$$(t^a)_{ij}(t^a)_{jk} = C_F \delta_{ik} \tag{B.2}$$

and

$$T^a_{bd}T^a_{dc} = f_{bad}f_{cad} = C_A\delta_{bc}, \tag{B.3}$$

where the numbers C_F and C_A are the Casimir operators of the fundamental and adjoint representation, respectively. They take the values (see for example [47])

$$C_F = \frac{N_c^2 - 1}{2N_c} \tag{B.4}$$

and

$$C_A = N_c. \tag{B.5}$$

Consider now the quark self-energies that were evaluated in Section 5.1. Let i denote the external parton color index. It is therefore not to be summed over. The color factor for the rainbow graph is

$$F_R = t^b_{ij}t^a_{jk}t^a_{kl}t^b_{li} = C_F^2\delta_{ii} = \frac{(N_c^2-1)^2}{4N_c^2}\delta_{ii}. \tag{B.6}$$

For the ladder graph, one finds

$$F_L = (-if_{abc})(-if_{cbd})t^a_{ij}t^d_{ji} = C_A\delta_{ad}t^a_{ij}t^d_{ji} = C_AC_F\delta_{ii} = \frac{N_c^2-1}{2}\delta_{ii}. \tag{B.7}$$

For the cloud graph, one obtains

$$F_C = (-if_{acb})t^a_{ij}t^b_{jk}t^c_{ki} = -\frac{N_c^2-1}{4}\delta_{ii}, \tag{B.8}$$

where the relation (see for example [47])

$$-if_{abc}t^at^b = \frac{C_A}{2}t^c \tag{B.9}$$

has been used. The color factor for the exchange graph is

$$F_E = t^a_{ij}t^b_{jk}t^a_{kl}t^b_{li} = -\frac{N_c^2-1}{4N_c^2}\delta_{ii}, \tag{B.10}$$

where the relation [47]

$$t^at^bt^a = \frac{-1}{2N_c}t^b \tag{B.11}$$

has been used. Finally, for the quark-loop graph the color factor is given by

$$F_{\rm QL} = t^a_{ij}t^b_{ji}{\rm tr}(t^at^b) = \frac{N_c^2-1}{4N_c}\delta_{ii}. \tag{B.12}$$

In an expansion in $1/N_c$, some of the self-energy diagrams are subleading. For details see Chapter 6.

Bibliography

[1] K. Geiger and B. Müller, *Nucl. Phys.* **B 369** (1992) 600.

[2] K. Geiger and B. Müller, *Phys. Rev.* **D 50** (1994) 337.

[3] K. Geiger, *Phys. Rev.* **D 54** (1996) 949.

[4] S. Mrówczyński and U. Heinz, *Ann. Phys. (N.Y.)* **229** (1994) 1.

[5] D.S. Isert and S.P. Klevansky, hep-ph/9912203.

[6] S.P. Klevansky, A. Ogura, and J. Hüfner, *Ann. Phys. (N.Y.)* **261** (1997) 37.

[7] J. Schwinger, *J. Math. Phys.* **2** (1961) 407.

[8] L.V. Keldysh, *JETP* **20** (1965) 1018.

[9] H. Umezawa, H. Matsumoto, and M. Tachiki, *"Thermo Field Dynamics and Condensed States"*, North-Holland Publishing Company, Amsterdam, 1982.

[10] K. Werner, *Phys. Rep.* **V 232** (1993) 87.

[11] J.C. Polkinghorne, *J. Math. Phys.* **4** (1963) 503; **4** (1963) 1393; **4** (1963) 1396.

[12] J.R. Forshaw and D.A. Ross, *"Quantum Chromodynamics and the Pomeron"*, p. 26, Cambridge University Press, Cambridge, 1997.

[13] R.E. Cutkosky, *J. Math. Phys.* **1** (1960) 429.

[14] N.P. Landsman and Ch.G. van Weert, *Phys. Rep.* **145** (1987) 141.

[15] Ch.G. van Weert, in *"Proc. Workshop on Thermal Field Theory, Banff, 1993"*, (F.C. Khanna, R. Kobes, G. Kunstatter, and H. Umezawa, Ed.), p. 1, World Scientific, Singapore, 1994.

[16] M. van Eijck, *"Thermal Field Theory and the Finite-Temperature Renormalization Group"*, Thesis, University of Amsterdam (1995).

[17] M. Le Bellac, *"Thermal Field Theory"*, Cambridge University Press, Cambridge, 1996.

[18] J.I. Kapusta, *"Finite-temperature field theory"*, Cambridge University Press, Cambridge, 1989.

[19] H. Umezawa, *"Advanced field theory - Micro, Macro, and Thermal Physics"*, AIP Press, Woodbury, NY, 1993.

[20] A. Niégawa, *Prog. Theor. Phys. Suppl.* **129** (1997) 105.

[21] P. Aurenche and T. Becherrawy, *Nucl. Phys.* **B 379** (1992) 259.

[22] M.A. van Eijck, R. Kobes, and Ch.G. van Weert, *Phys.Rev.* **D 50** (1994) 4097.

[23] L.D. Landau and E.M. Lifschitz, *"Course of theoretical Physics, Physical kinetics"*, vol.10, Pergamon Press, Oxford, 1981.

[24] K.-C. Chou, Z.-B. Su, B.-L. Hao, and L. Yu, *Phys. Rep.* **118** (1985) 1.

[25] W. Botermans and R. Malfliet, *Phys. Rep.* **198** (1990) 115.

[26] L.P. Kadanoff and G. Baym, *"Quantum Statistical Mechanics"*, Benjamin, New York, 1962.

[27] P. Danielewicz, *Ann. Phys.* **152** (1984) 239.

[28] S. Mrówczyński and P. Danielewicz, *Nucl. Phys.* **B 342** (1990) 345.

[29] J.E. Davis and R.J. Perry, *Phys. Rev.* **C 43** (1991) 1893.

[30] R.L. Kobes and G.W. Semenoff, *Nucl. Phys.* **B 260** (1985) 714.

[31] R.L. Kobes and G.W. Semenoff, *Nucl. Phys.* **B 272** (1986) 329.

[32] P.F. Bedaque, A. Das, and S. Naik, *Mod. Phys. Lett.* **A 12** (1997) 2481.

[33] F. Gelis, *Nucl. Phys.* **B 508** (1997) 483.

[34] A. Niégawa, *Phys.Rev.* **D 57** (1998) 1379.

[35] H.A. Weldon, *Phys. Rev.* **D 28** (1983) 2007.

[36] J.-P. Blaizot and E. Iancu, *Nucl. Phys.* **B 557** (1999) 183.

[37] R. Baier, M. Dirks, and K. Redlich, *Phys.Rev.* **D 55** (1997) 4344.

[38] H. Matsumoto, I. Ojima, and H. Umezawa, *Ann. Phys. (N.Y.)* **152** (1984) 348.

[39] Y. Fujimoto and R. Grigjanis, *Z. Phys.* **C 28** (1985) 395.

[40] Y. Fujimoto, H. Matsumoto, H. Umezawa and I. Ojima, *Phys. Rev.* **D 30** (1984) 1400.

[41] T. Altherr and D. Seibert, *Phys. Lett.* **B 333** (1994) 149.

[42] T. Altherr, *Phys. Lett.* **B 341** (1995) 325.

[43] I. Dadić, *Phys. Rev.* **D 59** (1999) 125012.

[44] P.F. Bedaque, *Phys. Lett.* **B 344** (1995) 23.

[45] C. Greiner and S. Leupold, *Eur. Phys. J.* **C 8** (1999) 517.

[46] C. Greiner and S. Leupold, *Annals Phys.* **270** (1998) 328.

[47] Yu.L. Dokshitzer, in *"Lecture Notes in Physics"* (F. Lenz, H. Grießhammer, and D. Stoll, Ed.), Vol. 496, p. 87, Springer-Verlag, Heidelberg, 1997.

Danksagung

Als erstes danke ich ganz herzlich Prof. Sandra P. Klevansky für die intensive Zusammenarbeit. Die Diskussionen mit ihr waren hilfreich und haben sehr viel Spaß gemacht. Die sehr gute Betreuung, die seit ihrem Wechsel im letzten Jahr in den IT-Bereich unter erschwerten Umständen stattfand, rechne ich ihr hoch an.

Mein Dank gilt auch Prof. Jörg Hüfner und Prof. Michael G. Schmidt für ihre stetige Diskussionsbereitschaft und für hilfreiche Anregungen. Außerdem danke ich Prof. Schmidt für die Übernahme des Zweitgutachtens.

Der ganzen Arbeitsgruppe spreche ich meinen Dank aus für die freundliche Atmosphäre. Dr. Yuri Ivanov danke ich für die schnelle Hilfe bei Computerproblemen.

Dankbar verbunden bin ich Annabella Rauscher, Jochen Meyer und Kai Schwenzer für viele gute Gespräche - nicht nur über Physik - und für das Korrekturlesen von Teilen meiner Arbeit. Annabella danke ich auch für die Aufmunterungen in der stressigen Endphase.

Schließlich danke ich für die Unterstützung in vielerlei Hinsicht meiner Familie und vielen guten Freunden.

Soli Deo gloria